Forward dynamic model for rowing performance; driven by rower specific data and variable rigging setup

Master Thesis

by

J.T. Voordouw

to obtain the degree of Master of Science
at the Delft University of Technology,
to be defended publicly on 30 April 2018

Biomechanical Design
Department of Biomechanical Engineering
Faculty Mechanical, Maritime and Materials Engineering
Delft University of Technology

Student number: 4152689

Thesis committee:		
	Dr. Ir. A. L. Schwab,	Supervisor, TU Delft
	Prof. Dr. Ir. H. Vallery,	TU Delft
	Prof. Dr. Ir. M. Wisse,	TU Delft
	Dr. M. J. Hofmijster,	VU Amsterdam
	Ir. E. Meenhorst,	KNRB

Abstract

Introduction Every crew has its own rowing style and every rower has her own technique. Combining rowers with different techniques in one crew is a challenge, but very important, because a crew that rows in better synchrony will perform better. In order to make a crew row in better synchrony, coaches often expect the rowers to adjust their technique into a common stroke of the boat. However, in practice professional rowers are only able to change very few aspects of their technique, they maintain an individual biomechanical fingerprint (rowing signature).

To study the influence of the rower behavior on the boat performance, a one-dimensional rowing model is created, based on one rower individual specific stroke. The model is driven with data that is measured in the boat during a (practice) race. It can be validated with the measured boat motions and expected rower motions. Also the influence of the rigging parameters on the rower and boat movements is investigated.

Background The rowing stroke is a periodic movement of the rower, the oar and the blade. The periodical application of the propulsive forces makes the velocity of the boat fluctuate within the cycle. Also the movement of the crews' center of mass relative to the (lighter) boat cause extra velocity fluctuations. The state of art rowing models can be classified in different research fields. Most models use a generalized movement pattern to describe the athletes motions. The human factor must be included in a model, preferably in a individualized approach. A model does not necessarily have to be absolutely accurate, if it can predict a trend, it already has an added value.

Data The data used in this study comes from a light weight women's double, the rowers of which are members of the KNRB. The sensors used are the measurement oarlock, foot stretcher force sensor, seat position sensor and the boat acceleration sensor (IMU) of the PowerLine measurement system. The raw data is cut into strokes, beginning at the catch, averaged and combined into one stroke.

In the stroke based data differences between rowers are found. The data is used to create a normalized force-angle curve for every rower. Clear differences are found between the normalized force-angle curves of the rowers. A constant angle segment of a rower may alter when the rigging parameters are changed. The relative displacement of the rower is assumed to be constant despite rigging changes. In order to predict the relative displacement of the rower, a model has to be created modeling rower and boat movements.

Model The free body diagrams of the system, the rower, the oar and the boat show the forces acting on the objects. The forces on the rower and boat are only considered in x-direction and the rower is modeled as a point mass. This results in a one-dimensional rowing model. The distribution of the masses in the system is slightly changed. All drag forces on the system are assumed to be viscous and proportional to the square of the boat velocity. The lateral forces on the blade and the oar deformation are neglected.

The relative motions of the rower are predicted based on different approaches, the most individualized approach is to use the forces acting on the rower. The acceleration of the boat can be described with the forces acting directly on the boat, or combining the acceleration of the system with the relative acceleration of the rowers. The last gives a better prediction on the boat acceleration. Changing some of the estimated model parameters improves the fit for the boat acceleration, but does not reach an optimum. Adding an extra resistance force to the rower results in a better relative movement of the rower and slightly better boat acceleration. The best fit for the boat acceleration and relative movement of the rower is found by changing the offset and gain of the measured foot force of the rowers. The total change of the foot force is at most 12%.

The rigging parameters in the model are changed under the assumption that the rower is a force constrained system and posses no restrictions on the movements of the handles. The rowers forces and motions in x-direction are assumed to remain constant, as well as the drag force. The changes

in boat motions for a different rigging setup are caused mainly by changes of the blade forces. The handle power applied by the rower is decreased when the boat velocity is increased. This indicates a deviation in the energy balance of the system.

Results Various methods are used to predict the boat acceleration. After comparison with the measured boat acceleration, the best obtained qualitative and quantitative (RMSE = 0.2152 m/s^2) fit for the boat acceleration is found with the method that uses the systems and relative rowers' accelerations with optimized gain and offset on the measured foot force.

For predicting the relative motions of the rower also various methods are used. The motions of the rower should be modeled with an individualized approach. The best qualitative result for the relative movement of the rower is found by using the forces acting directly on the rower with the optimized gain and offset for the foot force. The result is compared to the seat displacement and handle displacement for quality, the relative displacement is as expected.

Changing individual rigging parameters did not result in big differences between the rowers. Changing the lever ratio of the oar, by increasing the inboard length, leads to a bigger covered oar angle and a higher boat velocity. Moving the footstretcher towards the bow of the boat shifts the oar angle and leads to a higher boat velocity as well.

The energy balance of the system is not preserved, the work per stroke at the handle is decreased while the average boat velocity is increased. There have been made too much simplifications in calculating the blade forces. The found results of the modeled boat performance on changes in the rigging setup, should be interpreted as a sensitivity analysis and not a realistic prediction.

Discussion The model is build on a single dataset and the equations describing the motions of the rowers and the boat are all transferable to other datasets. However, the optimization that is done for the gain and offset of the foot forces is not.

The rower's technique is assumed to be constant, the receptivity of the rower to external influences changes per athlete. A power constraint per rower may improve the results for the different rigging setups. In order to gain a clear image of the rower's motions, measurements with a fully equipped boat have to be done regularly.

The kinematic complexity of this model is limited. When changing the rigging setup of the boat, the blade forces play a big role in the resulting boat motions and the model simplifications on that part may not be justified. A more complex model may result in better prediction of the blade forces under different rigging setups and show new insights on the effects of synchronization.

Conclusion The relative motions of the rower are best predicted with calculations based on the forces acting directly on the rower, after correction of the measured the foot force.

The best obtained qualitative and quantitative result for the boat acceleration is found with a method and that is based on the acceleration of the entire system and the relative accelerations of the rowers, after a correction is done on the gain and offset of the foot forces.

The blade forces have a leading role on the resulting boat motions when changing the rigging parameters. However the blade forces might not be realistically modeled. Changing the lever ratio of the oar, by increasing the inboard length, leads to a bigger covered oar angle, a smaller handle work per stroke and a higher boat velocity. Moving the footstretcher towards the bow of the boat shifts the oar angle and leads to an increase in boat velocity as well as a decrease in the applied work per stroke at the handle.

The boat performance is increased by changing the rigging setup of the boat, however there are no indications that this is the result of a better synchrony between the rowers. The model simplifications of the blade forces may not be justified. After implementation of a more complex modeling of the blade forces improvement could occur due to better synchronization.

Preface

This thesis is the result of my graduation project on the effects of the individual rower movements and rigging setup on the boat performance. In this thesis a model is presented with a new approach that calculates the rowers movement based on individual data. The project is a part of the graduation requirements of the study Mechanical Engineering at Delft University of Technology. I started the project in March 2017 with a literature thesis and I have been working on this dissertation until April 2018.

The first five years of my university career, I have rowed on a semi-professional level and during my research internship doing work on a rowing simulator at the ETH Zurich, I developed an academic interest in the sport as well. After I met Jelte Doeksen and Arend Schwab, I wanted to try and build a dynamic rowing model, in order to understand more about the sport. Via the Sports Engineering Institute contact is established with the Dutch Rowing Federation (KNRB) and the Vrije Universiteit Amsterdam (VU). Together we found a goal for a co-operation project; improve the boat performance by investigating the synchronization of the rowers.

While the synchronization of rowers is frequently investigated, a way to improve the synchronization for individual rowers is not found, this is a point where we can bring innovation. The ultimate plan was to develop an application (or simulation) that would use data from individual rowers as input and give their individualized rigging set-up for the best boat performance as output. However through time, we found there are plenty of problems to tackle before such a tool can be made. 'How can the synchronization of a crew be defined?' is the first question we answered in a small literature report. After this report we still wondered what the relation between different synchronization measures and boat performance is, this became the main topic of Jeltes graduation project.

Another unanswered question is the effect of the individual rower movements on the boat performance. In current models, only generalized rower motions are used, so a new approach is needed and presented in this thesis. At the end of my project, we have come a small step further in understanding how the rowing system works.

Throughout the project I have learned to conquer not only technical challenges, but also logistic problems and I have found ways to systematically present ideas or models so that people with different backgrounds can understand. I had to respond to changes in the project (direction) quite a few times, which taught me to be flexible towards the end goal and in my planning. For example, in the last week of my thesis I received extra datasets from Conny Draper, this is gratefully received, had to be analyzed really fast and fortunately the results supported my findings.

For his guidance and enthusiastic support during my research I would like to thank Arend Schwab. Daan Bregman: thank you for setting the collaboration with the VU Amsterdam. I would like to thank Mathijs Hofmijster for the introduction with the KNRB, the technical discussions and critical feedback and Eelco Meenhorst for the pleasant cooperation, supplying the various datasets and new ideas for the project. A special thank-you goes to Jelte, I enjoyed our cooperation, because we could discuss the technical challenges, as well as the "feeling" of rowing. The fact that we could work together on the project in the beginning was a big stimulant. The other students from the bicycle lab were a pleasure to work and to watch and discuss sports with, especially during the Olympics. Mats, Rob, Leonoor, Martine and Niek, thank you for reviewing my thesis when it was almost finished. Your feedback hopefully made it easier to read. At last I would like to thank Gerbrand and my parents for their unconditional support. Especially in times that were stressful for me or when I found myself in a stagnation point, you always knew how to reassure me, cheer me up and motivate me to tackle the problem.

I hope you will enjoy reading my thesis.

J.T. Voordouw
Delft, April 2018

Contents

Abbreviations & Symbols

Abbreviations

CoM	Center of mass
EOM	Equations of motion
FBD	Free body diagram
KNRB	Koninklijke Nederlandse Roeibond, the Dutch Rowing federation.
LW2x	Lightweight women's double sculls, two women with each two oars rowing together in the lightweight class (crew average 57 kg, no rower over 59 kg).
M4x	Men quadruple sculls or Men quad, four men each with two oars rowing together in the open weight class.
M4-	Men four, four men with one oar each rowing together in the open weight class.
RMSE	The root mean square of the error.
W2x	Women's double sculls, two women each with two oars rowing together in the open weight class.

Symbols

θ	The oar angle [rad]
C	The drag coefficient [-]
F_x	The force in x-direction; the moving direction of the boat [N]
F_y	The force in y-direction; perpendicular to the center line of the boat [N]
F_{blade}	The force acting on the blade [N]
F_{drag}	The drag force acting on the hull of the boat [N]
F_{foot}	The force acting on the footstretcher [N]
F_{gate}	The force on the gate [N]
F_{handle}	The force applied by the rower on the handle [N]
l_{boat}	The length of the boat [m]
$l_{inboard}$	The length of the inboard of the oar; from the collar to the tip of the handle [m]
l_{oar}	The length of the oar; from the tip of the blade to the tip of the handle [m]
$l_{outboard}$	The length of the outboard of the oar; from the collar to the tip of the blade [m]
m_b or m_{boat}	The mass of the boat [kg]
m_{oar}	The mass of the oar [kg]
m_r or m_{rower}	The mass of the rower [kg]
r1 = rower 1	The stroke rower
r2 = rower 2	The bow rower
t_0	is zero, t_0 is the start of the averaged stroke [s]
t_{final}	the time that the averaged stroke ends [s]
u_i	The relative position of object i in the boat[m]
x_b or x_{boat}	The position of the center of mass the boat [m]
x_r or x_{rower}	The position of the center of mass of the rower [m]

Rowing glossary

Concept	Definition
Accelerometer	Acceleration measurement device
Blade cant angle	The angle between the blade chord and the oar shaft axis
Bow	The front of the boat (fig. 1.1)
Bow angle	The angle between the oar shaft and the longitudinal axis of the shell
Bum-shoving	A technical error where the rower moves her seat backwards faster than her shoulders
Catch	The part of the stroke when the blade enters the water
Catch slip	The part of the catch when the blade is not completely submerged in the water
Checking the boat	Deceleration of the boat (mainly at the catch). The momentum of the rower(s) sends the boat in opposite direction
Collar	Plastic ring attached to the oar, which pushes in the oar shaft axis direction against the oarlock
Cox (or coxwain)	The person that steers the boat and gives commands to the rowers
Double	A two persons boat where both rowers have two oars (sculling)
Drag	The drag force; the component of the hydrodynamic force in the direction of the fluid flow
Drive	The propulsive part of the stroke between the catch and finish when the blade is in the water and the rower pulls the oar
Drive time	Time to complete the drive
Drive length	The displacement of the middle handle from catch to finish
Drive-recovery ratio	The ratio between the drive time and the recovery time
Entry	Vertical movement of the blade into the water
Feathered blades	Blades are turned parallel to the waterline (above the water)
Finish	The furthest point of the oar handle towards the bow of the boat
Forward control	Predicts the (movement) data based on set parameters and motor commands (forces)
Foot stretcher (Footboard)	An angled plate in the shell on which the rowers feet are secured (with shoes), adjustable in height, angle and longitudinal position
Four	A four persons boat where each rower has one oar (sweeping)
Gate (oarlock)	A device that swivels around a rigger pin and holds the oar (fig. 1.4)
Gunwhales	The top rail of the shell
Gyrometer	A device that measures angular speed
Handle	The end of the oar a rower holds in her hand
Hull	The watertight body of the boat
Inboard length	The length of the oar measured from the outside of the collar to the handle (fig. 1.2)
Inverse control	Computes parameters and motor commands (forces) based on (movement) data, also called Kinematic control
Lift	The lift force; the component of the hydrodynamic force normal to the direction of the fluid flow

Concept	Definition
Micro Electro Mechanical System	Small embedded systems that consist of a combination of electronic, mechanical and possibly chemical components. In this report they refer to small acceleration measurement devices
Oar	A leaver by which the rower pulls the handle against the oarlock and the blade through the water
Oarlock (gate)	A device that swivels around a rigger pin and holds the oar (fig. 1.4)
Outboard length	The length of the oar from the outside of the collar to the tip of the blade (fig. 1.2)
Pair	A two persons boat where each rower has one oar (sweeping)
Port side	The left-hand side of the boat, facing forward (fig. 1.1)
Power stroke	see drive
Pin	The vertical metal rod on which the rowlock rotates (fig. 1.4)
Quad	A four persons boat where each rower has two oars (sculling)
Recovery	The part of the stroke between the finish and the catch, when the oar is feathered and the seat is returned to the aft end of the slides
Recovery time	Time to complete the recovery
Release	The period of time where the blade moves vertically from fully covered till completely out of the water
Release slip	Part of the release where the blade is not completely emerged from the water
Rigger	The metal (or carbon) frame that supports the oarlock (fig. 1.4)
Rigging	The adjustment and alternation of the adjustable parts in and on the shell (riggers, footstretchers, oars) to maximize the rowers efficiency
Sculling	Rowing with two oars (the oars in sculling are also called sculls)
Shell	A rowing boat
Skiff	A single persons boat, always sculling
Slides	The rails over which the bench rolls
Span	The distance between two rigger pins of the boat in sculling (fig. 1.2)
Spread	The distance from the centerline of the boat to the oarlock in sweep rowing (fig. 1.2)
Squared blades	The blades are turned perpendicular to the waterline
Starboard side	The right-hand side of the boat, facing forward (fig. 1.1)
Stern	The back of the boat (fig. 1.1)
Stroke	The complete cyclic movement through the boat in order to move the boat through the water using oars
Stroke time	Time to complete one stroke (the period)
Stroke rate	The number of strokes per minute
Sweeping (or sweep rowing)	Rowing with one oar held with both hands

List of Figures

List of Tables

Introduction

Rowing is one of the oldest Olympic disciplines and in the last century the rowing boats are getting faster and faster [50]. In an Olympic rowing race the goal is to move the boat as fast as possible over a distance of 2000m. The differences between winning and losing can be 0.01 seconds at the finish. When observing the boats in a rowing race, several things can be noticed. At first it may seem as if the crew with best endurance and strength will win the race. But there are more differences between the crews and even differences between the rowers of one crew.

Every crew has its own rowing style and every rower has his or her own technique. This personal technique depends on the skill level of a rower and her body proportions and anatomy. Combining rowers with different techniques in one crew is a challenge, but very important, because a crew that rows in better synchrony will perform better [15, 26, 40, 60]. Despite the well-known tendency of humans to synchronize their movements [46], rowing in synchrony does not come automatically. In order to make a crew row in better synchrony, coaches often expect the rowers to adjust their technique into a common stroke of the crew. However, in practice professional rowers are only able to change very few aspects of their technique, they maintain an individual biomechanical fingerprint (also referred to as a rowing signature) [26, 30, 60]. This is why the coach of the Dutch mens sculling team (KNRB), Eelco Meenhorst, had the following question:

> *"Can the rowing performance be improved by tuning the rowers in a certain way, for example by changing the rigging?"*

Synchronization project

The ultimate goal of the project is to provide the KRNB with advice in how to tune the rigging parameters in the boat per rower. Such that rowers can row in better synchrony without changing much in their own technique. As a start, has to be defined what synchronization is and how it can be measured. This is done in a literature study [56]. The relationship between synchronization and performance is researched by Jelte Doeksen in his thesis.

For this thesis a goal is to obtain more knowledge on the individual behavior of the rower and the necessary relative motions of the rowers with respect to the boat. To study the influence of the rower behavior on the boat performance, a one-dimensional rowing model is created, based on one individually specific stroke per rower. The model is driven with forces and motions that are measured in the boat during a (practice) race. Technically the model is partly a forward dynamic model as well as partly an inverse model, due to the oar motions that are used. It can be validated with the measured boat motions and expected rower motions. The model is partly based on other models in literature [56], however most models generalize the rowers' movements, which is exactly the opposite of what this model is trying to accomplish.

A second goal in this thesis is to study the influence of the rigging parameters on the rower and boat movements. With the forward dynamic model of the rowers and the boat the following research questions can be answered:

- How can the individual rower behavior be modeled?
- How can the boat motions be modeled?
- What is the effect of changes in the rigging parameters on the rower and boat motion?

Thesis outline

The thesis starts with some background information on rowing and definitions of rowing terms (chapter 1). For guidance, most of the used rowing terminology can also be found in the rowing glossary. In chapter 2 the measured data is discussed and some processing of the data is done to create useful input data for the model. To draft the equations of motions of the different parts in the rowing system, several free body diagrams are needed. These are shown and supported in chapter 3. The

model with the individual movements of a rower and the resulting motions of the boat is explained in chapter 4. The effects of changes in the rigging parameters on the individual movements of the rower and the boat performance are shown in chapter 5. The results are presented in chapter 6 and critically reviewed in the discussion after which a conclusion is drawn. The final part of the thesis consists of some recommendations that can improve future studies with the same goal.

1

Background information & Definitions

Rowing is a sport with much history and although many people have a general idea of the sport, there is a lot of terminology that is not always clear to uninitiated readers. In section 1.1 and section 1.2 the basic principals and definitions around the rowing boat and the rowing stroke will be explained, in order to make sure that the interpretation of all the terms is correct. In the rowing glossary (page xi and xii) a list is made of rowing related terms used in this thesis.

In section 1.3 the current state of art rowing models are discussed, in preparation of the thesis model. A more detailed study regarding rowing measurements and models is done in the literature study preceding this thesis [56].

1.1. Rowing boat

One of the most important parts in the rowing system is the boat (or shell). The hull of the boat is the actual body; there are hulls of different materials, weights and width. In this report only the racing shells for rowing on elite levels are considered.

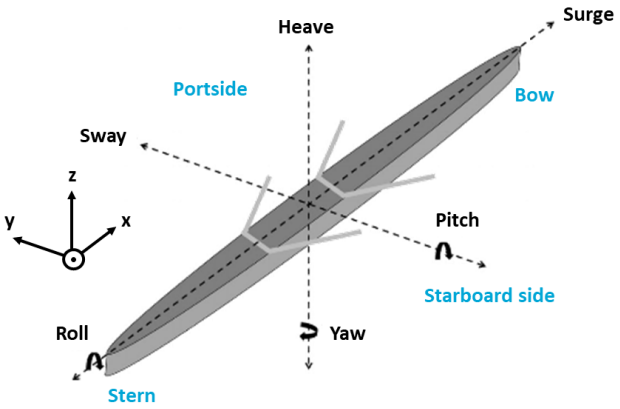

Figure 1.1: The movements of the boat shown in a double scull (Figure adjusted from Cuijpers et al. [15]). The translational movements of the boat are called surge (longitudinal boat direction), sway (perpendicular to the boat) and heave (vertical direction). The rotational movements in the boat are roll (around surge direction), pitch (around sway direction) and yaw (around heave direction).

The boat can make rotational and translational movements around each axis, see fig. 1.1. With yaw the boat can be steered in another direction and sway can be caused by water and wind conditions and can make the boat drift from its course. However, the only boat movement taken in consideration in this research is surge, since the velocity fluctuations in this direction cause the most detrimental force on the speed of boat.

Rowing is divided into two classes: sculling and sweep rowing. In sculling a rower holds one oar in each hand, in sweep rowing a rower holds only one oar. The amount of people in a boat can vary from one, two, four or eight rowers and possibly a cox. The skiff (or single scull) is the one-man boat and can only be used for sculling. On international level the eight is only used for sweep rowing. If the rowers are sweep rowing in a two-men's boat, this is called a pair, for sculling it is called a double. In a four-men's boat sweep rowing is simply called a four and sculling a quad.

The rower seated closest to the bow is called the bow (seat) and the rower closest to the stern is called the stroke (seat). The stroke is the one rower that every other crew member can see and is therefore important in determining the rhythm of the boat.

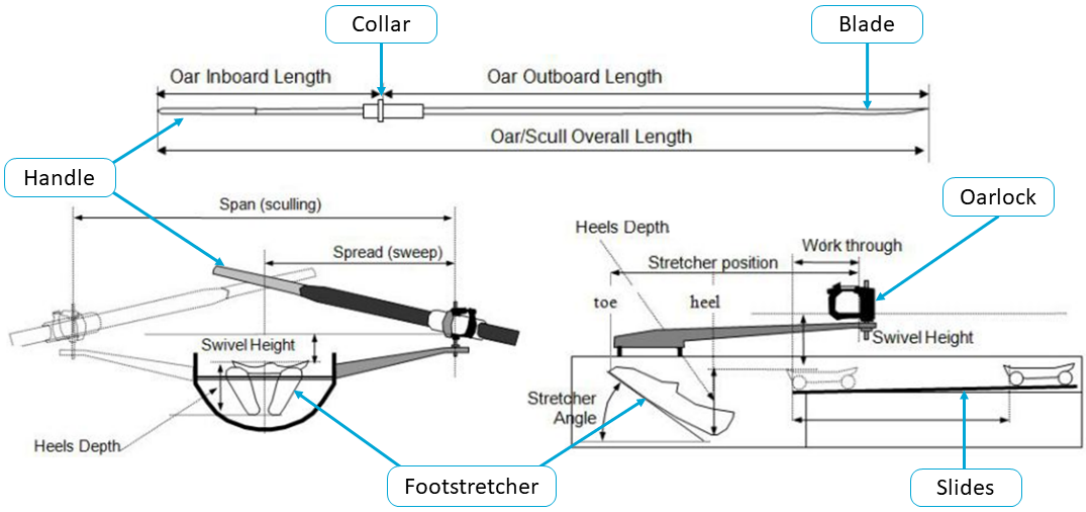

Figure 1.2: The set-up (adjustable parameters in the rigging) of the oar and the boat. (Figure adjusted from Gianchandani [21]).

Which class of rowing can be done with the boat is dependent on which type of riggers are mounted on the boat. Riggers are the metal (or carbon) frames that attach the oars to the boat, via an oarlock (or gate). The set-up (fig. 1.2) of the boat are adjustments that can be done, for example the position of the riggers, the pin or the length of the oars.

The total length of the oar is changeable, within a certain range. The inboard and outboard length of the oar can be changed independently, by changing the position of the collar. The type of oar shaft is also a factor to take into account, the thickness and stiffness of the shaft differ per brand and type. The blade characteristics can be chosen as well, the blade area and its shape can be altered. There are a few different shapes in blade form that are used in rowing (fig. 1.3), some claim to be better at the entry and others will go faster through the water.

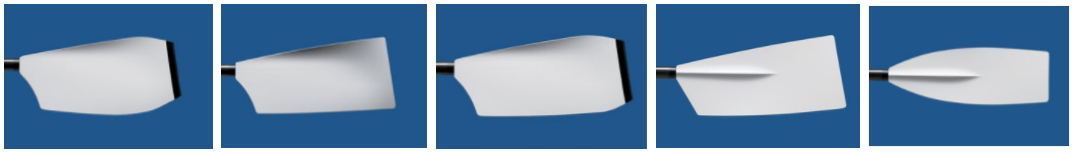

Figure 1.3: The different blade shapes of Concept2 [12]. From left to right: the Fat blade, Smoothie and Smoothie with vortex edge, Big blade and the Macon blade.

The span of the boat is the distance between the two pins on either side of the boat (when sculling). In sweep rowing this measure is called the spread and is measured from the pin to the middle of the boat. In combination with the inboard and outboard length of the oar the span or spread will determine the moment with which the force applied on the oar handle will be transferred to the water. The rower pushes against the footstretcher, an angled plate in the boat where the rowers shoes are attached to. The position and the angle of the footstretcher are adjustable to the rowers. Also the position of the slides can be adjusted, in both position and angle.

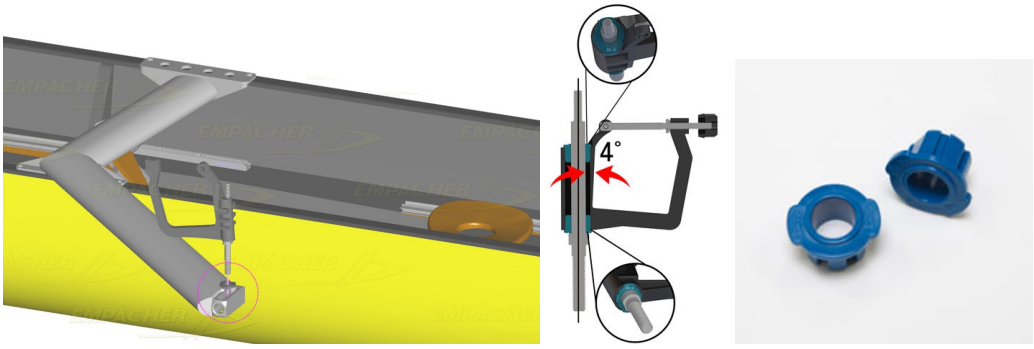

Figure 1.4: The sweep wing rigger of Empacher [18] (left). The oarlock is mounted on the rigger around a pin. In the middle figure is shown how the blue bushings determine the pitch angle of the oarlock, in this case 4°[13]. The right figure shows the bushing separately.

The oarlocks rotate around a pin which is fixed to the rigger. Due to bushings the pitch angle of the oarlock with respect to the pin can be adjusted. Assuming that the pin is perfectly perpendicular to the boat, the bushings do determine the angle of the blade with respect to the water. The height of the oarlock can also be adjusted.

1.2. Rowing stroke

Technique is an important factor for the efficiency in rowing. Rowing technique describes the movement pattern of the rower and the application of the forces of the rower on the boat. The most optimal technique in rowing is still discussed, however the general movement pattern is the same [53].

Figure 1.5: Four phases of the movement of the rower. Catch (1), leg drive (2), back swing (3), finish (4). The drive is the movement from catch to finish position (left to right). The recovery is the movement from finish to the catch position (right to left).

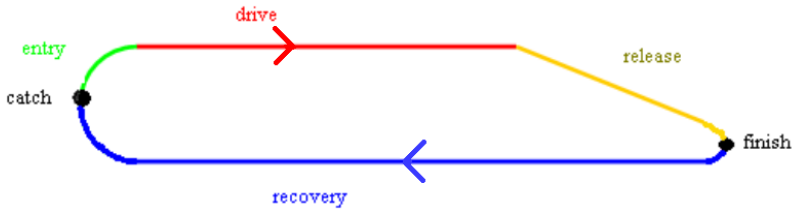

Figure 1.6: The handle path of the four phases in a rowing cycle, slightly adjusted from Coker [11]. The arrows show the direction in which the handle travels.

The rowing stroke is a cyclic movement that is roughly described by four phases; the entry, the drive, the release and the recovery, as shown in fig. 1.5 and fig. 1.6. In the catch position, the rower has moved the oar handle furthest towards the stern. The entry phase starts at the catch and is the vertical movement of the blade from the catch position until the blade is fully submerged in the water. The drive phase is the propulsive part of the stroke where the blade is moving from the catch to finish while in the water. The drive is roughly separated in three phases, the leg drive, back swing and arm pull. The release is the phase where the blade moves vertically from fully submerged to completely out of

the water. The finish is the furthest reach point of the oar handle towards the bow of the boat. The recovery phase is the non-propulsive phase of the stroke where the blade moves from the finish to the catch position and is not in the water. In the recovery phase the blades are feathered (turned parallel to the water).

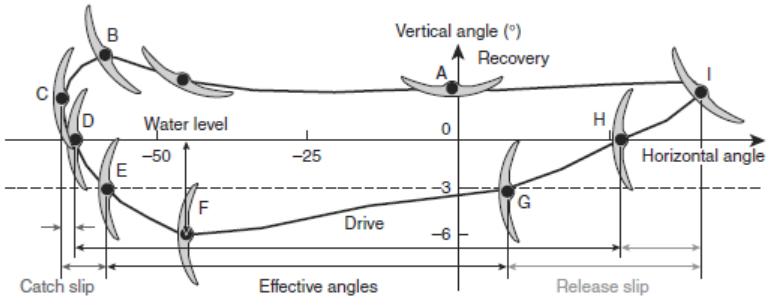

Figure 1.7: The movement of the blade with respect to the boat during one stroke from the side. The blade is feathered during the recovery and squared during the drive [31].

During the drive phase, the blade moves almost at the same speed as the boat, but not entirely. This leads to slip in both the catch and the finish. The catch slip occurs in the part of the entry when the blade is not completely submerged in the water, the release slip in the part of the release where the blade is not completely emerged from the water. In fig. 1.7 the movement of the blade with respect to the boat is shown, as well as a schematic representation of the catch and release slip. If there is no slip at all, the movement of the blade would be like the blue line in fig. 1.8b. Which describes the path of an oar blade without any load. The red line shows the locus of the ”normal” movement of a loaded blade through the water.

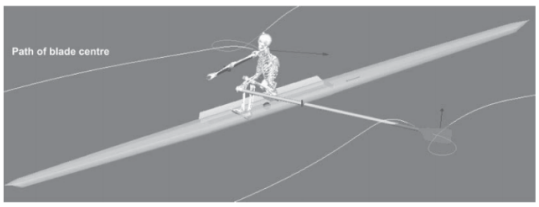

(a) A 3D simulation of the path of the blade center through the water by Serveto et al. [51].

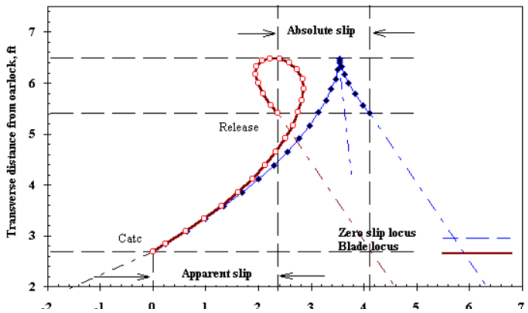

(b) The path of the blade through the water seen from above, simulated by Atkinson [3]. The blue line represents the blade simulated with no force, if drifts freely sternward. The red line is the normal blade locus.

Figure 1.8: The blade path through the water, in 3D and from above.

The periodical application of the propulsive forces makes the velocity of the boat fluctuate within the rowing cycle. And the movements of the crews' center of mass relative to the (lighter) boat cause extra velocity fluctuations. The power to overcome hydrodynamic drag is related to the velocity of the shell squared [15, 17, 31]. Reducing the surge velocity fluctuations will thus increase the efficiency.

1.3. Models

Modeling the rowing system is a challenging task because it involves many fields such as multibody dynamics, biomechanics, hydrodynamics and physiology. The difficulty arises from the fact that these fields are fully coupled. Good models and valid assumptions about the whole system and interactions are needed in order to simulate the system accurately. One of the most important coupling points is the one between the rower motion and the boat dynamics, because of the heavy oscillating masses of the rowers with respect to the light boat.

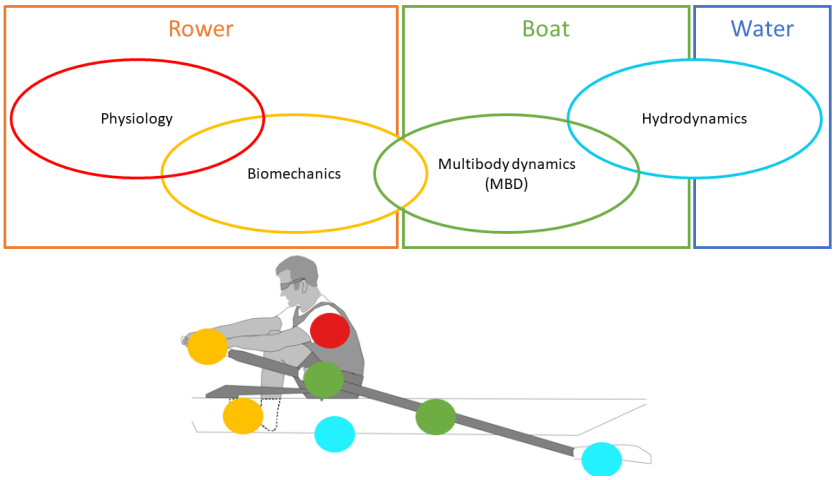

Figure 1.9: Overview of the different research fields in rowing that have been studied with models. Figure modified from [29].

Physiological models Physiological models of rowers are found in different sizes and with different purposes. Mathematical models are able to predict the rowing performance. For example they can predict race times, based on individual allometric data of the athletes [25, 37]. When interested in the movements of the rower, simulation models are an useful tool. How many and which body segments need to be used in a simulation is dependent on the focus of the study [14, 23, 51]. Also the choice in how to simulate the human joints differs per study and is dependent on the goal of the study. When muscle models are introduced [2], instead of direct joint torques, this will lead to a better estimate on the force development of the rower. These results are used to estimate pre-evaluate Functional electrical stimulation (FES) systems before applying FES in a training of a paraplegic on an ergometer.

Biomechanical models Alexander [1] made quite a complete basic model, but was presumably limited by the lack of data and computational power. In his footsteps many researchers created biomechanical models to analyze the forces and motions of the rowers. A five segment human body model is created by Caplan and Gardner [10], it is driven with kinematic data obtained from an ergometer. The five segments improved the simulation of the main features of the on-water data. However, the kinematic data from the ergometers differ from the kinematic data in the boat, as studied by Ritchie [47]. Cabrera et al. [8] also used the five segment model and found that oar slip proves to be necessary for accurately predicting the force generated at the oar handle. Cabrera's model is also used by Pettersson et al. [44] in which the movement pattern of the rower is optimized by minimizing a cost function with the hydrodynamic power losses and the control forces. Whether this optimized movement can be used as an example for the optimal stroke is debatable, because no activation dynamics are used. So far models have been able to reasonably reconstruct data measured in the boat, however improvements that can help the boats row faster is still limited. Due the fact that the individual (movement, force and physiological) capabilities of the rowers have not been taken into account.

Multibody dynamical models The dynamics of the system and its separate components are similar in all models; rower, oar and boat. However, the details of every component are modeled differently. The rower is often modeled between 1 and 5 body segments (see biomechanical models). The oar flexibility is sometimes introduced, but this might be unnecessary according to Cabrera et al. [8]. Hofmijster et al. [27] draw an opposing conclusion and say that oar flexibility is important in a model.

Multiple models study variable parameters in the boat. A bigger blade area leads to less blade losses [3, 39, 55]. The higher gearing of the inboard and outboard length of the oar also seems more optimal because a bigger outboard length leads to less blade slip losses [44, 55]. Although Ottenhoff [39] states that the trade-off between the blade losses and the reaction forces needed should be made. A higher gearing also leads to a lower stroke rate.

The recovery is a point of discussion as well, according to Atkinson [3] and van Holst [55] the speed during the recovery is not important for the average velocity of the boat, but Ritchie [47] states that the recovery is the phase where the technique is most important. Roosendaal [49] agrees but for the reason that the timing of the catch is very important and that this is easier done with a slower seat velocity in the end of the recovery. According to Ottenhoff [39] an early catch is beneficial, but van Holst [55] says that the catch angle should not pass 60° or the blade losses will increase.

It is hard to decide which studies give better results, because the assumptions made vary between studies. However it can be stated that the models that used real rowing measurements to validate their findings seem more credible.

Hydrodynamical models The hydrodynamic forces on the system can be separated in hull drag forces and blade forces. To calculate the drag forces on the hull, a geometric and physical similarity can be assumed for all rowing boats [35, 42]. The velocity fluctuations due to the movements of the rowers, do not change the drag coefficient very much, the coefficient is mainly dependent on the boat shape [7, 8]. The vertical and rotational movements of the boat should be included in calculating the drag force according to Formaggia et al. [19], Rongere et al. [48].

The blade forces are modeled by either using only the force perpendicular to the blade (normal force) or by decomposing the blade force in a lift and a drag component (drag in direction of fluid flow, lift perpendicular to drag). Cabrera et al. [8] argue that the second option is necessary to model the slip of the blade. Barré and Kobus [4] says that the propulsive force is overestimated in this approach, it is better that the simplified model of the normal force. Caplan and Gardner [9] study the shapes of the blades and the influences it has on the propulsion, an asymmetric blade shape (such as Big Blade) can increase the hydraulic efficiency.

It can be concluded that modelling in rowing has many challenges. When the model is too simplistic or it is not possible to quantify all variables, this reduces the accuracy of a model. The human factor must also be involved, which cannot be generalized too much, an individualized approach is even preferred. The difficult thing is to determine where to draw the borders of the model. Should a model include physiological parameters like the muscle activation, the control effort of the rowers, or even include the mental strength of the rowers?

Rowing races get won or lost by differences of centimeters at the finish, but the assumptions that have to be done in order to create a model, may neglect greater effects. Fortunately, an absolute accurate model is not needed to predict the effects of changes in the boat. With a sensitivity analysis, predictions can be made whether it is useful to investigate the influence of one parameter in an on-water experiment. Most models strive to predict the boat fluctuations as accurately as possible, while the true value of modelling may be the possibility to change parameters (even out of a currently used range) and see what effect it has on the boat performance.

Summary Chapter 1

There is a lot of terminology in rowing that is explained in this chapter. The rowing stroke is a periodic movement of the rower, the oar and the blade. The periodical application of the propulsive forces makes the velocity of the boat fluctuate within the rowing cycle. Also the movements of the crews' center of mass relative to the (lighter) boat cause extra velocity fluctuations. The power to overcome hydrodynamic drag is related to the velocity of the shell squared. Reducing the surge velocity fluctuations, which will increase the efficiency. The movement of the blade through the water at slightly different speed than the boat causes slip in the catch and finish. The current state of art rowing models are classified in different research fields. The human factor must be included in a model, but the borders of the model are hard to determine. A model does not necessarily have to be absolutely accurate, if it can predict a trend, it already has an added value. A more detailed study regarding rowing measurements and models can be found in the literature study preceding this thesis.

2

Data Acquisition & Processing

From a literature study [56] can be concluded that the main features interesting for this research are measurements of the boat and rower behavior. Measured on the boat are the following motions: distance, velocity and acceleration (three translational directions and three rotations). The boat movements in the moving direction are best measured with an impeller or an accurate and high frequency sampled GPS device. Other boat motions can be measured with a 3D-accelerometer.

The gate sensors that measure both gate force and oar angle give the most precise data on the forces and movements of the oar and are easy to use. From the gate force, the handle and blade force are derived. The individual movements of the rower are estimated based on the handle movements (oar angle) and seat position. However for a better prediction information is needed on the foot force, which is measured with an instrumented footplate.

The PowerLine Rowing Instrumentation and Telemetry measurement system [41] has the possibility to measure these variables and obtain a complete dataset of the forces and motions of the boat and rowers. This system is also chosen because of the convenience that the measurement system is in possession of the KNRB and complete datasets are available.

In this chapter information of the crew and rowing equipment from which the data is originated is given in section 2.1. The specific sensors used in this study are shown and explained in section 2.2. The data is processed into stroke based data in section 2.3, so that it can later be used as an input in the model. Section 2.4 goes one step further and combines the data in such a way, that it can describe an individual rower's behavior.

2.1. Rowing crew & rowing equipment

In this section, the features of the rowing boat, oars and crew are explained. The rowers are members of the KNRB and the data is gathered during their (practice) races.

M4x The original plan was to use measurements of a M4x with a crew that competed at international races. The dataset that is available contained measurements of gate force, oar angle and boat motions at race pace (±36 str/min). However, during the study it became clear that more data is needed. There were however complications with the installation of the footstretcher sensor in the quad. Therefore the choice is made to use the data of another boat type that is available.

LW2x From the LW2x data is available at different rowing paces (20, 24, 28, 32 and max str/min). In this dataset measurements foot force and seat position are also included. From the foot force data combined with oarlock force, the net force applied by each rower to the hull can be calculated. Unfortunately this dataset did not hold boat velocity data from the MiniMax or impeller. The velocity can only be based on the integration of the acceleration data of the boat of every timestep.

The crew of the LW2x consists of two lightweight female rowers. Both rowers weigh 59.0 kg, they are 20 years old and have an average length of 1.75 m (±3 cm). The boat that is used is a lightweight

women's double scull, with a length of 8 m and a mass of 27 kg. The oars that are used have a mass of 1.5 kg.

The athletes are rowing on a slightly lower level than the M4x (competing in World Championships under 23 years old). However due to the fact that the athletes have a more similar weight and height, the data may lead to interesting conclusions. The produced force-curves are alleged to be more similar than for athletes competing in the open weight class. Differences found between the rowers can be attributed to individualized patterns more than when rowers have bigger allometric differences.

The average race velocity that is added to the integral of the boat acceleration to calculate the boat speed can be derived from boat velocities of the same boat in rowing races. A fairly good finish time for a LW2x over 2000m is 7 minutes and 15 seconds, which would lead to an average speed of 4.6 m/s.

2.2. Sensors

The PowerLine system is used to perform measurements on the rowing system. It consists of several sensors connected to a network (fig. 2.1a). The sensors used in this study are the PowerLine oarlock (fig. 2.2a), the inertial measurement unit (IMU) (fig. A.1a), the footstretcher (fig. 2.3a) and the seat position sensor (fig. 2.4a). An impeller (fig. A.1a) can be added to the system as well, however during the measurements used in this study no impeller was present. With a logger (fig. 2.1b) the data of the sensors is recorded with a frequency of 50 Hz.

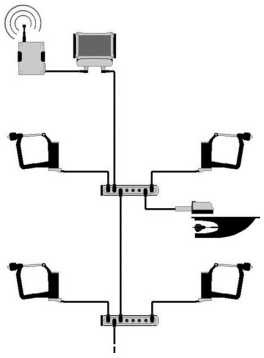

(a) The network of an installed PowerLine system consists of one logger and one IMU, also for each rower a junction box and oarlocks. To the network other PowerLine sensors can be added.

(b) The logger of the PowerLine system records the sensor values at a sample frequency of 50 Hz. It has several real-time functions, used as feedback in the boat. The logger has to be connected to the computer to read out the data, using the PowerLine software.

Figure 2.1: The network and logger of the PowerLine system [41].

The original way of the PowerLine system to measure the boat motions is to use an impeller with an IMU (fig. A.1a). The IMU measures the linear acceleration in three axes and yaw, pitch and roll angles. For the measurements to be accurate, the IMU should be placed horizontally on a flat surface. It must line up with the longitudinal axis of the boat. The impeller should be attached to the bottom of the hull, where it measures the speed of the water along the boat. In the measurements of the LW2x no impeller or other type or velocity sensor is used.

The measurement gate is placed over the "normal" pin as in fig. 1.4. The base of the sensor should be aligned towards the hull. The sensor is accurate to 2% full scale and can be overloaded 200%. In addition to forces, the oarlock can measure the gate angle and angular velocity as well, see fig. 2.2b. The gate angle is zero when the oar is perpendicular to the boat and the positive direction is towards the finish. The angle is measured with an accuracy of 0.5 °.

The foot force and seat position measurements are added to the measurements on the LW2x. During the project is discovered that to determine the motions of the rower, data on the applied foot force could be very useful. The seat position helps in estimating the motions of the rower, in particular the leg velocity. The foot and seat sensor used in this study are shown in respectively fig. 2.3 and fig. 2.4.

(a) The measurement oarlock of PowerLine [41]. This sensor belongs to the "standard" PowerLine measurement system.

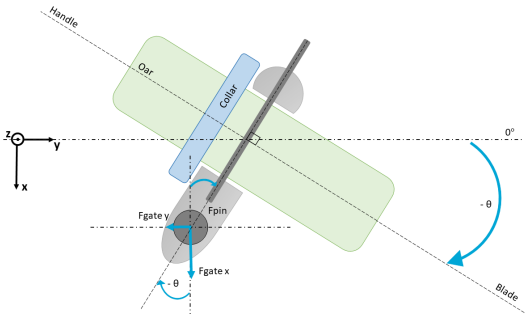

(b) A schematic picture of the gate sensor, showing the forces that are measured ($F_{gate,X}$ & $F_{gate,Y}$). The oarlock also measures the gate angle (θ).

Figure 2.2: The measurement oarlock measures the forces between the oarlock and the pin in x- and y-direction. The sensor is accurate to 2% full scale and can be overloaded 200%. In addition to forces, the oarlock measures the gate angle as well. The gate angle is zero when the oar is perpendicular to the boat and the positive direction is towards the finish. The angle is measured with an accuracy of 0.5 °.

(a) The foot stretcher force sensor of the PowerLine system [41].

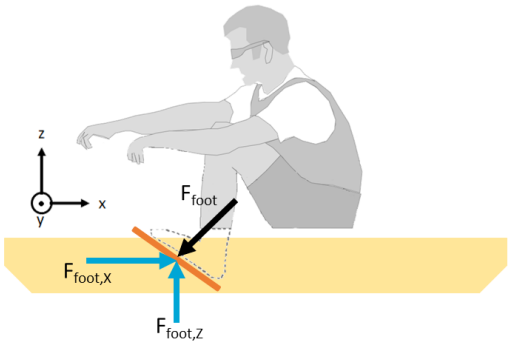

(b) A schematic picture of the foot force sensor, showing the forces that are measured ($F_{foot,X}$ & $F_{foot,Z}$).

Figure 2.3: The footstretcher sensor is added to the "standard" PowerLine measurement system (fig. 2.1a). The output from the sensor is the force in x- and z- direction. Other sensor outputs that are not used are: a ratio between the force distribution on the footstretcher between the left and right foot and between the top and bottom of the footstretcher.

(a) The seat position sensor of the PowerLine system [41].

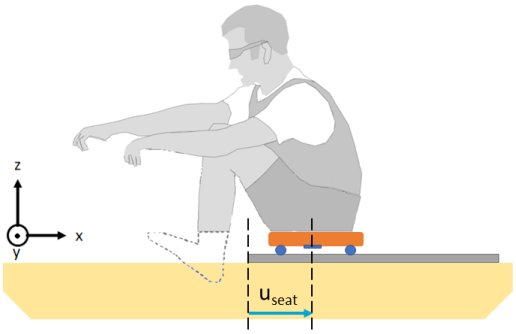

(b) A schematic picture of the seat position sensor, showing the distance that is measured (u_{seat}).

Figure 2.4: The seat position sensor is added to the "standard" PowerLine measurement system (fig. 2.1a). A sensor is connected to the bottom of the sliding seat of the rower and an extra rail is taped to the deck of the boat.

2.3. Raw data and averaged data per stroke

The data obtained with the PowerLine sensors, consists of large files over the complete time of the race. First relevant rowing segments are selected. In these segments a constant pace and boat speed is needed to make sure that the strokes within the segment can be compared to each other. In the dataset obtained from the KNRB of the LW2x, the practice race is cut into segments of the same rowing pace; 20 , 24, 28, 32 and max str/min. Each segment lasts roughly 40 seconds which holds between 14 and 21 strokes. For most of the calculations the race segment of pace 32 str/min is used, because it holds the most strokes and this is a good approximation of the race pace.

Raw data The force measurements coming from the PowerLine system are measured in [kgf] and the seat position and velocity in respectively [mm] and [mm/s]. The data is first converted to SI units. In fig. 2.5, the raw data obtained from the gate sensors is shown in SI units. In the appendix A (fig. A.3, fig. A.4 and fig. A.2) the raw data from the other sensors is shown.

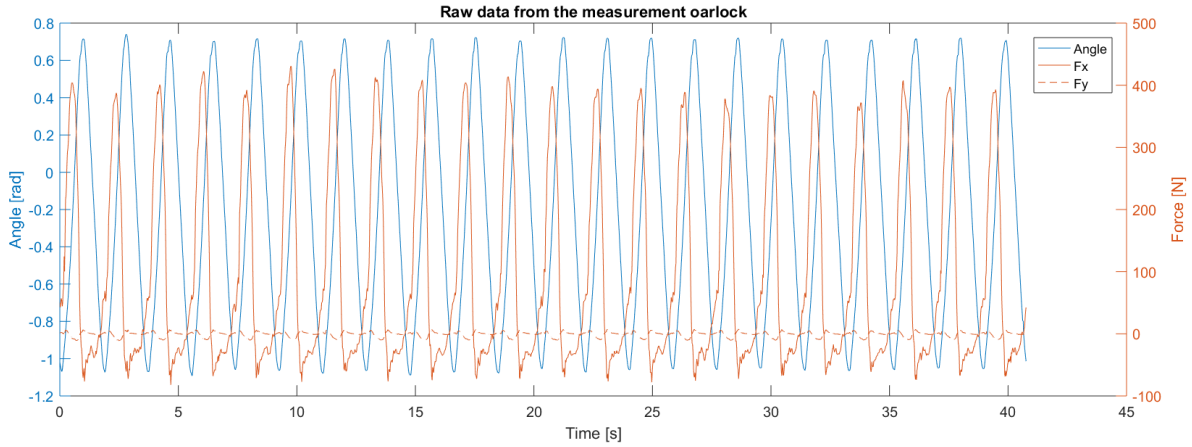

Figure 2.5: Raw data of the gate force in x- and y-direction and the gate angle, obtained with the Portside PowerLine oarlock from a LW2x at pace 32 str/min, for a period of ±40 seconds (21 strokes).

Filtering To improve the peak identification and the identification of the catch and finish in the stroke, the oar angle data is filtered. This is done to reduce the sensor noise on the signal and obtain a smooth gate angle, so that the catches that are found are unique points. A fourth order Butterworth filter is selected with a cutoff frequency of 5 Hz. In tests, there is found that for a smaller cutoff frequency, the minimum and maximum values of the oar angle change a lot.

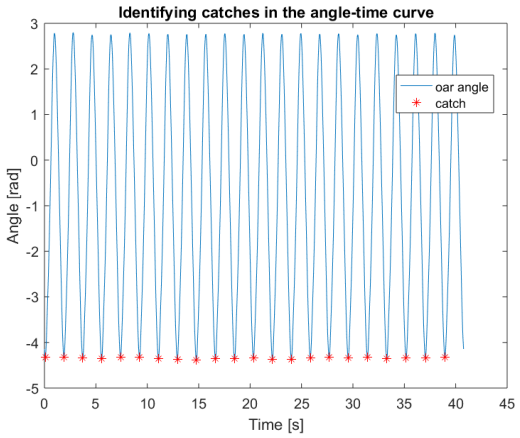

Figure 2.6: The identification of the catch of each stroke, based on filtered oar angle.

Average data per stroke To compare the data of different rowers and for different rowing intervals, the data is averaged per stroke. First the data has to be cut into segments of one stroke each. The beginning of the stroke is defined in the catch. The catch is identified as the minimal oar angle (fig. 2.6). After the signal is cut into strokes, these strokes are averaged. Taking the average is not straightforward, because not every stroke has exactly the same amount of measurement points. First all the stroke vectors are interpolated into vectors of the same length. Then for every data point in the stroke the average is taken over all strokes. In case of the gate measurements (gate angle and gate force), the port side gate and starboard side gate measurements should be averaged, since a symmetrical movement is assumed for all rowers. The averaged data is shown in fig. 2.7 and fig. 2.8. The vertical line in the figures shows the point of the average finish in the averaged stroke. This means that the part to the left of the "finish-line" is the drive phase and right of the line is the recovery.

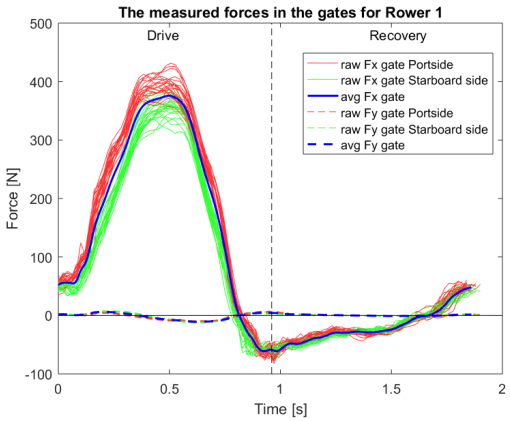

(a) The measured gate forces on portside and starboard side and their average in x- and y-direction for rower 1.

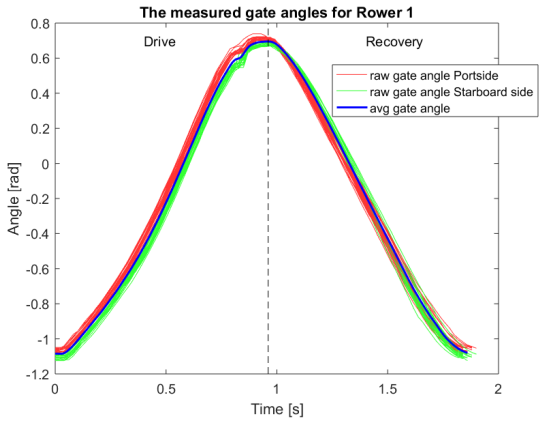

(b) The measured and average gate angles on portside and starboard side in x- and y-direction for rower 1.

Figure 2.7: Raw and average data per stroke obtained with the PowerLine oarlocks at a pace of 32 str/min. The vertical striped line in the middle of the graphs is the "finish-line", left of this line is the drive phase of the rowing stroke and at the right hand side of the line is the recovery.

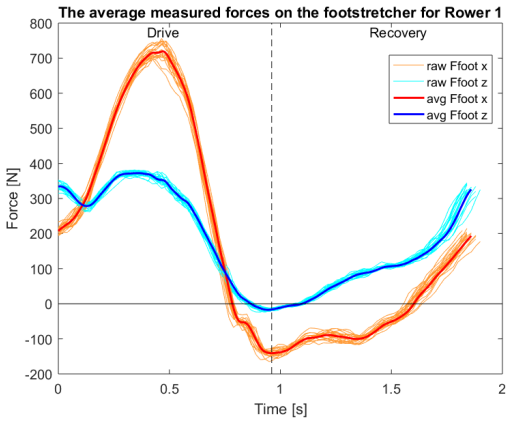

(a) The measured and average foot forces in x- and z-direction, of rower 1.

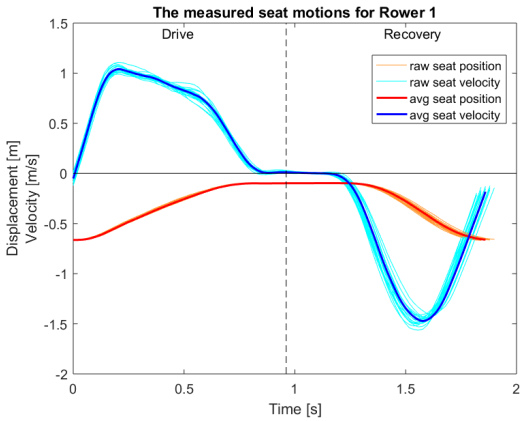

(b) The measured and average seat position and velocity of rower 1.

Figure 2.8: Raw and average data per stroke obtained with the PowerLine foot force and seat position sensor for rower 1 at a pace of 32 str/min.

2.4. Identifying biomechanical fingerprints

After preparing the average data curves per stroke for every rower, the curves are compared. From the averaged strokes some personal features of the curve per rower can be conducted. For example, the peak of the gate and foot force of rower 1 is quicker reached than for rower 2 (fig. 2.9).

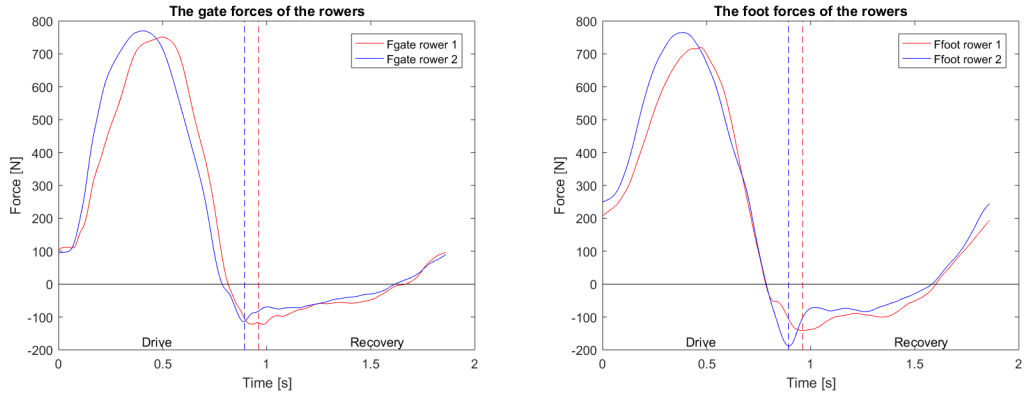

Figure 2.9: The averaged gate (left) and foot (right) forces in x-direction of rower 1 and 2.

Different studies found that experienced rowers produce a characteristic individually shaped force time pattern [26, 28, 30, 60]. This is also found in practice by Eelco Meenhorst (KNRB). To find a good fit of rowers for a crew boat is challenging, because the ability to adapt one rower's technique to others in a crew, differs per person. Currently, subjective and qualitative measures are the main methods used to select the fastest crew. Gravenhorst et al. [22] used a data-driven approach to select the most relevant features that make the rower's technique unique. They found that the "finish slip" is the most discriminative feature for the identification of a rower. However, to run a model based on individual rower characteristics, defining only the finish slip is not enough. Therefore another way to define the unique rower behavior through the whole stroke should be investigated.

Normalized force-angle curves rowers

One approach is to create an averaged force-angle curve for the rowers, that is normalized over a constant angle segment. The meaning of the stroke angle segment is shown in fig. 2.10a. The length of the drive of a stroke of the rower is calculated as the total angle covered from the catch to the finish, the minimum and maximum oar angle. This is done as well for the recovery phase. For all strokes, the segment of the drive and recovery is calculated. The average segments of the drive and recovery are calculated for one rower.

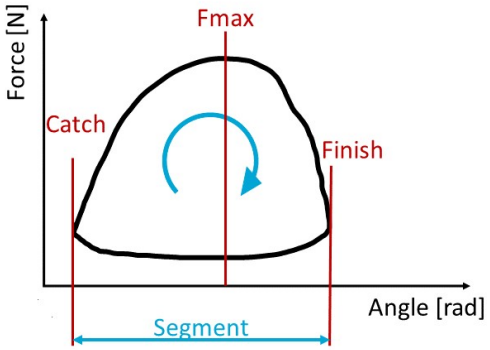

(a) Graphical representation of the segment of a rowing stroke in the force-angle curve. The cyan arrow in the curve indicates the direction of the stroke.

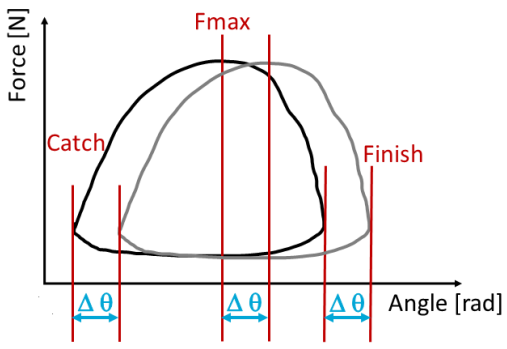

(b) Graphical representation of the assumption that stroke shifted with an angle $\Delta\theta$ will hold the same shape.

Figure 2.10: The stroke angle segment and shifted force-angle stroke with constant segment.

Next, the (average of starboard side and portside gate) force-time of all strokes is split in drive

and recovery. Such that the force-angle curve of the drive and the force-angle curve of the recovery can be determined per stroke (with the constant stroke angle segment). This data is interpolated over the length of the average segment of the drive and recovery respectively. For the interpolation an unique dataset is required. This is done for all the strokes in the dataset. These normalized strokes are averaged between themselves, so that one averaged normalized force-angle curve is made for every rower (drive and recovery), shown in fig. 2.11.

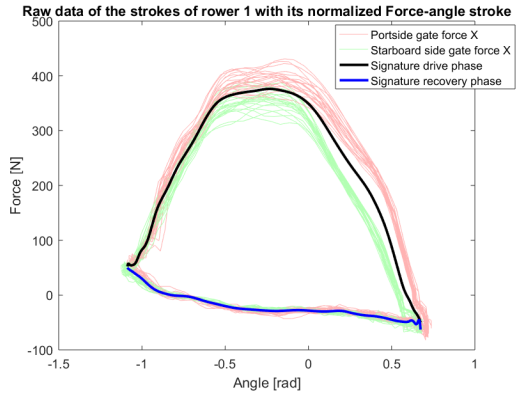

(a) The normalized gate force-angle curve of rower 1 with raw data.

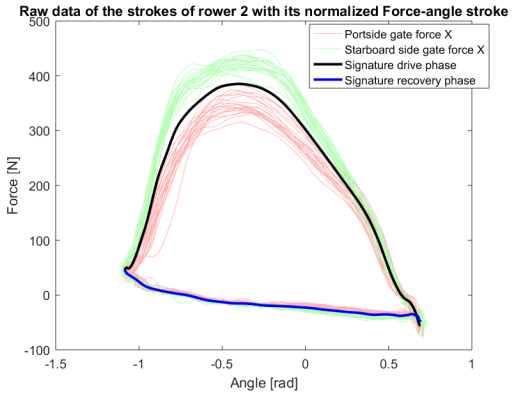

(b) The normalized gate force-angle curve of rower 2 with raw data.

Figure 2.11: The raw data of the gate force-angle curves of rower 1 and 2 and the averaged and normalized strokes obtained from this data; the signature drive and recovery phase. The data comes from a practice race at a pace of 32 str/min.

The resulting normalized average force-angle curve is plotted for different paces of a rowing (practice) race in fig. 2.12a. It appears that the shape of the force angle curve is roughly similar for different paces of rowing. This means that the rower generates the same force per angle under different circumstances.

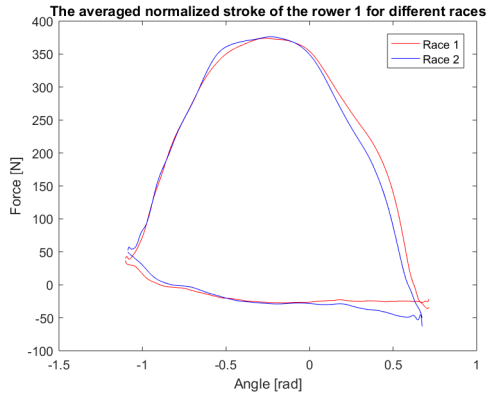

(a) Normalized averaged gate force-angle curves for rower 1 at a pace of 24 str/min (Race 1) and at a pace of 32 str/min (Race 2).

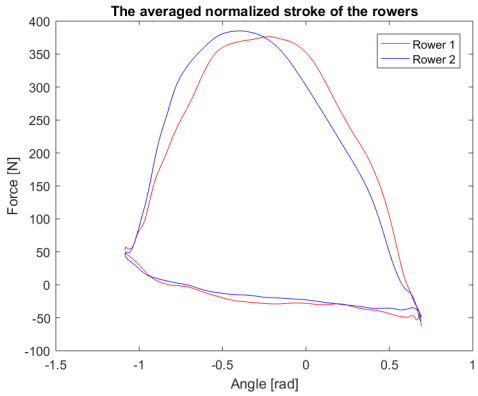

(b) Normalized averaged force-angle curve of a stroke for rower 1 and 2 at a pace of 32 str/min compared.

Figure 2.12: Comparison of the average normalized gate force-angle curves of one rower for different races and between rowers. The shape of the normalized force-angle do not differ much within a rower, but they do differ between different rowers.

If the average normalized force-angle curves of all rowers in a boat are plotted (fig. 2.12b), difference in shape between the force-angle curve of the rowers are found. This is also done for the rowers of a M4x, which show even more differences in shape (fig. A.5). These graphs give a strong indication that these curves can be used as a signature curve of a rower.

Segment based on CoM displacement

When the rigging properties change, it is not proven that the force-angle curve remains the same. Especially when the position of the footstretcher with respect to the gate changes, the catch angle will change and there is a suspicion that the force distribution over the shifted angle will change. It would be unexpected if the rower would not be influenced by the different angles of the handles, in applying her force. So the assumption shown in fig. 2.10b is not proven.

To overcome this uncertainty, the constant segment can be based on the center of mass displacement of the rower (fig. 2.13). Then the force distribution over the segment is not dependent on the rigging of the boat. A change in x-position of the rower would lead to the same force distribution on the handle and the footstretcher, as long as the movement of the rower is not limited by other factors. To create a force-u_{com} curve, the relative motions of the rower with respect to the boat have to be calculated. This is why a model is build.

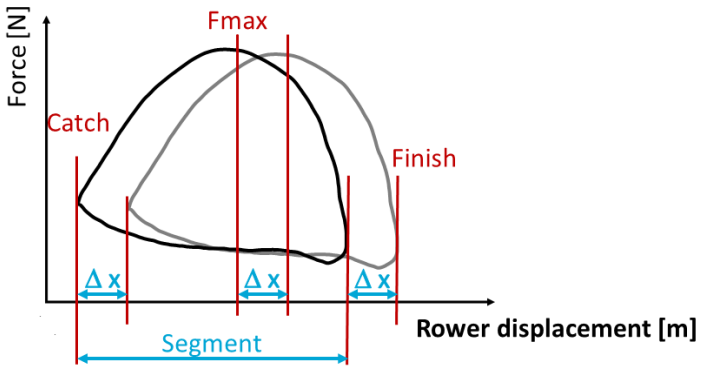

Figure 2.13: Graphical representation of the segment of a rowing stroke in the force-u_{CoM} curve.

Summary Chapter 2

The data in this study comes from a LW2x, the rowers of which are members of the KNRB. The sensors used are the measurement oarlock, foot stretcher force sensor, seat position sensor and the boat acceleration sensor (IMU) of the PowerLine measurement system. The raw data is cut into strokes, beginning at the catch (minimal oar angle), averaged and combined into one stroke. The data of the port side and starboard side gates is averaged, since a symmetric movement is assumed.

In the stroke based data differences between rowers are found. The data is used to create a normalized force-angle curve for every rower, based on the assumption that the angle segment of the rower is constant for rowing at different paces or in different races. Clear differences are found between the normalized force-angle curves of the rowers. A constant angle segment of a rower may alter when the rigging parameters are changed. Therefore a segment has to be found that is constant despite rigging changes: the relative displacement of the rower. In order to predict the relative displacement of the rower, a model has to be created modeling rower and boat movements.

3

The mechanical rowing model: Free body diagrams

In the free body diagrams (FBD's) the principal forces acting on an object are demonstrated. The FBD's are needed to compose the linear and angular momentum balances of an object. In this chapter the free body diagrams of the rowing system and its different parts are presented. The parts of the rowing system are the rower, the oar and the boat. The calculations of the forces in the free body diagrams are discussed as well as the assumptions whether some factors may be neglected. In chapter 4 the equations are used to model the motions of the different parts of the rowing system. The linear and angular momentum balances of an object are drafted as in the following equations.

$$\sum F_x = m \cdot \ddot{x} \qquad \sum M = I \cdot \ddot{\phi}$$

The momentum balances are needed to determine the equations of motion of the different parts in the rowing system through the rowing stroke. In this chapter, the momentum balances for the total system and for the rower, oar and boat separately are discussed.

3.1. Total system

The equation of motion for the averaged mass of the total is derived from the free body diagram of the system fig. 3.1. The whole system has a lot of forces acting on it. To simplify, a big border is drawn around the system and only the external forces on the system remain.

$$\sum F_x = F_{m,system} = m_{system} \cdot \ddot{x}_{system} = F_{blades,X} - F_{drag} \tag{3.1}$$

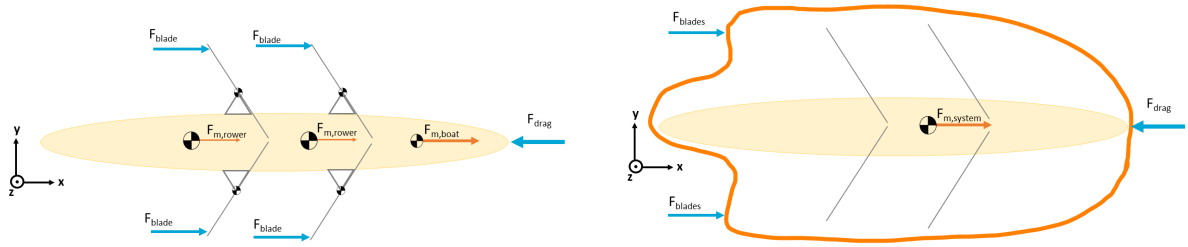

(a) A free body diagram of the complete rowing system. (b) A reduced FBD of the system.

Figure 3.1: Free body diagrams of the system on different scales,. From the reduced FBD, eq. (3.1) is derived.

3.2. Rower

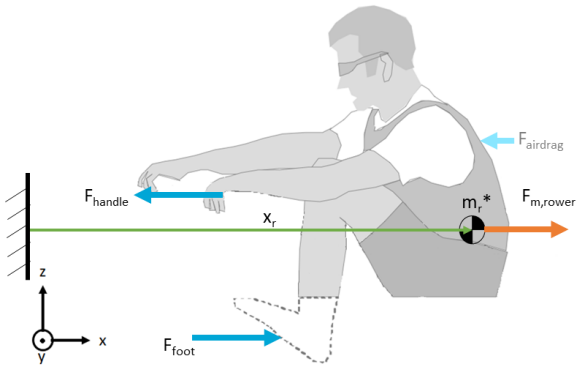

Figure 3.2: The free body diagram of the rower. Showing the external forces on the rower, F_{handle} and F_{foot} and the coordinate definition of x_r. Figure adjusted from In Motion Software & Sports Technology [29].

For the rower, the linear momentum balance in x-direction is shown in eq. (3.2).

$$\sum F_x = F_{m,rower} = m_{rower} \cdot \ddot{x}_{rower} = F_{foot,X} - F_{handle,X} - F_{airdrag} \tag{3.2}$$

$F_{handle,X}$ is the component of the handle force in x-direction and $F_{foot,X}$ of the foot force. The rower also applies a force on the handle in y-direction $F_{handle,Y}$ and a force on the footstretcher in z-direction $F_{foot,Z}$. Both of these forces are neglected, because they will not influence rower movements in the x-direction and that is the only direction modeled in this thesis.

m_{rower} is the rower's mass and x_{rower} the rower's center of mass position relative to the world ($\ddot{x}_{rower}$ is the second derivative of x_{rower}). The air drag on the rower $F_{airdrag}$ is often neglected. In the next section is calculated whether this is a valid assumption for this model.

3.2.1. Air drag on rower

In many models, the air drag force on the rower is not taken into account. In other sports the opposite is true and air drag is reduced as much as possible. In cycling and ice skating for example, is seen that trailing behind another athlete reduces the air drag on an athlete and thereby reduces the effort that the athlete has to provide to reach the same speed. However, all rowers in a boat work on the same boat speed. Thus the only thing that can be concluded is that the rowers should move straight through the boat in order to create less air drag force on the system.

$$F_D = \frac{1}{2}\rho C_{D,rower} A v^2 \tag{3.3}$$

To calculate the air drag on every rower separately, a simplified drag function is used, shown in eq. (3.3). ρ is the air density, $C_{D,rower}$ is the drag coefficient, A is the frontal area and v is the velocity of the object. The air density is taken for a temperature of 15 °C; 1.225 $\frac{kg}{m^3}$. The frontal area A is determined based on the torso (the width of the trunk times the height of the shoulders with respect to the seat). The drag force coefficient is more difficult to determine, in literature often a combined factor drag area $C_{D,rower}A$ is used, this is the product of the frontal area and drag coefficient and relates the drag force to the dynamic pressure ($\frac{1}{2}\rho v^2$). The drag area is typical for an athlete in a certain position. For racing cyclists the drag area lies around 0.35 m^2 [16, 43, 54, 59]. Expected is that for a rower the drag should be a little smaller. For a trunk width of 0.4 m and a shoulder height of 0.55 m, the frontal area of a rower is estimated at 0.22 m^2. A drag coefficient ($C_{D,rower}$) of 0.9 [54] is a conservative guess, a sitting person probably has a drag factor around 0.6. The drag coefficient of 0.9 would lead to a drag area of 0.2 m^2 which is of the same order of magnitude as that of the cyclist, but may expected to be slightly smaller.

Also the rowers in one boat do not experience the same drag force, because they are sitting behind each other. In cycling, research has been done to determine the drag force reduction when cyclists

ride behind each other [6]. Since the distance between the bodies of the cyclists and the bodies of the rowers in a boat is comparable, the results of this research are translated in reduction percentages for rowers in a quad and double as well. Of course these percentage are still a bit dependent on the specific size of the rower in front of another rower, but they present a general idea.

Seat	Reduction
Bow rower	3 %
Stroke rower	14 %

Table 3.1: Reduction percentages of air drag force on the positions in a rowing boat, deduced from a study on two cyclists riding behind each other [6].

The absolute velocity of the rower is composed of the boat velocity and her relative velocity with respect to the boat. The air drag forces on the rowers calculated with the absolute velocity are shown in fig. 3.3. For the absolute velocity of the rowers, the boat velocity and seat velocity are added. The seat velocity is an estimate of the rowers relative velocity (section 4.2.2), but for the estimation of the drag force it is accurate enough.

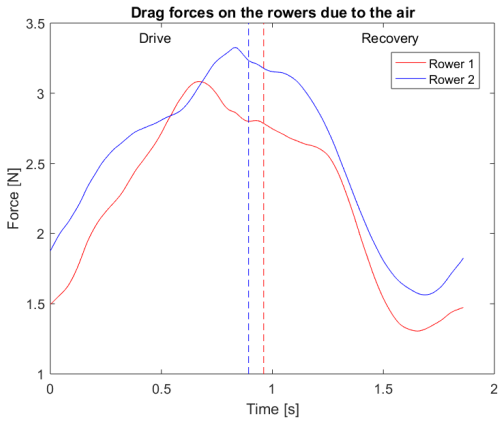

(a) The air drag forces on the rowers, using the absolute velocity of the rowers based on u_{seat} and measured boat speed, ρ is 1.225 $\frac{kg}{m^3}$ and C_D is 0.9.

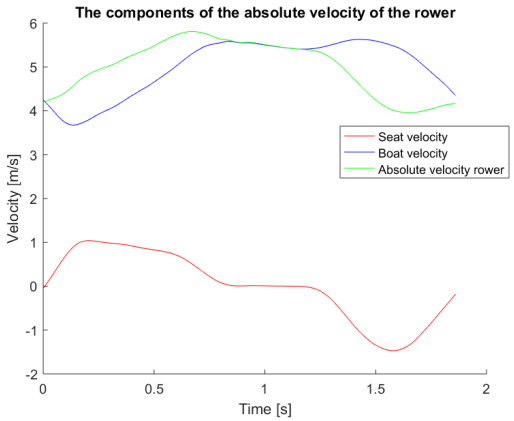

(b) The different components from where the absolute velocity of one rower is calculated; the boat velocity and seat velocity.

Figure 3.3: Air drag forces on the rowers and the absolute velocity of a rower.

As shown in fig. 3.3a, the bow rower (2) does encounter more drag force than the stroke rower, due to the reduction percentages as given in table 3.1. The magnitude of the air drag forces that are calculated is of a smaller scale than the other forces that act on the rower ($F_{handle} \approx 500$ N and $F_{foot} \approx 700$ N). Therefore in further calculations on the force balance of the rower (eq. (3.2)), the air drag force is neglected.

3.3. Oar

It is important to describe the momentum balances around the oar accurately, because the oar is connecting the rower to the boat and the boat to the water. The measurements are done at the oarlock (gate). Therefore in this section the force calculations in the gate are discussed first. The linear and angular momentum balances of the oar are presented and the blade forces will be investigated.

3.3.1. Oarlock

The forces on the gate are measured in the longitudinal direction of the boat ($F_{gate,X}$) and perpendicular to the boat ($F_{gate,Y}$). The oar angle is defined as the angle in the xy-plane and is zero when the oar is exactly perpendicular to the boat. The direction rotation is positive during the drive phase of the stroke (this means a negative angle in the catch and positive angle in the finish position). The measured variables are shown in fig. 3.4 with the cyan arrows.

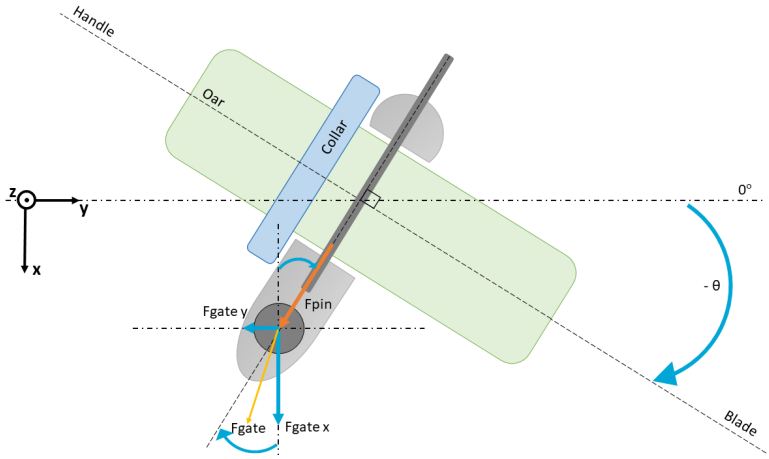

Figure 3.4: The forces that are measured with the PowerLine gate are the $F_{gate,X}$ and $F_{gate,Y}$ (cyan arrows). The oar angle θ can also be measured by the measurement gate. F_{gate} is the sum of the forces measured in the gate in x- and y-direction, F_{pin} is the force from the oar perpendicular to the oar.

$$F_{gate} = \sqrt{F_{gate,X}^2 + F_{gate,Y}^2} \tag{3.4}$$

$$F_{gate,v} = F_{pin} = F_{gate,X} \cdot \cos(\theta) + F_{gate,Y} \cdot \sin(\theta) \tag{3.5}$$

F_{gate} is the sum of the forces measured in the gate in x- and y-direction. This force also includes the force in longitudinal direction of the oar. However this force does not have an influence on the propulsive forces on the oar and the boat and has to be corrected for. F_{pin} is the force from the gate perpendicular on the oar.

3.3.2. Oar

The oar works like a lever between the blade and the handle. Via force on the pin, the boat is moved forward. The free body diagram of the oar with forces and lever arms is shown in fig. 3.6.

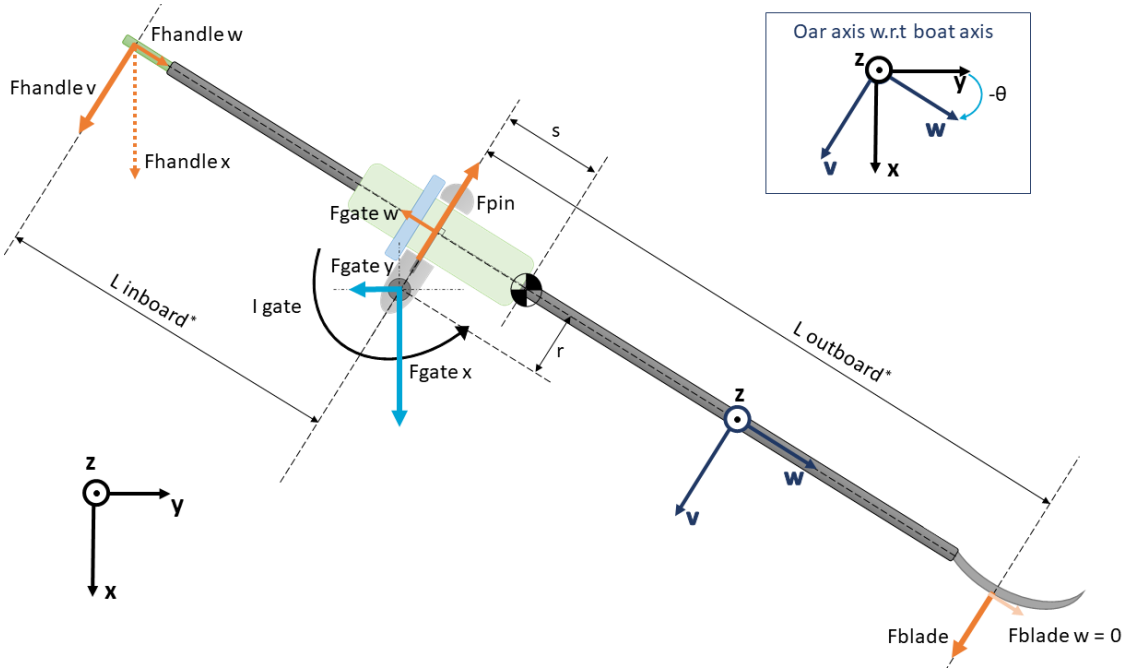

Figure 3.5: The free body diagram of the oar, with the defined lengths of the in- and outboard. The relative axial system of the oar is defined with w in longitudinal direction of the oar, and v perpendicular to the oar. The axial system is shifted with θ from the axial system of the boat. Length r and s are assumed to be zero, so that the center of mass of the oar lies in the gate, and the oar rotates exactly around it's center of mass. The axial force at the blade is also assumed zero, because there is no practical way to measure it.

From the free body diagram the following formulas are derived.

$$\sum F_v = m_{oar} \cdot \ddot{v}_{oar} = F_{pin} - F_{blade} - F_{handle,v} \tag{3.6}$$

$$\sum F_w = m_{oar} \cdot \ddot{w}_{oar} = F_{handle,w} - F_{gate,w} \tag{3.7}$$

$$\sum M_{gate} = I_{gate} \cdot \ddot{\theta} = F_{handle,v} \cdot {l_{inboard}}^* - F_{blade} \cdot {l_{outboard}}^* - m_{oar}(s \cdot \ddot{v}_{oar} + r \cdot \ddot{w}_{oar}) \tag{3.8}$$

$$F_{handle,v} = \frac{F_{pin} \cdot {l_{outboard}}^* + I_{gate} \cdot \ddot{\theta} + m_{oar} \cdot \ddot{v}_{oar}(s - {l_{outboard}}^*) + m_{oar} \cdot \ddot{w}_{oar} \cdot r}{{l_{outboard}}^* + {l_{inboard}}^*} \tag{3.9}$$

$$F_{handle,w} = F_{gate,w} + m_{oar} \cdot \ddot{w}_{oar} \tag{3.10}$$

$$F_{blade} = \frac{F_{pin} \cdot {l_{inboard}}^* - I_{gate} \cdot \ddot{\theta} - m_{oar} \cdot \ddot{v}_{oar}({l_{inboard}}^* + s) - m_{oar} \cdot \ddot{w}_{oar} \cdot r}{{l_{outboard}}^* + {l_{inboard}}^*} \tag{3.11}$$

$$F_{handle,x} = F_{handle,v} \cdot \cos(\theta) + F_{handle,w} \cdot \sin(\theta) \tag{3.12}$$

In all following calculations it is assumed that the center of mass of the oar lies in the gate and that the distance between the pin and the middle of the oar is negligible. Thus distance r and s are assumed to be zero. The effect of s on the handle force is shown in appendix A.4. This results in $\ddot{v}_{oar}(t) = \ddot{x}_{oar}(t) \cdot \cos(\theta(t))$ and $\ddot{w}_{oar}(t) = \ddot{x}_{oar}(t) \cdot \sin(\theta(t))$, where $\ddot{x}_{oar}$ is equal to the boat acceleration. The effect of the oar acceleration on the calculated handle forces is shown in appendix A.4. For the force balances, the variables of the oar are calculated according to eq. (3.13 & 3.14). In eq. (3.15) the rotational inertia of the oar is calculated as if the oar would be a perfect rod. The influence of the oar inertia on the handle force is really small (appendix A.4), thus a more precise estimate is not necessary.

$$l_{oar} = l_{inboard} + l_{outboard}$$

$$l_{inboard}^{*} = l_{inboard} - l_{handle\ center} \quad (3.13)$$

$$l_{outboard}^{*} = l_{outboard} - l_{blade\ center} \quad (3.14)$$

$$I_{gate} = \frac{m_{oar} \cdot l_{oar}^{2}}{12} + m_{oar} \cdot s^2 - m_{oar} \cdot r^2 \quad (3.15)$$

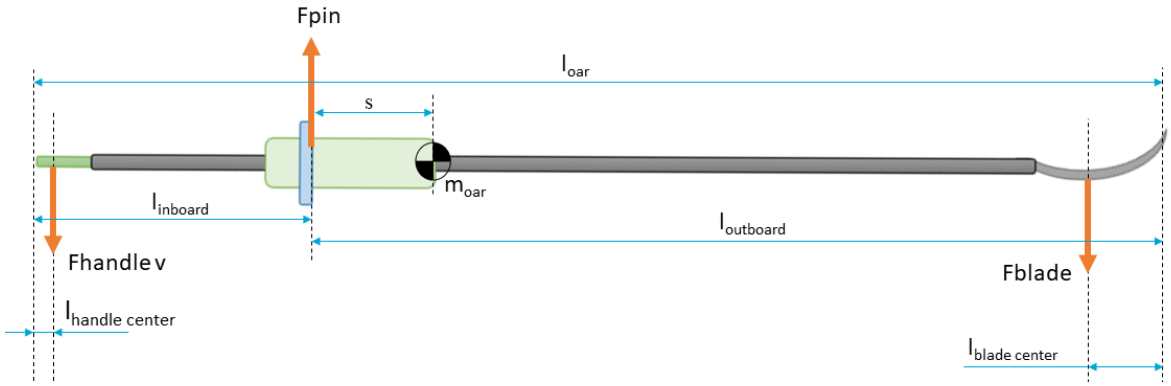

Figure 3.6: The oar with the definition of different lengths. The lever arms $l_{inboard}^{*}$ and $l_{outboard}^{*}$ are calculated according to eq. (3.13 & 3.14).

The oar properties that are used in eq. (3.13, 3.14 & 3.15) are shown in table 3.2.

Parameter	Value	Description
l_{oar}	2.88 m	The length of the oar.
$l_{inboard}$	0.88 m	The inboard length of the oar.
$l_{outboard}$	2.00 m	The outboard length of the oar.
$l_{handle\ center}$	0.04 m	The distance from the tip of the handle to the handle center.
$l_{blade\ center}$	0.225 m	The distance from the tip of the blade to the center.
s	0 m	The distance from the collar to the oar CoM.
r	0 m	The distance from the pin to the midline of the oar.
m_{oar}	1.5 kg	The mass of the oar.
I_{gate}	1.0368 kgm^2	The moment of inertia of the oar around the gate.

Table 3.2: The oar properties, with their value and description.

Oar deformation There has been a debate whether introducing oar flexibility would improve the quality of a model. Although it is more realistic, it is hard to implement the oar deformation. Cabrera et al. [8] state that oar flexibility does not improve the quality of their model fit. However, Hofmijster et al. [27] have done a detailed analysis on incorporating the oar deformation in the reconstruction of blade kinematics. They found that the oar deformation had an effect on the power losses at the blade ($P_{blade} = F_{drag} \cdot \dot{v}_{blade}$). When taking the average over the whole stroke the power loss at the blade is not affected.

For practical reasons (it is not measured) is chosen not to implement oar flexibility in the model used in this thesis. In the analysis of the results, there should be a critical view on the neglected effect.

3.3.3. Blade

In modeling the blade force, there are roughly two approaches that are used; only using the force perpendicular to the oar or separating the blade force in two components (lift and drag). The blade model of Pope [45] assumes that only the blade force perpendicular ($\vec{v}$-direction) to the blade is propulsive. The blade force is calculated as in eq. (3.16). C_2 is the blade force coefficient, calculated by

$C_2 = \frac{1}{2}\rho C' A'$, where A' is the area of the face of the oar blade and C' is a shape-determined constant.

$$F_{blade} = C_2(\dot{x}_{blade} \cdot \vec{v})^2 = C_2 \cdot \dot{v}_{blade}^2 \tag{3.16}$$

$$\dot{v}_{blade} = l_{outboard} \cdot \dot{\theta} + \dot{x}_{boat}\cos(\theta) \tag{3.17}$$

When C_2 is known, a validation of the blade force according to eq. (3.11) is done. This parameter however is dependent on the blade shape C' which is unknown.

Cabrera et al. [8] discovered that including the lift forces in addition to the drag forces in the calculation of the blade forces is important to determine the slip of the blade (explained in chapter 1). The lift and drag forces are calculated as in eq. (3.18 & 3.19). The lift and drag coefficients C_L and C_D are functions of the angle of attack ϕ. ϕ is the angle between the blade velocity relative to the fluid and the longitudinal axis of the oar ($\vec{w}$).

$$F_{lift} = C_L|\dot{x}_{blade}|^2 = C_L{}^{max}\sin(2\phi)|\dot{x}_{blade}|^2 \tag{3.18}$$

$$F_{drag} = C_D|\dot{x}_{blade}|^2 = C_L{}^{max}(1-\cos(2\phi))|\dot{x}_{blade}|^2 \tag{3.19}$$

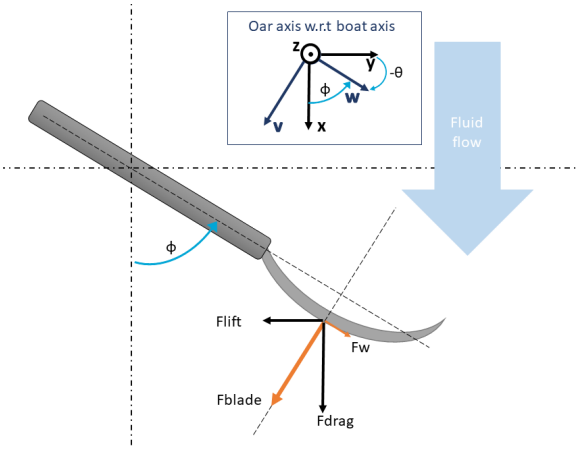

(a) The forces on the blade, the resultant fluid force (F_{drag}) on the oar blade is broken up into lift and drag force. The angle of attack, ϕ, is the angle between $\dot{x}_{blade}$ and the longitudinal axis of the oar ($\vec{w}$). Fw is the force in the longitudinal direction of the oar (neglected).

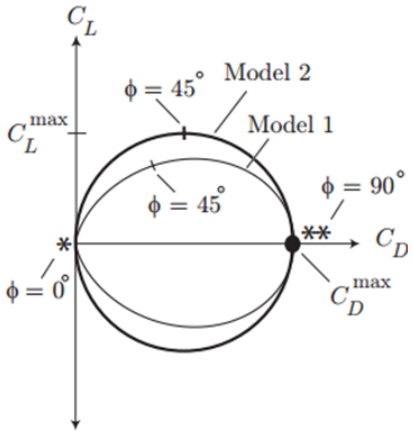

(b) The relationship between the lift and drag coefficients is shown on the right for both models of the oar blade force. The model of Pope [45] is model 1 and the model of Cabrera [8] is model 2. The equivalent lift and drag forces are multiplied with sin(ϕ). When ϕ = 0 or 180°(*), there is no lift and the drag force is at a minimum. When ϕ = 90°(**) the plate is perpendicular to the flow and the lift is zero but the drag now attains its maximum value. In rowing, the region near ϕ = 90°(**) is most relevant. Figure modified from Cabrera et al. [8].

Figure 3.7: The forces on the blade and the relationship between the blades lift and drag coefficient.

Barré and Kobus [4] studied the differences between the models as well. Their conclusion was that only using the drag force of the blade underestimates the propulsion force, but using the lift and drag force overestimates the propulsion force. They also concluded that the coefficient $C_L{}^{max}$ is the most important quantity to be evaluated for modeling the propulsive force, however the problem is how to accurately determine it.

Parallel blade force Fw neglected When neglecting Fw, in the beginning and at the end of the stroke, F_{drag} is underestimated, whereas in the middle part of the stroke ($\phi \approx 0$), F_{drag} is overestimated. In the first half of the stroke Fw is acting inwards on the blade, during the second half it acts outwards. Hofmijster et al. [27] calculated that the estimated power losses at the blades are 18% higher when parallel blade force (Fw) is incorporated. However, there is no practical way of measuring the parallel blade force, so this systematic error is generally accepted.

3.4. Boat

The free body diagram of the boat is shown in two different views; the xz- and xy-plane. This is because the forces on the boat act at specific points. The points of application do not influence the linear momentum balance, however for the completeness of the FBD's it is interesting to show.

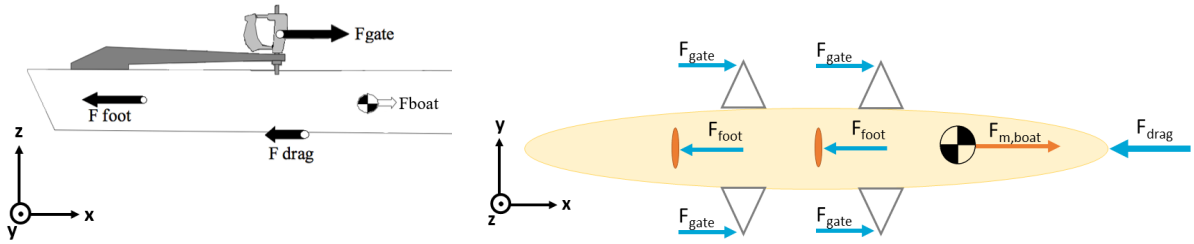

(a) The FBD of a boat from the side (xz-plane). Figure adjusted from In Motion Software & Sports Technology [29].

(b) A FBD of a double in the xy-plane. F_{gate}, F_{drag} and F_{foot} are the external forces. $F_{m,boat}$ is the resultant force that causes the boat to move.

Figure 3.8: The free body diagram of a boat in side and top view.

$$\sum F_x = F_{m,boat} = m_{boat} \cdot \ddot{x}_{boat} = F_{gates,X} - F_{drag} - F_{foots,X} \tag{3.20}$$

The linear momentum balance for the boat is shown in eq. (3.20). It is important because it shows the relation between the boat acceleration and the forces applied on the boat. The boat velocity is what best shows the boat performance. In the model the boat acceleration should be calculated accurately. The drag force of the boat is dependent on the boat velocity. In the next section, the calculation of the drag force on the hull will be explained.

3.4.1. Drag force hull calculation

When an object is moving through fluid, the drag is dependent on two factors, viscosity (ν) and form of the object. Drag is a difference in pressure that has to be overcome.

A first assumption in calculating the drag force of the boat is that only the horizontal movements of the boat are taken into account and only in the direction of the movement of the boat (so only motions in x-direction). This means that all detrimental movements of the boats in the five other degrees of freedom (fig. 1.1) are neglected. There are studies that take (some of) these movements into account [19, 20, 48] and found significant results. However, to keep the model simple, there is chosen not to implement this movements.

The drag force on a boat consists of form drag, skin friction, wave drag and induced drag of the hull.

$$F_{drag} = F_{form} + F_{skin} + F_{wave} + F_{induced} = \frac{1}{2}\rho C_{D,boat} A v^2 \tag{3.21}$$

$$C_{D,boat} = C_{form} + C_{skin} \tag{3.22}$$

$$C_{form} = \frac{1}{\rho v^2 A}\int_A (p - p_0)(\hat{n} \cdot \hat{\imath}) dA \tag{3.23}$$

$$C_{skin} = \frac{\tau_w}{\frac{1}{2}\rho v^2} = \frac{2}{\rho v^2 A}\int_A \tau_w (\hat{t} \cdot \hat{\imath})\ dA \tag{3.24}$$

$$\tag{3.25}$$

Wave drag is the drag that a boat encounters by producing waves. Since a rowing boat barely produces waves this can be neglected, although in some studies a small percentage of 7% or 8% is taken [8, 35, 45].

Induced drag is caused by protruding parts of the boat, since a rowing boat is very smooth. Only the fin or the steer could cause this kind of drag when the boat is not perfectly balanced. And because only the horizontal boat movements are modeled, the induced drag is neglected as well.

Form drag is also called profile drag or pressure drag and arises due to the shape of the hull. The shape of the hull, the ratio between the hull length and width is the same for all types of rowing boats. This phenomena is called geometric similarity [32, 35]. The form drag is calculated as in eq. (3.23), where p_0 is the pressure on the outside of the interference area and p is the pressure on the boat hull. The form drag scales with the Froude number (eq. (3.27)).

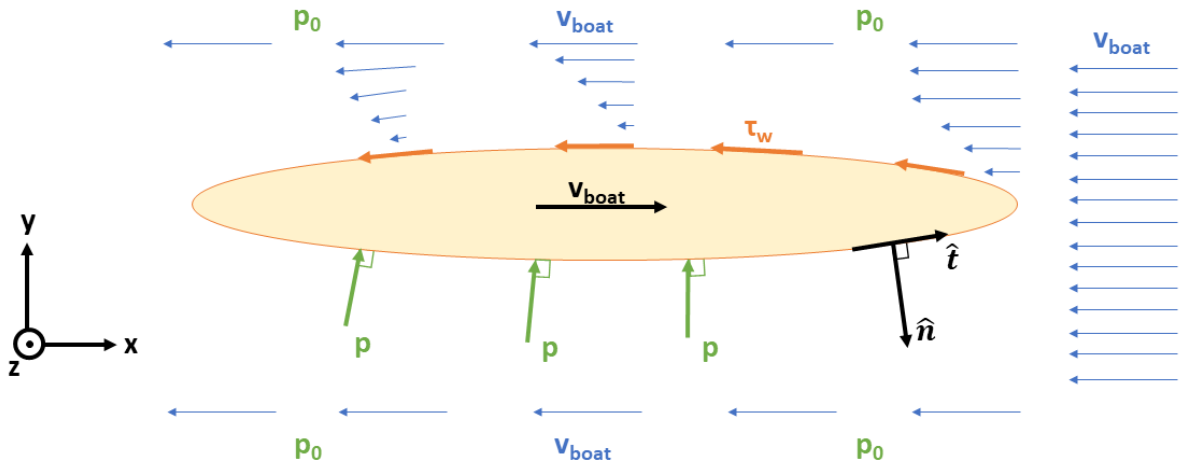

Figure 3.9: A graphical representation of the different components of the hydrodynamic drag force on the hull of the boat

Skin friction (drag) arises from the friction of the fluid against the skin of an object, in this case the hull of the boat. The skin friction is directly related to the wetted area ($A_{surface}$) of the boat. Skin friction is caused by the viscous drag in the boundary layer around the hull. The boundary layer of the front of the hull (the bow) is relatively thin, which results in a laminar flow. However, towards the stern the flow of water becomes more turbulent with a thicker boundary layer. The transition point (between the laminar and turbulent flow) of a rowing hull lies due to the small, long shape and smooth surface of the boat quite far toward the stern. The skin friction drag scales with the Reynolds number, eq. (3.26).

$$Re = \frac{\rho v L}{\mu} = \frac{v L}{\nu} \tag{3.26}$$

$$Fr = \frac{v}{\sqrt{gL}} \tag{3.27}$$

In practice, the skin friction is often determined with a flat plate drag test. A flat plate (almost only skin drag, no form drag) with the same wetted surface and smoothness as the boat is pulled through a tank, and the amount of drag force is determined.

Most of the time however, the total drag of the boat is approached with a combined drag force coefficient ($C_{D,boat}$) [59]. Drag tests [7, 58] confirm the quadratic relationship of the drag force of rowing boats and the boat velocity. Due to the geometric similarity [35, 42]), the drag coefficient is dependent on a ratio between the boats (form drag: Froude number) and the Reynolds number (skin drag). Wellicome [58] determined from a drag test, the drag force on a racing eight (probably wooden in the year 1967) (fig. 3.10).

Cabrera et al. [8] state that the fluctuations in boat velocity during a stroke are typically on the order of ±25% of the average velocity and therefore the Reynolds number does not vary much during the stroke. Also it is very convenient that there is a constant drag coefficient. In that case the drag coefficient should be mostly dependent on the boat shape, which is similar for all boats, $C_{D,boat}$ is taken as a constant. The drag force is only dependent on boat characteristic area, which is measured with the wetted area or projected cross-sectional area. The drag coefficient of Cabrera is calculated by: $C_1 = \frac{1}{2}\rho C_{D,boat} A$, where A is the characteristic area of the boat (eq. (3.28)).

$$F_{drag} = C_1 v^2 = \frac{1}{2}\rho C_D A v^2 \tag{3.28}$$

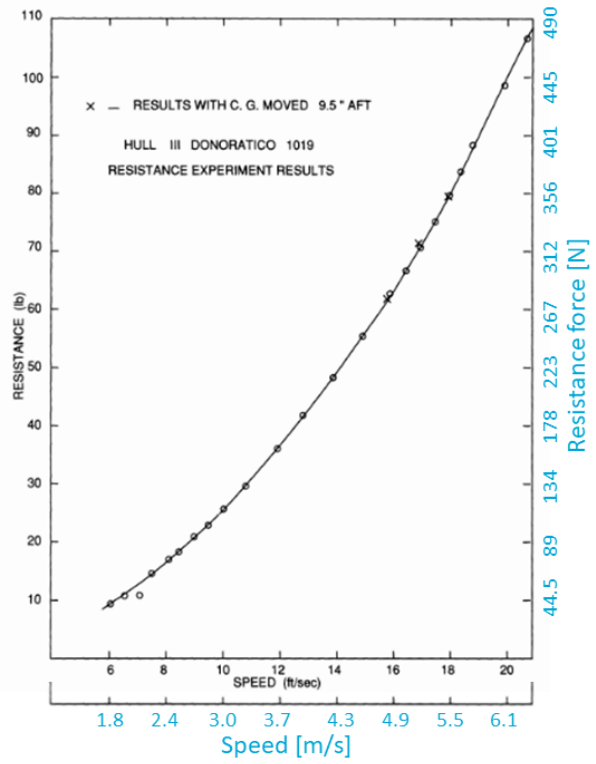

Figure 3.10: The hull resistance in lb wt versus speed in ft/sec for a typical racing eight hull, with permission of British Maritime Technology Limited [58]. The figure is adjusted by converting the axes into SI-units (cyan). A speed of 5.5 m/s leads to a drag force of 355 N, thus 11.74 $N/(m/s)^2$.

Assuming that the characteristic area of the boat scales with the number of rowers, $C_{D,boat}$ is calculated from the drag test by Lazauskas [32] with an eight (C_1 = 11.8 $\frac{N}{(m/s)^2}$). From Wellicome [58] there is found a similar value for C_1 for an eight (11.7 $\frac{N}{(m/s)^2}$). For a double this would mean that C_1 is 4.6829 $\frac{N}{(m/s)^2}$.

$$C_1 = \frac{11.8}{4^{2/3}} = 4.6829 \frac{N}{(m/s)^2}$$

If a small wave drag of 7 % is included, C_1 = 1.07 · 4.6829 = 5.01 $\frac{N}{(m/s)^2}$. This drag coefficient might be a bit conservative, due to the wave drag and the fact that it is reduced from a drag test from 1967 (probably with heavy men's rowers).

It remains a challenge to determine the drag force on the hull separately from the total drag on the system. The question can be asked if the effect of the air resistance may be neglected. This is already assumed for the rower, thus imaginable, however headwind definitely leads to slower race times. If the air drag is neglected, the total drag coefficient of the system is also valid as the drag coefficient of the hull.

Summary Chapter 3

The free body diagrams of the system, the rower, the oar and the boat are presented in this chapter. The forces on the rower and boat are only considered in x-direction and the rower is modeled as a point mass. The air drag on the rower is neglected, as well as the lateral forces on the blade and the oar deformation. The drag force on the hull is assumed to be proportional to the square of the boat velocity.

4

The mechanical rowing model: Forward dynamic model

This chapter describes the calculations done to obtain possible relations between the measured variables and modeled variables. The free body diagrams are presented in chapter 3. Often a combination of the equations composed from the FBD's is used to establish equations that describe motions of a part of the rowing system. The focus lies on modeling a double, because the available dataset is from a lightweight women's double (LW2x). In fig. 4.1 the definitions of the coordinates of this system are shown.

Complexity To reduce the complexity of the model, there is chosen to make the model of the rower and boat in one-dimension. This means that all movements of the boat and rower in lateral and vertical direction are neglected, also the yaw, pitch and roll motions of the boat are neglected. Due to this assumption only forces in x-direction on the boat and rower are used. Therefore F_{gate} has to be read as $F_{gate,X}$, F_{foot} as $F_{foot,X}$ and F_{handle} as $F_{handle,X}$. The X is left out in the subscript because of the clarity in the notation when other variables, such as rower numbers, are introduced. Because of the rotation of the oar, a shifted axial system is used for the oar. The calculations of the forces on the oar are officially two-dimensional calculations. The resulting forces on the rower and boat are only considered in one dimension.

To make the model more realistic, some slight changes have to be made to distributions of the masses in the system.

Added mass In fluid mechanics, added mass is an inertial mass of the water added to the system. This is done to make the model more realistic. To move a boat, some volume of the water has to be moved or deflected. The added mass can be seen as a small layer of water travelling attached to the hull.

Alexander [1] assumed an added mass of 20 % of the displaced mass. Cabrera et al. [8] state this is a big overestimation (maybe due to another hull used in the time of Alexander). Cabrera et al. use an added mass of 0.65 % of the displaced mass, they use eq. (4.1) for a Rankine ovoid. Later they increased the percentage to 4.3% to obtain a better fit.

$$\frac{m_{added}}{m_{displaced}} = \frac{w_{boat}}{3 \cdot l_{boat} - w_{boat}} = \%_{m,added} \tag{4.1}$$

For a double the added mass is calculated as 0.0169*$m_{displaced}$. $m_{displaced}$ is the mass of the whole system, for a LW2X this is approximately 151 kg, which means that m_{added} is 2.55 kg.

Rower mass As in several rowing models found in literature [1, 3, 8, 44, 55], in this thesis the rowers mass will be assumed to be a point mass located around the belly button. However not all of the body segments move with the gut, for example, the feet of the rower are attached to the boat.

Therefore a variable is introduced that defines a percentage of the rower's mass attached to the boat ($\%_{m,rowerboat}$). Naturally, the other part of the rower's mass is the moving mass of the rower ($m_r{}^*$).

$$m_r{}^* = m_r(1 - \%_{m,rowerboat}) \tag{4.2}$$

These mass distributions lead to the following changes of the boat (m_b) and system mass (m_{sys}).

$$m_{sys} = m_b + 4 \cdot m_{oar} + \sum_{i=N}(m_{r,i}) \tag{4.3}$$

$$m_b{}^* = m_b + 4 \cdot m_{oar} + \%_{m,added} \cdot m_{sys} + \%_{m,rowerboat} \cdot \sum_{i=N}(m_{r,i}) \tag{4.4}$$

$$m_{sys}{}^* = m_{sys}(1 + \%_{m,added}) \tag{4.5}$$

In fig. 4.1 the coordinates and relative displacements of the different masses in the model are shown.

Parameter	Value	Description
$m_{boat} = m_b$	27 kg	The mass of the (hull and the riggers of the) boat.
m_{oar}	1.5 kg	The mass of the oars.
$m_{rower} = m_r$	59 kg	The mass of one rower.
m_{sys}	151 kg	The mass of the total system.
$\%_{m,added}$	1.69 %	The percentage of m_{sys} added to the boat as water inertia.
$\%_{m,rowerboat}$	5.0 %	The percentage of m_{rower} attached to the boat.

Table 4.1: The different masses and mass percentages used in the model for the LW2x, with their value and description. There is one m_r given, because both rowers have the same weight.

Other parameters that are used in the model are the oar properties as given in table 3.2 and the model parameters shown in table 4.2.

Parameter	Value	Description
l_{boat}	8 m	The length of the boat.
C_1	5.01 $\frac{N}{(m/s)^2}$	The coefficient to calculate $F_{drag} = C_1 \cdot v^2$.
v_{avg}	4.5 m/s	The average velocity of the boat over a race.
l_{arms}	0.53 m	The assumed length of the arms of the rowers.

Table 4.2: The remaining model parameters, with their value and description.

Initial velocity From the measured boat acceleration data over the total rowing practice, the PowerLine measurement system calculates the boat velocity by integrating the acceleration signal. This means that the "measured" velocity fluctuates around 0 m/s. The measurements for the rowing segment used in the model are started after the boat has reached a constant actual speed. With the integrated measured acceleration over the whole practice, the measured velocity is determined for the segment of ±20 strokes. This measured velocity is cut into strokes in the same way as all other data. The resulting average measured velocity of the stroke is a periodic signal, but smaller than zero in the catch of the stroke (t_0).

The average speed over the measured rowing segment of ±20 strokes is assumed to be 4.5 m/s (v_{avg}). This is a constant offset that is added to the measured velocity signal. A realistic boat velocity is needed to determine the drag force on the hull (see section 3.4.1).

In the start of the modeled stroke, the initial velocity is determined (v_{init}). The initial velocity of the system, boat and rower are assumed to be the same. The rower sits still in the catch position, this means there are no relative speed differences between the different masses in the system at t_0.

$$v_{realistic} = v_{measured} + v_{avg} \tag{4.6}$$

$$v_{init} = v_{measured}(t_0) + v_{avg} \tag{4.7}$$

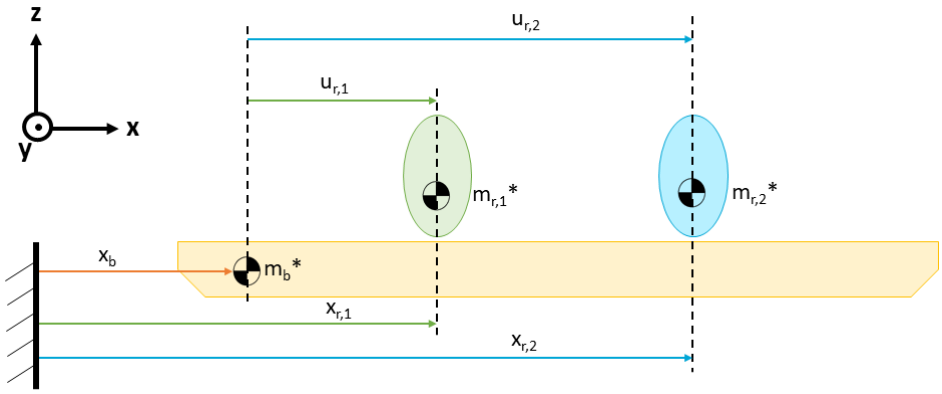

Figure 4.1: The schematic picture of the definition of the coordinates of the different masses in the model.

4.1. System

The position of the center of mass of the system is the weighted average of the centers of mass of the rowers and boat. The weighing is done by the weight of the masses. The position of the system is calculated in eq. (4.8). During the stroke, the position of the boat and the rowers change with respect to each other. The position of the center of mass of the system is expected to move gradually towards the finish.

$$x_{sys} = \frac{x_b \cdot {m_b}^* + x_{r,1} \cdot {m_{r,1}}^* + x_{r,2} \cdot {m_{r,2}}^*}{{m_{sys}}^*} \tag{4.8}$$

$$\dot{x}_{sys} = v_{init} + \int_{t_0}^{t_{final}} \ddot{x}_{sys}\, dt \tag{4.9}$$

From the free body diagram of the system the equation eq. (3.1) is derived. The drag force on the hull is determine based on the measured boat velocity and combined drag coefficient C_1 as shown in eq. (3.28). Other drag forces on the system are neglected.

$${m_{sys}}^* \cdot \ddot{x}_{sys} = F_{blades} - F_{drag} \tag{3.1}$$

The forces acting on the system and the motions of the center of mass of the system are shown in fig. 4.2. The absolute displacement of the center of mass (CoM) of the system in one stroke is approximately 7.5 m. In the end of the stroke, the displacement of the rower and boat must be the same, and equal to the diplacement of the total system.

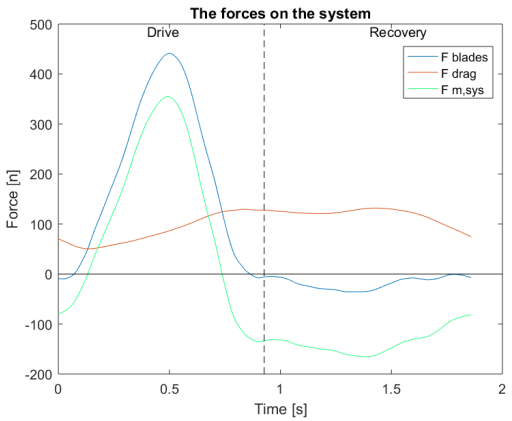

(a) The forces acting on the system.

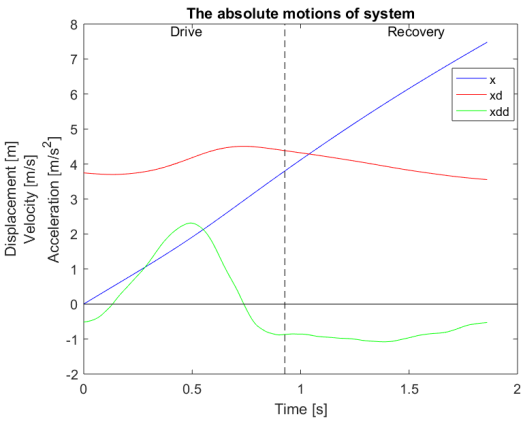

(b) The absolute motions of the system.

Figure 4.2: The forces acting on the system and the resulting absolute motions of the CoM of the system.

4.2. Rower

From fig. 3.2 eq. (3.2) is derived. The calculated and measured forces acting on the rower are shown in fig. 4.3a.

$$\sum F_{m,rower} = m_r{}^* \ddot{x}_r = F_{foot} - F_{handles} \tag{3.2}$$

The rower is modeled as a point mass, the displacement of the center of mass of the rower x_{CoM} is thus the same as x_r.

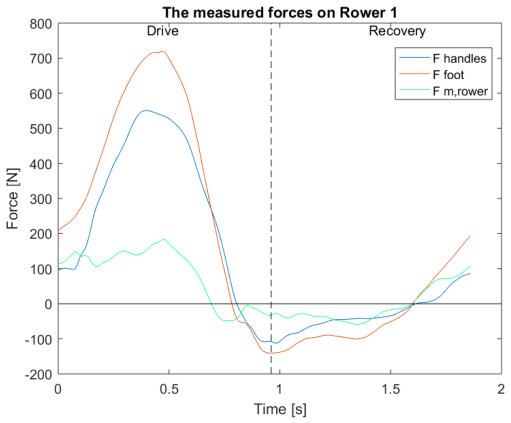

(a) The measured forces on rower 1, F_{handle} and F_{foot}, and the resulting $F_{m,rower}$.

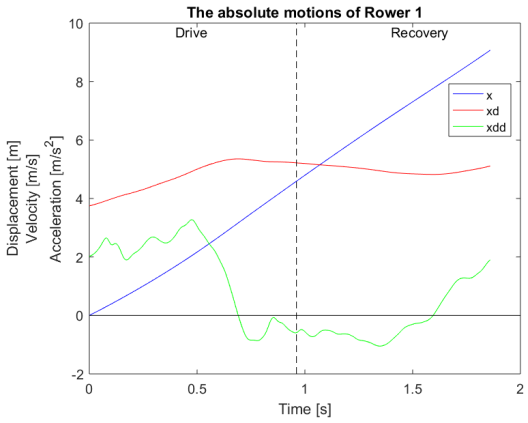

(b) The absolute acceleration, velocity and displacement of rower 1, based on the $F_{m,rower}$ calculated in fig. 4.3a.

Figure 4.3: The forces acting on and absolute motions of the CoM of rower 1.

4.2.1. Absolute motions

The absolute acceleration of the rower $\ddot{x_r}$ is described by rewriting eq. (3.2);

$$\ddot{x}_r = \frac{F_{foot} - F_{handles}}{m_r{}^*}$$

By integrating the absolute acceleration of the rower once and twice, respectively the absolute velocity ($\dot{x}_r$) and absolute displacement (x_r) of the rower is found. In case of the model t_0 is the time of the catch and t_{final} the time step before the catch of the next stroke. The acceleration is thus integrated of the period of the stroke.

$$\dot{x}_r = v_{init} + \int_{t_0}^{t_{final}} \ddot{x}_r \, dt \tag{4.10}$$

$$x_r = \int_{t_0}^{t_{final}} \dot{x}_r \, dt \tag{4.11}$$

At the end of the stroke, the absolute displacement of the rower should be equal to the absolute displacement of the system (7.5 m). The absolute displacement of the rower is over 9 m, this is bigger than the absolute displacement of the system. This means that the rower would move away from the boat ($\approx$ 1.5m), which is not possible.

4.2.2. Relative motions

The absolute movement of the rower x_r is described as a sum of the absolute movement of the boat x_b and the relative movement of the rower u_r, eq. (4.12). The definitions are shown in fig. 4.1.

$$x_r = x_b + u_r \tag{4.12}$$

$$\ddot{x}_r = \ddot{x}_b + \ddot{u}_r \tag{4.13}$$

The relative motions of the rower are described with different approaches;

- as a function of the displacement of the handle (u_{handle})
- as a function based on the boat acceleration ($\ddot{x}_b$) and the foot force (F_{foot})
- based on the seat displacement (u_{seat})

The rower is modeled as a point mass, the relative displacement of the center of mass of the rower u_{CoM} is thus the same as u_r. In the explanation of the following approaches it is easier to use u_{CoM}, because the CoM is introduced in the graphical representation of the coordinates.

u_{CoM} based on u_{handle}

The movement of the center of mass of the rower ($u_{CoM} = u_r$) has been modeled before as a cosine function [39]. This approach shows potential, but the relative movement between the handle and the CoM has to be described more accurately. To do so, not a normal cosine is used, but the distance between the handle and the CoM is only changed during the movement of the back and arms. During the leg drive, the relative distance between the handle and CoM remains constant (approximately an arms length (l_{arms})). During the back-arms swing the handle moves towards the CoM, thus the relative distance decreases, until it is zero in the finish. Back forward, the relative distance increases again, until the rower is only using the seat to go forward again. This function and the velocity and acceleration of the center of mass of the rower are shown in fig. 4.5.

$$
\begin{aligned}
u_{CoM} &= u_{handle} + \Delta u_{handle-CoM} \\
u_{handle} &= l_{inboard} \cdot \sin(\theta_{oar}) \\
\Delta u_{handle-CoM}(i) &= \begin{cases} l_{arms} & \text{for the legdrive} \\ \frac{l_{arms}}{2} \cos(2\pi \cdot f^*_{back-arms}(i)) + \frac{l_{arms}}{2} & \text{for back-arms swing} \end{cases}
\end{aligned}
$$

Where $f^*_{back-arms}$ is a function dependent on the back-arms swing (A.6)

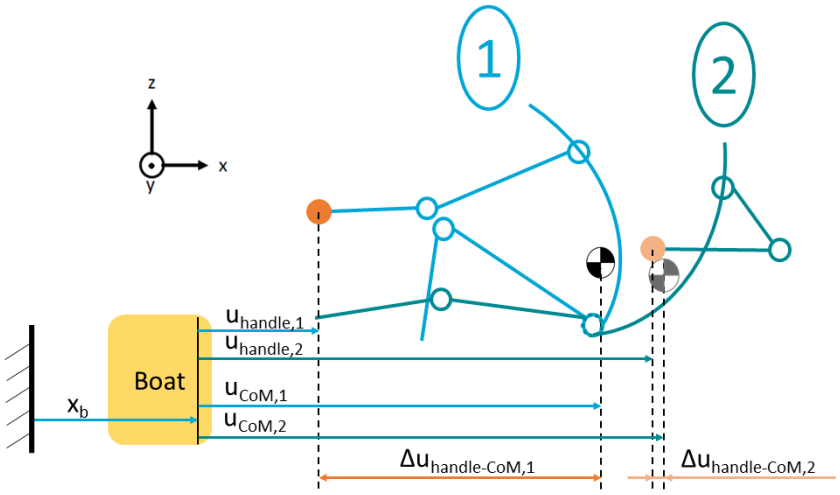

Figure 4.4: The definition of the relative distances of the handle (u_{handle}) and CoM of the rower (u_{com}) with respect to the boat, in two different positions in the rowing cycle (catch position 1 and finish position 2). And the relative distance between the CoM and the handle ($\Delta u_{handle-CoM}$).

When this method is applied on more rowers, clear differences are found in the motions of the CoM's of the rowers in a crew fig. A.11b. Small changes in the u_{CoM} of the different rowers result in big changes in the accelerations of the center of mass and will thereby cause a change in the net forces that the rowers apply on the boat.

Using this approach, the movement of the CoM of the rower is periodical, which means that the rower returns to the same position as she started ($u(t_0) = 0$ m & $u(t_{final}) = 0$). The drawback of this approach is that the movements of the different body segments of the rower with respect to each other is generalized for all rowers. Thus the movement of the CoM of the rower is individualized by the movement of the oar, but the movement pattern of the rower is generalized. The generalization of the movement patterns of the rower is one of the issues that is supposed to be tackled with the model.

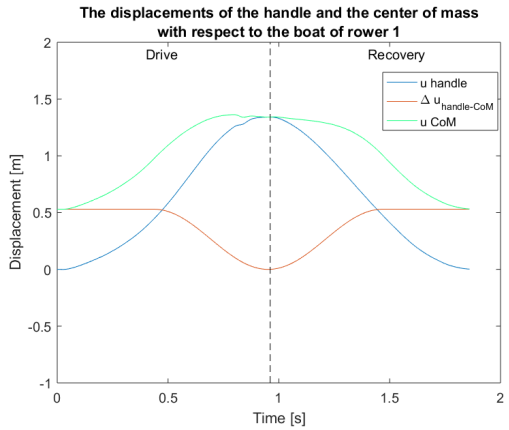

(a) The displacement of the handle of the rower (u_{handle}), the function for the relative movement of the handle and the CoM ($\Delta u_{handle-CoM}$) and the displacement of the CoM (u_{CoM}).

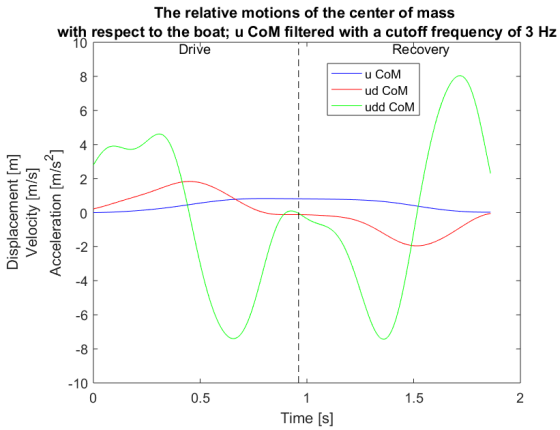

(b) The relative motions of the center of mass of the rower, after u_{CoM} is filtered with a cutoff frequency of 3 Hz.

Figure 4.5: The motions of the center of mass of rower 1, derived from the handle movement (u_{handle}).

u_{CoM} based on forces

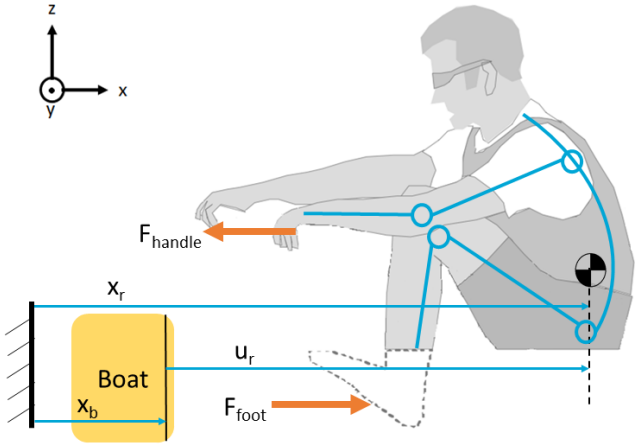

Figure 4.6: The definition of the coordinates x_b and x_r and relative distance u_r, together with the application points of the foot force (F_{foot}) and handle force (F_{handle}).

When substituting eq. (4.13) in eq. (3.2) a relation is found between the foot force, handle force and the relative acceleration of the rower.

$$m_r{}^*(\ddot{x}_b + \ddot{u}_r) = F_{foot} - F_{handles} \tag{4.14}$$

For the boat acceleration in this relation, the measured boat acceleration is taken, to make sure that no cumulative errors occur. Thus $\ddot{u}_r$ is calculated according to eq. (4.15).

$$\ddot{u}_{CoM} = \ddot{u}_r \quad = \quad \frac{F_{foot} - F_{handles}}{m_r{}^*} - \ddot{x}_b \tag{4.15}$$

Basically this approach uses the $\ddot{x}_r$ from section 4.2.1 in fig. 4.3b and then subtracts the measured boat accelerations. This leads to the relative motions of the rower as shown in fig. 4.7a.

In the relative motion, the CoM of the rower should return to the catch position, but in fig. 4.7a there is shown that this is not the case (u(t_0) = 0 m & u(t_{final}) ≠ 0). The velocity of the CoM of the rower does not become negative, which means that the CoM of the rower does not move backwards (to the stern) at all. The displacement of the CoM does indeed not become smaller in the recovery,

but still proceeds towards the bow. Physically this would mean that the rower would move out of the boat, which is not possible, because she is secured to the boat by the shoes on the footstretcher.

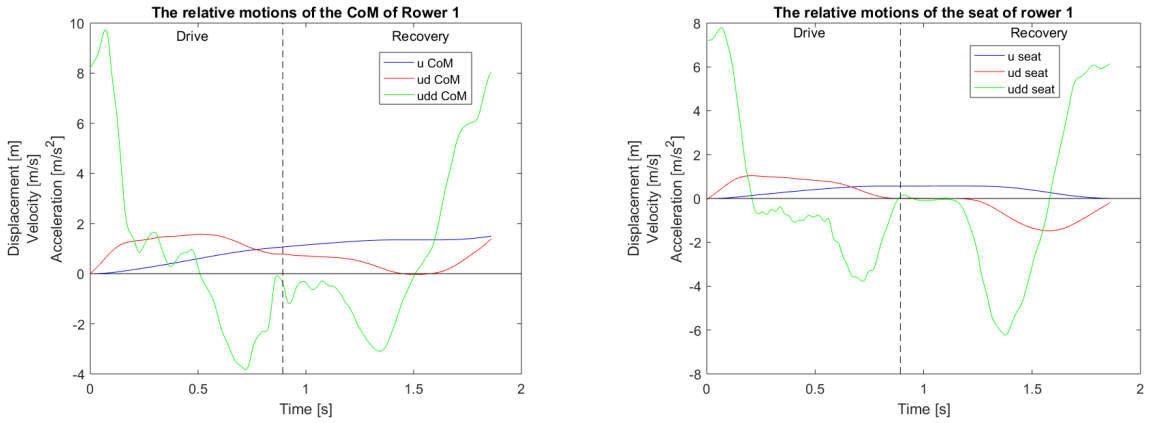

(a) The motions of the CoM of a rower based on F_{foot} and F_{handle}

(b) The motions of the CoM of a rower based on u_{seat}

Figure 4.7: The relative displacement, velocity and acceleration of the CoM of the rower with respect to the boat, based on the foot forces and based on the measured position of the seat.

u_{CoM} based on u_{seat}

The rower remains seated on the seat through the whole rowing cycle, the seat moves as a result of the leg drive. The assumption is made that the rowers center of mass is concentrated in her gut. It seems reasonable to use the seat displacement to estimate the position of the center of mass. In fig. 4.8 the coordinate definition of the seat and center of mass is given.

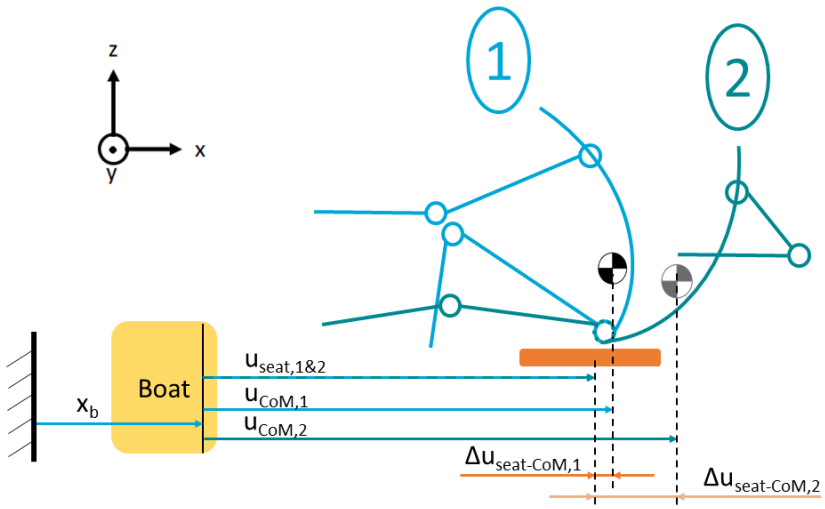

Figure 4.8: The definition of the relative distances of the seat (u_{seat}) and CoM of the rower (u_{CoM}) with respect to the boat and the relative distance between the CoM and the seat ($\Delta u_{seat-CoM}$). In two different positions in the rowing cycle; Position 1 is the catch position and position 2 is the finish.

In the current approach the assumption is made that $\Delta u_{seat-CoM}$ is zero through the whole stroke. This is not very realistic, as shown in fig. 4.8. In the finish the position of the CoM of the rower is displaced with respect to the catch. For the leg drive of the stroke, u_{seat} can be used to estimate u_{CoM}, but during the back and arm swing, this is not the case since the torso rotates around the hip.

In fig. 4.7b the seat displacement, velocity and acceleration are shown. The motions of the seat are periodical as expected, the seat does return to the same position as it started (u(t_0) = 0 m & u(t_{final}) = 0). If this were not the case the measurements with the seat sensor would be most likely be false.

Compare approaches

When the three different approaches to determine the motions of the center of mass are compared, the biggest differences are found in the recovery phase of the rowing cycle. The expected relative

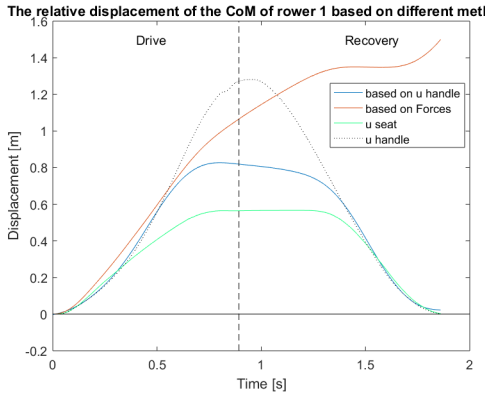

(a) The relative displacement of the CoM of the rower based on three different approaches.

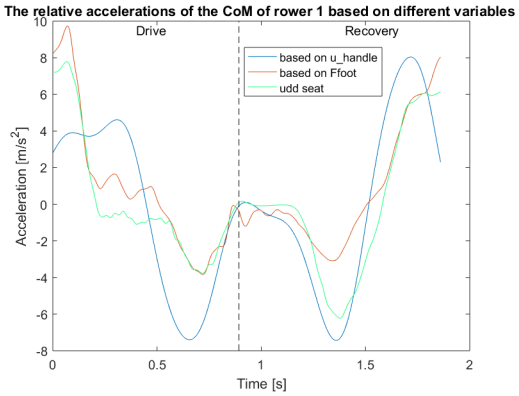

(b) The relative acceleration of the CoM of the rower based on three different approaches.

Figure 4.9: The relative displacement and acceleration of the CoM of rower 1 calculated based on three different approaches. The displacements of the handle and seat do not start at the absolute same x-position (for example with respect to the gate), both motions start in their own relative catch position (u(t_0) = 0).

displacement of the center of mass of the rower should be between the relative displacement of the handle and the relative displacement of the seat in the finish position. Looking at these restrictions, the relative displacements of the rower based on the handle displacement and based on the seat (naturally) meet the requirements. The approach where u_{CoM} is calculated based on the F_{foot} does not meet these requirements, because it does not return to the catch position.

Looking at the relative accelerations of the CoM of the rower, the results from the calculations based on the foot forces have the same shape as the measurements of the seat in the drive. In the recovery the accelerations from the approach based on the handle displacement have a better match with the seat accelerations, which results in the motion back to the catch position.

None of the approaches now used is optimal. Preferably the relative motion of the rower is estimated based on the forces measured on the rowers, because then the segment of the rower is calculated independent of the rigging parameters.

The approaches based on the handle movement and seat position are not optimal to use. When the distances $\Delta u_{seat-com}$ and $\Delta u_{handle-com}$ are described with a standard function for every rower, a generalization of the movement pattern of the rowers is done, which is what the model is trying to solve.

In section 4.4 the search for a good predictor of the relative movements of the rower continues.

4.3. Boat

The boat should be accurately modeled, because the measured performance of the system is dependent on the boat model and the boat accelerations have an influence on the relative motions of the rower. Also the boat is actually the part of the system on which all the sensors are attached, so the model starts in the boat (force & oar angle measurements) and finishes there as well (boat accelerations).

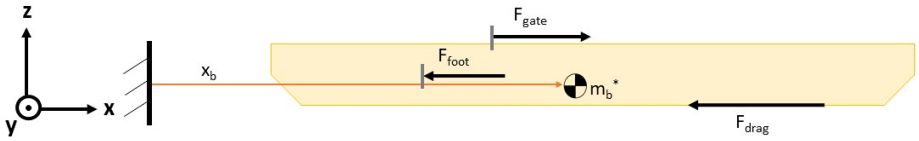

Figure 4.10: A schematic free body diagram of the boat, including the coordinate definition of x_b.

4.3.1. Boat motions

The boat motions are derived in different ways, two approaches are discussed in this section. The first approach looks at the forces directly acting on the boat, as shown in fig. 4.10. The second approach combines the forces acting on the system with the net forces applied on the boat by the rowers motions. The boat velocity is calculated with the integral of the boat acceleration and the initial velocity (eq. (4.16)).

$$\dot{x}_{boat} = v_{init} + \int_{t_0}^{t_{final}} \ddot{x}_{boat}\, dt \tag{4.16}$$

$$x_{boat} = \int_{t_0}^{t_{final}} \dot{x}_{boat}\, dt \tag{4.17}$$

Based on F_{gates} and F_{foots} (eq. (3.20)):

Looking at the forces that are acting directly on the boat, the gate forces have a positive effect on the boat accelerations and the foot and drag forces a negative effect. From fig. 4.10 eq. (3.20) is derived. The magnitude of the forces acting on the boat is shown in fig. 4.11a and the resulting accelerations of the boat ($\ddot{x}_b$) in fig. 4.11b.

$$\sum F_x = {m_b}^* \ddot{x}_b = F_{gates} - F_{foots} - F_{drag} \tag{3.20}$$

Where F_{gates} and F_{foots} are respectively the sum of all the gate forces and the sum of all the foot forces in x-direction in the boat. For the double eq. (3.20) is rewritten:

$$\ddot{x}_b = \frac{F_{gate,r1} + F_{gate,r2} - F_{foot,r1} - F_{foot,r2} - F_{drag}}{{m_b}^*}$$

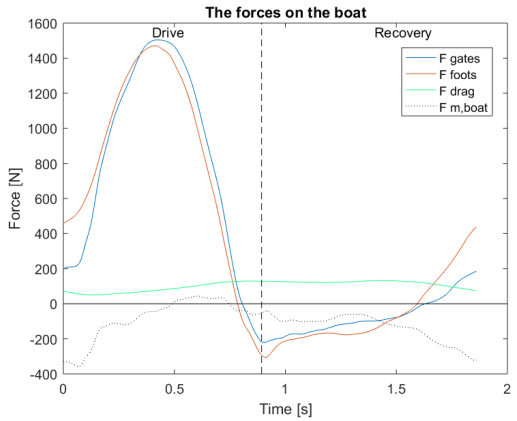

(a) The measured forces acting on the boat (m_b^*).

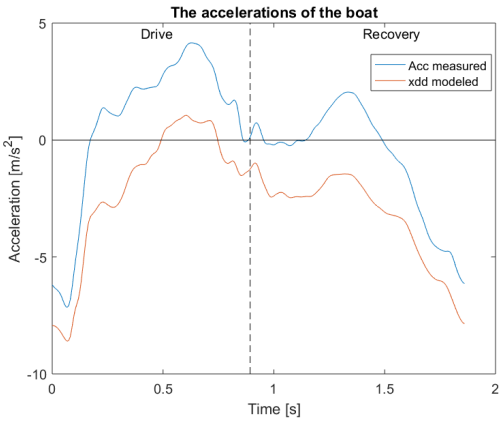

(b) Modeled and measured accelerations of the boat

Figure 4.11: The forces acting on the boat, considered in eq. (3.20) and the resulting accelerations of the hull.

The measured and modeled boat accelerations in fig. 4.11b do not match, although the shape of the acceleration curve is similar. There is some scaling issue that keeps the modeled boat acceleration much smaller than the measured boat acceleration. The resulting boat velocity and displacement will be too small as well.

Based on F_{blades} and the relative motions of the rowers ($\ddot{u}_r$) via m_{sys} (eq. (4.18)):

Another approach is to combine the equations for the motions of the system (eq. (4.8) and eq. (3.1)) and the relative motions of the rowers (u_r).

$$\begin{aligned}
\text{system:} \quad & m_{sys}{}^* \cdot \ddot{x}_{sys} = F_{blades} - F_{drag} \\
& x_{sys} = \frac{x_b \cdot m_b{}^* + \sum_{i=N} \left(m_{r,i}{}^* \cdot x_{r,i}\right)}{m_{sys}{}^*} \\
\text{rower:} \quad & \ddot{x}_{r,i} = \ddot{x}_b + \ddot{u}_{r,i} \\
\text{system with N rowers:} \quad & m_b{}^* \cdot \ddot{x}_b + \sum_{i=N} \left(m_{r,i}{}^* (\ddot{x}_b + \ddot{u}_{r,i})\right) = F_{blades} - F_{drag} \\
m_{sys}{}^* = m_b{}^* + \sum_{i=N} (m_{r,i}{}^*) \text{ , thus:} \quad & m_{sys}{}^* \ddot{x}_b = F_{blades} - F_{drag} - \sum_{i=N} \left(m_{r,i}{}^* \cdot \ddot{u}_{r,i}\right)
\end{aligned} \tag{4.18}$$

Eq. (4.18) describes the relationship between the relative movements of the rowers and the boat acceleration. Using eq. (4.18) the calculated boat acceleration is much more similar to the measured boat acceleration (see fig. 4.12b), however still a little smaller than it should be, resulting in a too small boat velocity and displacement.

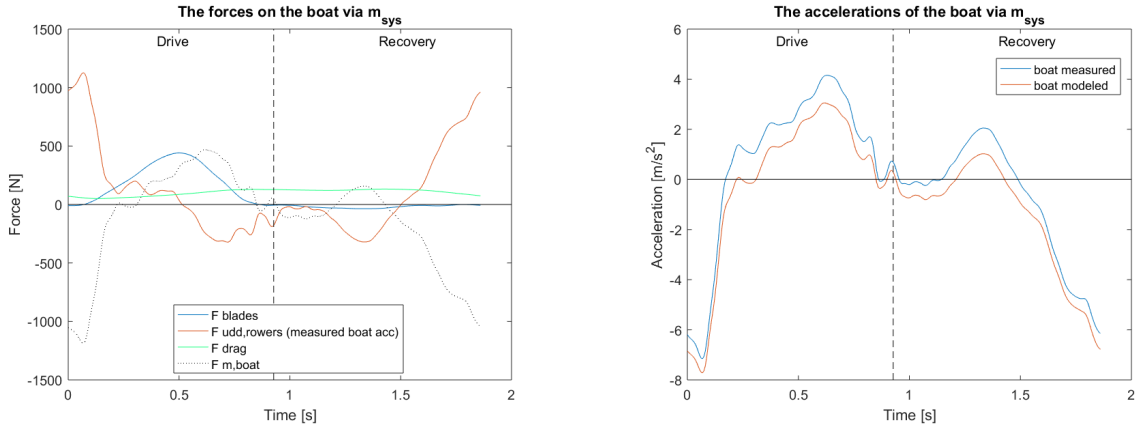

(a) Forces acting on the boat (via $m_{sys}{}^*$)

(b) Modeled and measured accelerations of the boat

Figure 4.12: The forces acting on the boat, considered in eq. (4.18) and the resulting accelerations of the hull.

Compare $\ddot{x}_{boat}$ based on F_{foots} (eq. (3.20)) and m_{sys} (eq. (4.18))

For the double two approaches are used to describe the boat acceleration. For simplicity, the approaches are called F_{foots} method and m_{sys} method, they are deduced from respectively eq. (3.20) and eq. (4.18).

$$\begin{aligned}
F_{foots} \text{ method} : \quad & \ddot{x}_b = \frac{F_{gate,r1} + F_{gate,r2} - F_{foot,r1} - F_{foot,r2} - F_{drag}}{m_b{}^*} \\
m_{sys} \text{ method} : \quad & \ddot{x}_b = \frac{F_{blades,r1} + F_{blades,r2} - m_{r,1}{}^* \ddot{u}_{r,1} - m_{r,2}{}^* \ddot{u}_{r,2} - F_{drag}}{m_{sys}{}^*}
\end{aligned}$$

The F_{foots} method uses the force acting directly on the boat, the m_{sys} method uses the forces acting on the system and the relative acceleration of the rowers. These equations should result in the same boat accelerations, however this is not the case. The gate forces take over the foot forces in fig. 4.11a at a later time step than the blade forces take over the forces due to the moving rowers in fig. 4.12a.

This results in a later time step where the boat acceleration becomes positive (compare fig. 4.11b and fig. 4.12b.) The fact that both of these results are smaller than the measured boat acceleration, lead to the suspicion that the model is not 100% correct. This is possible due to some parameters that are estimated. Therefore the effect of selected model parameters on the modeled boat acceleration has to be studied.

4.3.2. Improving model parameters

There are several parameters in the model that are assumed or estimated, therefore to improve the model it might be useful to look closer at the effects of these parameters. The parameters of which the chosen values are uncertain are: $\%_{m,rowerboat}$ = 0.05, $\%_{m,added}$ = 0.0169, C_1 = 5.01 $\frac{N}{(m/s)^2}$ and v_{avg} = 4.5 m/s.

Effect of the parameters separately

The effect of the four parameters on the boat acceleration calculations is best shown in a figure with different values for the parameter. In fig. 4.13, the effects on the boat acceleration of five different values of one parameter, while keeping the other parameters constant are shown. In fig. 4.13 the boat acceleration is calculated via the m_{sys} method. The accelerations of the boat calculated via F_{foots} (eq. (3.1)) are shown in fig. A.10. These results are worse than those obtained via m_{sys} and the effects of the parameter changes are roughly the same.

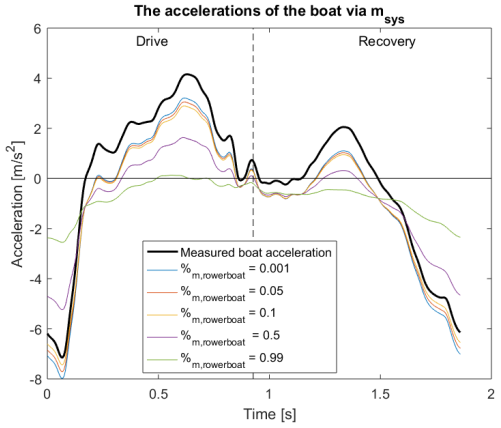

(a) The effect of the percentage of the rowers mass attached to the boat ($\%_{m,rowerboat}$).

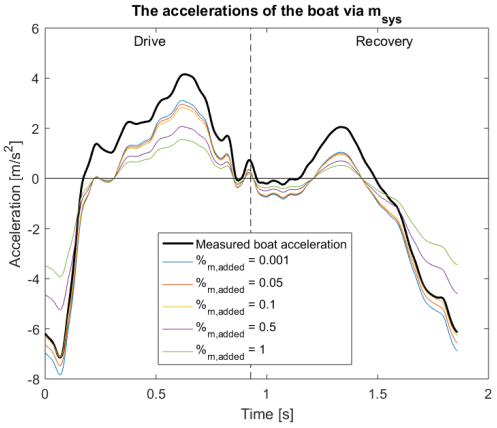

(b) The effect of the percentage of the system mass used as added mass on the boat ($\%_{m,added}$).

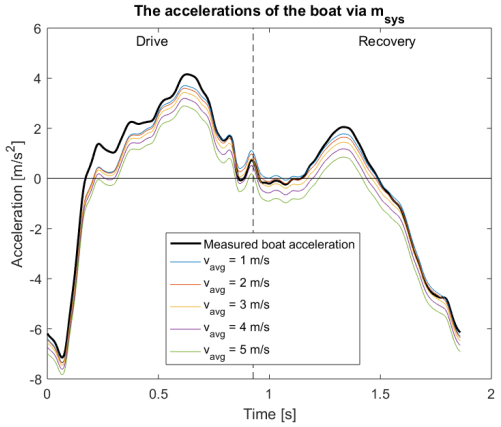

(c) The effect of the estimated average velocity of the stroke (v_{avg}).

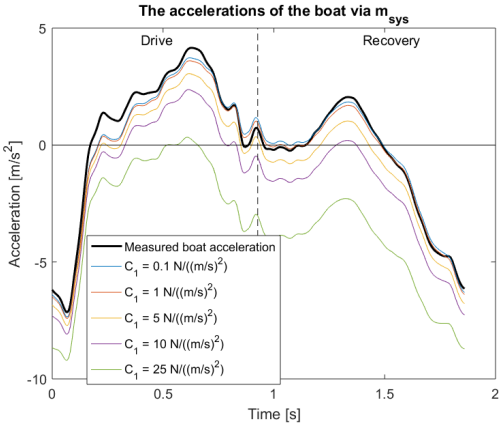

(d) The effect of the drag coefficient of the hull drag (C_1).

Figure 4.13: The effects of four different parameters on the modeled boat acceleration, calculated via m_{sys} (eq. (4.18)).

The effect of $\%_{m,rowerboat}$ and $\%_{m,added}$ is similar, which is not surprising since they both add more mass to the boat. A higher percentage of the rowers mass or added mass attached to the boat leads to

a flatter acceleration curve. The extra mass causes extra damping on the acceleration, because more mass has to be moved with the same forces.

The effect of v_{avg} and C_1 is also similar. Both of the parameters can translate the acceleration curve up or down, but seem to have a maximum that still lies beneath the measured boat acceleration. The drag force is directly influenced by both parameters, because C_1 is the drag force coefficient in eq. (3.28) and according to the equation the drag force is dependent on the velocity squared. v_{avg} determines the average stroke velocity and thus plays a big part in the calculated drag force.

Concluding, none of the parameters seems to have the ability to really raise the modeled acceleration curve above the measured curve. This may point to an offset in one of the measured forces, but first an optimization is done to see what a combination of the four parameters can accomplish.

Optimization of parameters

An optimization of the modeled boat acceleration toward the measured boat acceleration is done, by optimizing the four different parameters. Boundaries regarding the parameter values are needed. For the mass of the rower attached to the hull $\%_{m,rowerboat}$, minimal 1 % is assumed and the maximum amount of mass attached to the hull is set to 50%. For the added mass of the water, the minimal percentages is set to 0.1 % and the maximum again to 50 %. The drag coefficient is less a guess than the mass percentages, therefore a smaller range is assumed; C_1 should be between 1 and 10 $\frac{N}{(m/s)^2}$. The average speed of the LW2x is in the optimization allowed to differ from 1 m/s to 6 m/s.

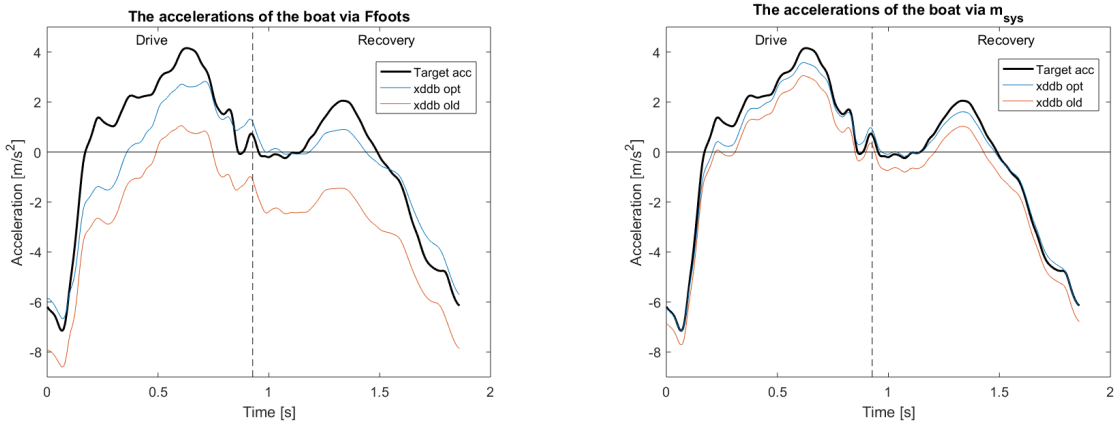

(a) The acceleration of the boat modeled with the F_{foots} method, with and without optimized parameters. The optimized parameters are: $\%_{m,rowerboat}$ = 0.0619, $\%_{m,added}$ = 0.0420, C_1 = 1 $\frac{N}{(m/s)^2}$, v_{avg} = 6 m/s.

(b) The acceleration of the boat modeled with the m_{sys} method, with and without optimized parameters. The optimized parameters are: $\%_{m,rowerboat}$ = 0.0998, $\%_{m,added}$ = 0.0010, C_1 = 1 $\frac{N}{(m/s)^2}$, v_{avg} = 6 m/s.

Figure 4.14: Optimization of the boat acceleration based on four different parameters for two different methods (F_{foots} & m_{sys}).

The optimization of the parameters leads to better fits between the modeled and the measured boat acceleration. However the modeled accelerations via both equations are still mostly below the measured acceleration. Also the boundaries of some of the parameters are met. The set boundaries are already quite extreme cases, which are unlikely to really occur. Nonetheless, in the optimization of the parameters two of the four parameters seek their lower boundary (C_1 and v_{avg}). Through the optimization the drag force is minimized, since both of these parameters have a direct influence.

In the optimization of the accelerations via F_{foots} the mass percentages stay within a reasonable range. However in the optimization of the accelerations via m_{sys}, $\%_{m,added}$ also finds its boundary.

Although the optimization of the parameters leads to better fits between the modeled and measured acceleration, the fits are not as good as they should be. Because almost all parameters strive towards their boundaries, the results are a minimization of all detrimental forces instead of due to a new nice combination of the parameters.

4.4. Improving the predicted rower and boat motions

The relative motions of the rower do not agree with the expectations based on the movement of the seat and the handle. Therefore different methods are tried to improve u_r, mainly by making it return to the catch position. This is done by adding an extra resistance force and changes in the foot force in the calculations of the relative motions of the rower.

All the while u_r is improved, the boat acceleration must be improved as well. The results of the boat accelerations are influenced by the rower motions in the boat.

4.4.1. Calculate the relative acceleration of the rower via the *System* method

For rower 1 of the double the relative acceleration is described in two ways. The *System* method is based on the forces on the total system, the boat acceleration and other rowers acceleration, based on eq. (4.18). The *Forces* method uses the direct forces on the rower via $\ddot{x}_r$ and the boat acceleration (eq. (4.15)).

$$\textit{System} \text{ via eq. 4.18}: \quad \ddot{u}_{r,1} = \frac{F_{blades,r1} + F_{blades,r2} - F_{drag} - m_{sys}\ddot{x}_b - {m_{r,2}}^{*}\ddot{u}_{r,2}}{{m_{r,1}}^{*}}$$

$$\textit{Forces} \text{ via eq. 4.15}: \quad \ddot{u}_{r,1} = \frac{F_{foot,r1} - F_{handle,r1}}{{m_{r,1}}^{*}} - \ddot{x}_b$$

In case there are more rowers in a boat, the forces on the boat are the sum of all the forces delivered by the separate rowers. For rower i, the *Forces* method can describe the relative motion with eq. (4.19), where all the forces are separated to show the influence of the different masses of the system on the relative acceleration of the rower.

$$\ddot{u}_{r,i} = \ddot{x}_{r,i} - \ddot{x}_b = \frac{F_{foot,i}}{{m_{r,i}}^{*}} + \frac{F_{foots}}{m_b^*} - \frac{F_{handle,i}}{{m_{r,i}}^{*}} - \frac{F_{gates}}{m_b^*} + \frac{F_{drag}}{m_b^*} \tag{4.19}$$

The relative motion of a rower will always be dependent on the boat motions and the other way around. To model the boat accelerations correctly, the rower motions should be known and to predict the rower motions the boat motions are needed.

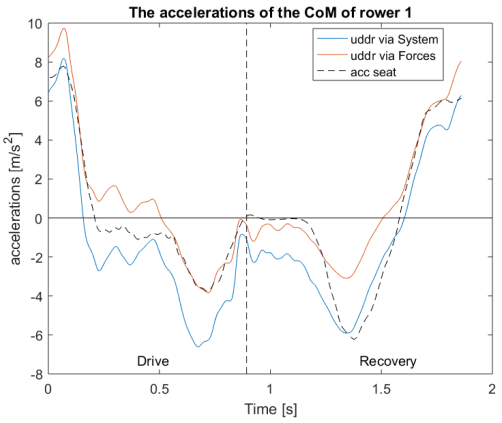

(a) The relative acceleration of the CoM of the rower calculated via two methods; the *System* method and the *Forces* method.

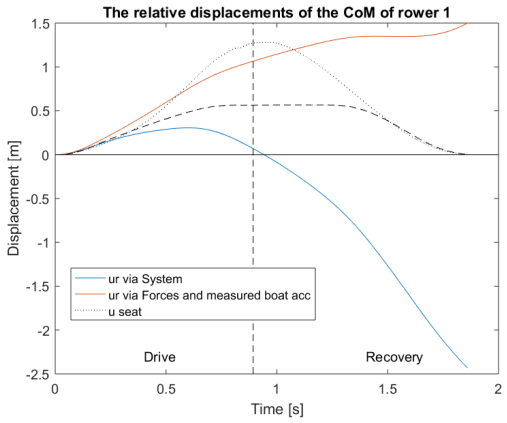

(b) The relative displacement of the CoM of the rower calculated via two methods; the *System* method and the *Forces* method.

Figure 4.15: The relative displacement (u_{r1}) and acceleration ($\ddot{u}_{r1}$) calculated with the *System* method, where the relative acceleration of rower 2 ($\ddot{u}_{r2}$) is calculated with the *Forces* method (eq. (4.15)). The relative acceleration of the rower is compared to the seat acceleration and the relative displacement or the rower with the seat and handle displacement.

In fig. 4.15, the accelerations and relative displacement of the CoM of rower 1 are shown according to the *System* and *Forces* methods. The relative acceleration of rower 2 is also calculated according to the *Forces* method. The relative accelerations of rower 1 seem to be better predicted by the *Forces*

method than by the *System* method, see fig. 4.15a. However, looking at the relative displacement of rower 1 (fig. 4.15b), neither of the equations lead to a CoM of the rower returning to the catch position.

The results for the *System* method are disappointing. To study the influence of rower 2 on the relative motion of rower 1, several inquiries are done. The relative acceleration of rower 2 is based on the measured seat acceleration, this leads to a u_r that roughly returns to the catch position (fig. A.12). Using the seat acceleration to predict the motions of rower 2 is not really using a self-containing model and is not in line with the goal to create a more precise estimate of the relative motions of the rowers. When the relative acceleration of rower 2 is completely neglected, actually the relative motion of rower 1 is still reasonable (fig. A.13). However these tests of the model are not very realistic and will therefore not be included in further modeling of the rower's motions.

There need to be made some changes to the estimation of the relative motions of the rower based on the *Forces* method, because in section 4.2.2, the foot forces were the worst predictor of the displacement of the center of mass of the rower. The calculation via the *System* method did not overcome this problem.

4.4.2. Virtual resistance force

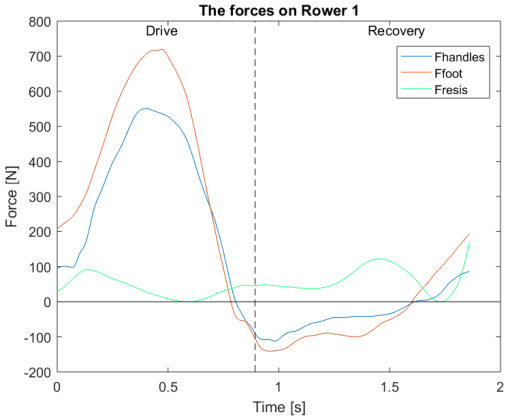

(a) The forces acting on rower 1 after introduction of F_{resis}.

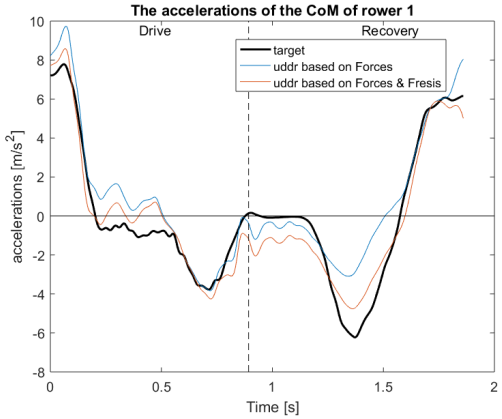

(b) The relative accelerations of rower 1 with and without introduction of F_{resis}.

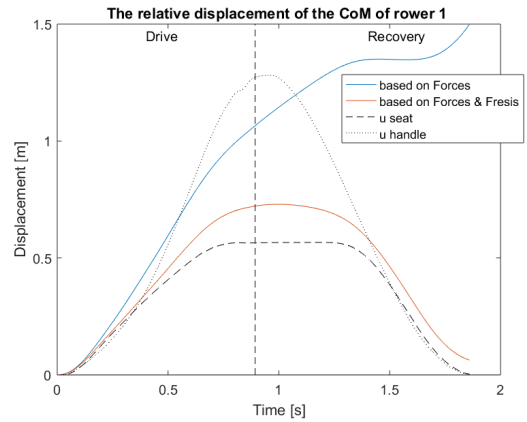

(c) The relative displacement of rower 1 with and without introduction of F_{resis}.

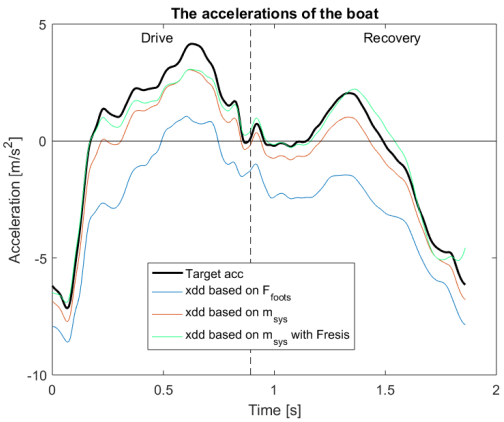

(d) The boat accelerations with and without introduction of F_{resis} on both rowers.

Figure 4.16: The introduction and effect of a virtual resistance force F_{resis} on the relative motions of the rowers and the boat acceleration.

Some small forces on the rower are neglected, such as the small ramp in the slides (small gravity force component in opposite x-direction), the friction in the slides and some turbulence around the blade. To cover these forces a virtual resistance force (F_{resis}) is introduced. This force must compensate

for the overshoot of the relative displacement of the rower (u_r) when modeling u_r based on the foot force. The resistance force is implemented in the *Forces* method as shown in eq. (4.20). The virtual resistance force is composed of multiplications of the boat displacement (x_b), boat velocity ($\dot{x}_b$), absolute displacement of the rower (x_r) and velocity of the rower ($\dot{x}_r$). The specific function of F_{resis} is given in appendix A.6.

$$\ddot{u}_{r,i} = \frac{F_{foot,ri} - F_{handle,ri} - F_{resis}}{m_{r,i}{}^{*}} - \ddot{x}_b \tag{4.20}$$

In fig. 4.16 the virtual resistance force is optimized for rower 1. The relative acceleration of the rower is optimized towards the measured seat acceleration to see if movements can be reached. The same resistance force is applied to both rowers to calculate the resulting boat acceleration.

The influence of the resistance force is larger during the recovery. The force itself has the biggest value there (121 N) and the foot and handle forces on the rower are much smaller in this phase. A relatively small force can make a big difference in the recovery.

The relative displacement of the rower (calculated via the *Forces* method) is improved after the introduction of F_{resis}. The CoM of the rower is almost in the same position at the end of the stroke as in the beginning. The maximum displacement lies properly between u_{seat} and u_{handle}.

The boat acceleration is improved for the m_{sys} method but not via the F_{foots} method (see previous section). This is logical, because in the F_{foots} method the relative motions of the rower are not directly implemented in the calculation of the boat acceleration. In this method the interaction force between the rower and boat is created by the foot forces.

The boat acceleration calculated via m_{sys} is definitely improved, although the maximum measured boat acceleration is not reached yet. Also the shape of the acceleration curve is changed, but now the shape matches less with the measured boat acceleration. The boat performance is thus not modeled in an optimal way by introducing the resistance force.

4.4.3. Changes in the foot force

The negative (pulling) forces of the footstretcher are smaller than expected. Adding an extra resistance force as in section 4.4.2 does solve some problems for u_r, but the shape of the boat modeled acceleration curve is changed into a less good version. It becomes more likely that the offset between the modeled and measured boat acceleration and thereby the relative movement of the rower are caused by the input data itself; the measured forces. Therefore in this section the measured foot forces are investigated, the effects of introducing a gain and adding an offset to the force are shown.

Scaling F_{foot}

By changing the gain of F_{foot} a calibration fault in the gain could be compensated. The standard gain of the foot force is 1 and by trial is found that bigger gains would result in worse fits for both u_r and $\ddot{x}_b$. Therefore there is chosen to show only the effects of five gains of smaller than 1. The gain the foot forces of rower 1 and 2 is changed with the same value in this sensitivity analysis.

As shown in fig. 4.17a, a smaller gain of the foot force leads to better results for u_r in the drive, but not in the recovery. For a too small gain, the rower does not move far enough, however for bigger gains, the rower does not return to the initial position.

For $\ddot{x}_b$ the results are better in the drive phase as well. However, in the recovery the gain does not influence the boat acceleration much. This is expected, because of the size of the original foot force in the recovery, with respect to the drive (fig. 4.3a). Changing only the gain of the foot force will not result in a better model prediction of u_r and $\ddot{x}_b$.

Adding an offset to F_{foot}

By changing the offset of F_{foot} there could be compensated for an offset in the sensor calibration. The footstretcher is subject to pushing and pulling forces, the pulling however does not occur directly at the sensor, but via the shoes attached to the footstretcher. Therefore the pulling forces are dependent on how tight the shoe laces are fastened, in other words some kind of backlash occurs in the shoes. A small offset in the foot force may compensate for this phenomenon. The offset of rower 1 and 2 is changed with the same value in this effect analysis. A positive offset caused worse fits for both the boat acceleration and relative displacement of the rower, therefore only negative offsets are shown.

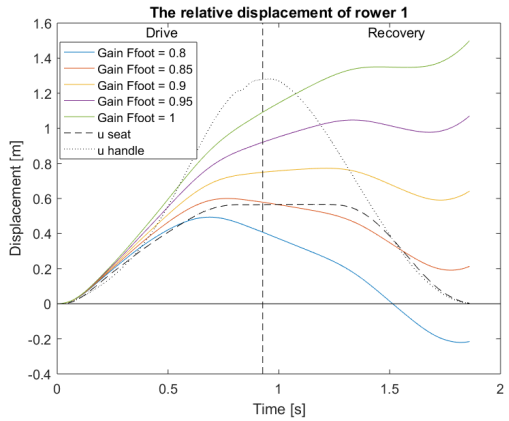

(a) The relative displacement of rower 1 for five different gains on the foot force.

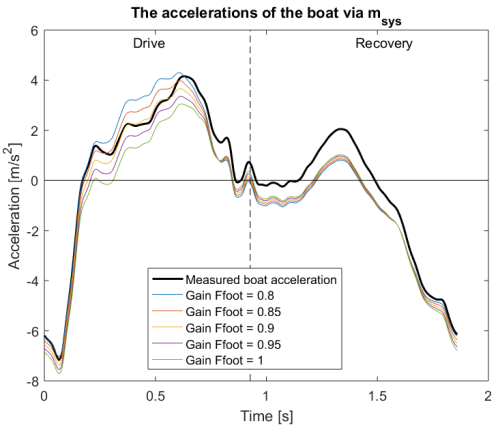

(b) The modeled boat acceleration for five different gains on the foot force.

Figure 4.17: The effect of five different gains for the foot force on the relative displacement of rower 1 and the boat acceleration. The different gains for which the results are presented are: 0.8, 0.85, 0.9, 0.95 and 1.

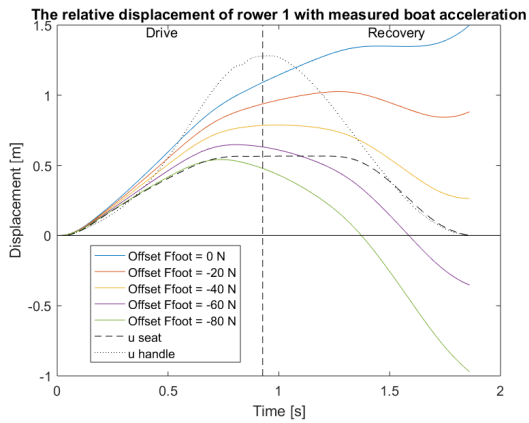

(a) The relative displacement of rower 1 for five different offsets on the foot force.

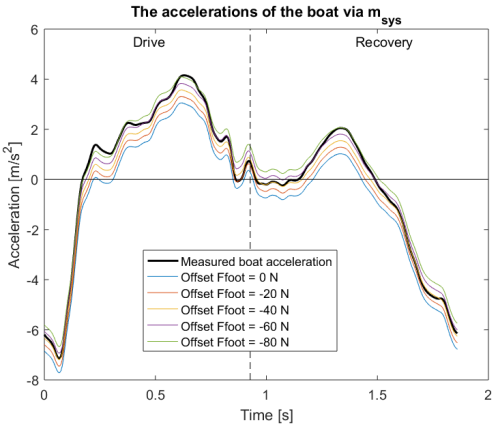

(b) The modeled boat acceleration for five different offsets on the foot force.

Figure 4.18: The effect of five different offsets for the foot forces on the relative displacement of the rower and the modeled boat acceleration. The chosen offsets are: 0 N, -20 N, -40 N,-60 N and -80 N.

By changing the offset of the foot force, the drive and recovery phase are both influenced. When looking at the trend of the different offsets, an offset of -50 N for rower 1, would result in a good curve of the relative movement. The boat accelerations would be optimal for an offset of approximately -70 N. Overall does changing the offset of the foot forces result in the best modeled movement and acceleration curves so far.

Potentially a combination of changing the offset and gain of the foot force per rower leads to the best results for the motions of both rowers and the boat acceleration.

Optimize offset and gain for F_{foot}

To find the best combination of offsets and gains for rower 1 and 2, an optimization is done with four parameters; [offset rower 1, offset rower 2, gain rower 1, gain rower 2]. The error function of the optimization is composed of the root mean square of the error between the measured boat acceleration and the modeled boat acceleration (via the m_{sys} method) and the difference between the final position of the relative movement of the rowers and their starting position.

$$\text{Error} = RMSE(\ddot{x}_{b,meas} - \ddot{x}_{b,mod}) + RMSE(\ddot{u}_{r,1}(t_{final}) - \ddot{u}_{r,1}(t_0)) + RMSE(\ddot{u}_{r,2}(t_{final}) - \ddot{u}_{r,2}(t_0)) \quad (4.21)$$

The final value for this error function after the optimization is 0.2059. The results of the optimization are shown in fig. 4.19. The relative displacement of the rowers in this optimization is still dependent on the measured boat acceleration.

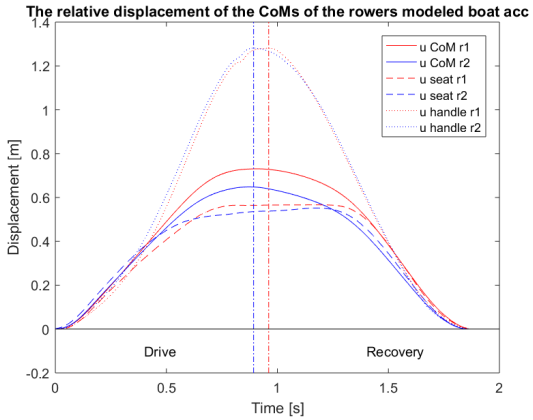

(a) The relative movement of both rowers calculated with an optimized offset and gain for F_{foot}, based on eq. 4.18 and with the measured boat acceleration.

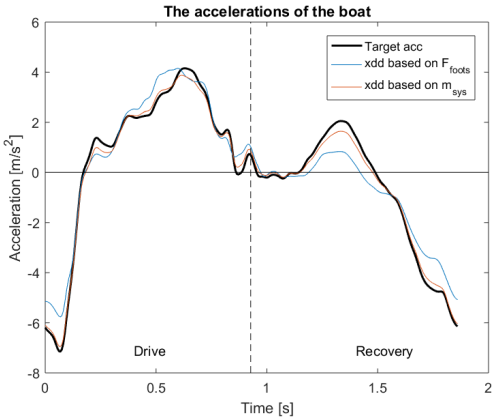

(b) The acceleration of the boat calculated with an optimized offset and gain for F_{foot}. The relative accelerations used in the m_{sys} method are the same as for the relative movement in fig. 4.19a.

Figure 4.19: The results for an optimized offset and gain for F_{foot}. The relative rower displacement in the error function is based on the measured boat acceleration (already optimal). The optimized variables that are found are; offset rower 1: -51.7709 N, offset rower 2: -48.7591 N, gain rower 1: 1.0114 and gain rower 2: 0.9295.

The results of the optimization are almost perfect, the rower's relative displacement lies between the seat and handle displacement and returns exactly to the starting position. The boat acceleration is almost a perfect fit. Although the boat acceleration calculated based on the m_{sys} method (eq. (4.18)) is optimized, the boat acceleration based calculated via eq. (3.20) is improved as well, with the new variables for the gain and offset of the foot force.

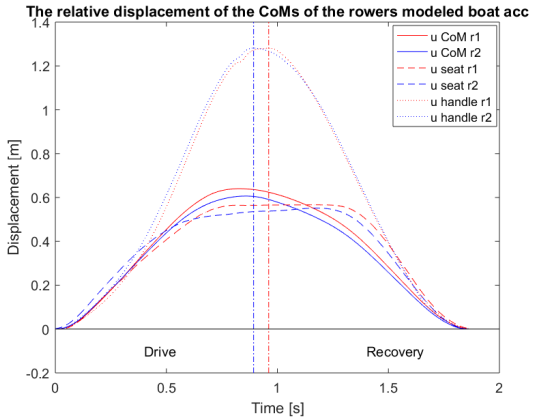

(a) The relative movement of both rowers calculated with an optimized offset and gain for F_{foot} based on eq. 4.18 and with the modeled boat acceleration.

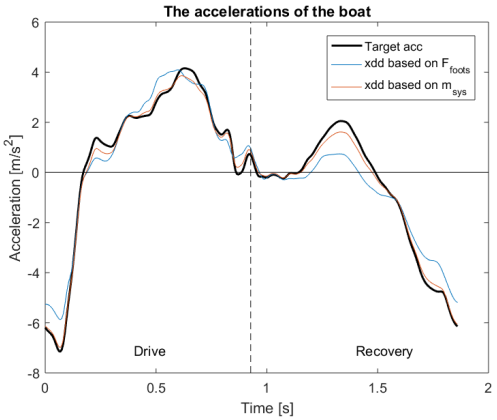

(b) The acceleration of the boat calculated with an optimized offset and gain for F_{foot}. The relative accelerations used in the m_{sys} method are the same as for the relative movement in fig. 4.20a.

Figure 4.20: The results for an optimized offset and gain for F_{foot}. This time the relative rower displacement in the error function is based on the modeled boat acceleration instead of the measured boat acceleration. The optimized variables that are found are; offset rower 1: -43.5337 N, offset rower 2: -52.0547 N, gain rower 1: 0.9895 and gain rower 2: 0.9471. The forces acting on the rowers are shown in fig. 4.21. The foot force of rower 1 is changed with 7.1% and the foot force of rower 2 with 12.1%.

The optimization of the gain and offset of the foot forces can also be done for the relative rower displacement based on the modeled boat acceleration (instead of measured boat acceleration). Ex-

pected is that the parameters will be a little different, but no large changes are allowed. The results of this optimization are shown in fig. 4.20. The resulting value of the error function is 0.2152, this is only slightly worse than the previous optimization. Considering that the relative displacement of the rower's CoM are now based on a modeled acceleration instead of an already "optimal" version.

Both optimizations result in a smooth curve for the relative movement of the rower. It exceeds the seat motion in the finish position, which is exactly what is expected (remember fig. 4.8). A three-dimensional model by Serveto et al. [51], predicts a similar curve for the displacement of the rower in x-direction. A higher maximum displacement of the center of mass of the rower with respect to the seat, would point to a rower with a larger "back-swing". A smaller maximum means that the rower sits more upright in the finish position.

There are also small differences, in fig. 4.20a the center of mass lies a bit below the seat in the drive phase. This is explainable, when the rower would move her seat backwards faster than the shoulders, this technical error is called "bum-shoving". The "bum-shoving" is an example of an error that is not recognized with the state of art ways to study/model the relative motions of the rower, but can now be noticed. In the recovery phase, the CoM of the rower lies typically in front of the seat. For the boat acceleration no significant differences are found.

The results of the optimized gain and the offset of the foot force are promising. The relative motion of each rower is within the expected range of the seat and the handle displacement and the measured boat acceleration is approached very closely.

The model might be improved further by optimizing the offset and gain of the gate forces, or optimizing for the model parameters $\%_{m,rowerboat}$, $\%_{m,added}$, C_1 and v_{avg}. In a new optimization these parameters might stay within their boundaries. However, it is more interesting to see if this model can predict some effects of changes in the rigging parameters, this is done in chapter 5.

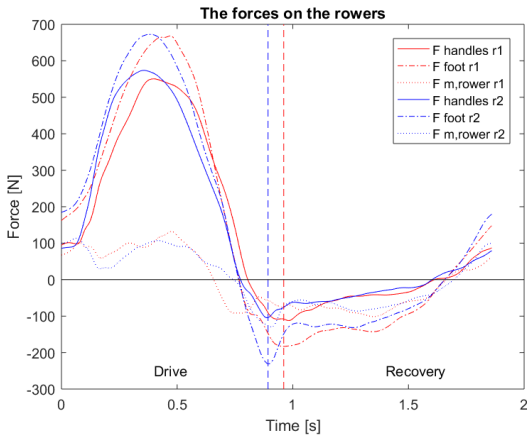

Figure 4.21: The forces acting on the rowers after changing the gain and offset of F_{foot}.

Summary Chapter 4

In this chapter an one-dimensional rowing model is presented and improved. A double is modeled, because the available data is measured in this boat type. The distribution of the masses in the system are slightly changed to make the model more realistic. The relative movements of the rowers are predicted based on different approaches, the most individualized approach is to use the forces acting directly on the rower.

The acceleration of the boat is described with different approaches; by the forces acting directly on the boat and combining the acceleration of the system with the relative acceleration of the rowers. The latter does a better prediction on the boat acceleration. Changing some of the estimated model parameters improves the fit for the boat acceleration, but does not reach an optimum. Adding an extra resistance force to the rower results in a better relative movement of the rower and slightly better boat acceleration. The best fit for the boat acceleration and relative movement of the rower is found by changing the offset and gain of the measured foot force of the rowers.

5

Changing the rigging setup

With the model established in the previous chapters, the boat acceleration is predicted with a reasonable accuracy. Using this model while changing some parameters in the rigging, can give more insight in the effect of these parameters on the boat performance. In this chapter a converted model is presented which is driven with the forces applied by the rower as calculated in the model, the drag force on the hull and the rower movements. Subsequently, the rigging parameters are changed and the effects on the boat acceleration and velocity are calculated, using the m_{sys} method.

In appendix C a graphical interface is presented in which multiple rigging setup parameters can be changed. The new rigging setup, handle and blade paths are shown in a graph. The effect of the parameter change on the force-angle curve of the rower and boat velocity is shown in figures in the interface as well. This tool would be a nice way to present rowing coaches with the modeled effects of a change in the rigging setup of a rower.

Important note: In this model, the rower is assumed to be a force constraint system, this means that she can deliver the same force over the handle displacement despite changes in the rigging setup. There are no restrictions in the power output of the rower. A power constraint system would probably be more accurate for rowing at race pace. The delivered power of the rower (at the handle) has to be monitored in the obtained results. The handle power is calculated with eq. (5.1) and the work over one stroke is the integral of power on both handles over the total stroke. No restrictions in the movement of the rower in y-direction are composed, it is assumed that the arms of the rower can reach any angle of the oar movement.

$$P_{handle} = {l_{inboard}}^{*} \cdot F_{handle} \cdot \dot{\theta} \tag{5.1}$$

$$W_{stroke} = \int_{t0}^{t_{final}} P_{handles}\, dt \tag{5.2}$$

5.1. The variable parameters

Two rigging parameters are changed in the model, one in the longitudinal (x-)direction of the boat and one in the oar length parameters. From the model, the forces and motions of the rower under the original circumstances are deduced. The model variables are assumed to remain constant: F_{handle}, u_{handle}, u_r and F_{drag} In reality the drag force is dependent on the boat velocity, which is probably changed due to the parameter changes, however the changes in the drag force are assumed to be negligible. Therefore the changes in boat acceleration are only dependent on the change of the blade forces.

$$\ddot{x}_b = \frac{F_{blades} - F_{drag} - \sum_{i=N} \left({m_{r,i}}^{*} \cdot \ddot{u}_{r,i}\right)}{{m_{sys}}^{*}} \tag{4.18}$$

The blade forces in eq. (4.18) are derived from the handle forces as shown in eq. (5.3), which is a simplified rewritten version of eq. (3.8). In this equation, the relation between the blade force, oar

angle (θ) and oar lever ratio is shown. The oar angle belonging to a changed rigging setup is calculated with eq. (5.4).

$$F_{blade} = \frac{F_{handle,X} \cdot \cos(\theta) \cdot {l_{inboard}}^* - I_{gate} \cdot \ddot{\theta}}{{l_{outboard}}^*} \tag{5.3}$$

$$\theta = \arcsin\left(\frac{u_{handle}}{{l_{inboard}}^*}\right) \tag{5.4}$$

Oar lever ratio The oar length parameters determine the lever ratio between the handle force and blade forces. The force applied by the rower at the handle is assumed to be constant for every rigging setup. Also the displacement of the handle in x-direction is assumed to stay similar under different rigging setups. By changing the lever ratio of the oar, the blade force applied on the water and the oar angle over the stroke is changed (see fig. 5.1). The power applied by the rower is also altered, but in reality this is not always possible for the rower to accomplish. The effects of the rigging parameters of the oar are more of a test whether the change in lever ratio does influence the boat performance and not whether the rower's behavior is improved. The parameter that is chosen to investigate the influence of the oar lever ratio on the boat motions is the inboard length of the oar. The inboard length is changed by changing the position of the collar on the oar. If the total oar length remains constant, this means that the outboard length of the oar changes as well with the same distance ($\Delta l_{inboard}$ = -$\Delta l_{outboard}$).

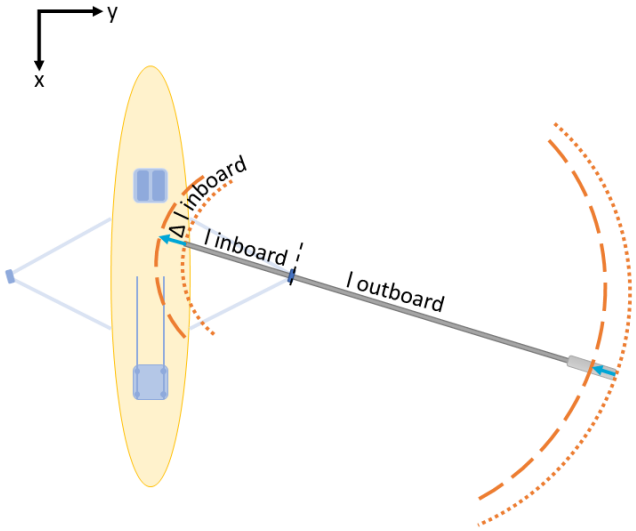

Figure 5.1: A simplified sketch of the effect of changing the inboard length of the oar in the model. The handle displacement in the boat remains constant, thus for a smaller $l_{inboard}$, θ increases and the distance traveled by the blade as well.

Change of position of the footstretcher A change of the position of the footstretcher with respect to the gate would theoretically lead to the same displacement of the rower with respect to the gate (Δx_{foot} = Δx_{CoM}). Since the coupling between the handle position and the rowers CoM is not established, the same shift in x-position of the handle is assumed (Δx_{foot} = Δx_{handle}). When the change of the position of the footstretcher is studied, a shift of oar displacement in x-direction is used in the model, see fig. 5.2. This assumption is done because the rower is modeled as a point mass and her movements in other directions than x-direction are neglected.

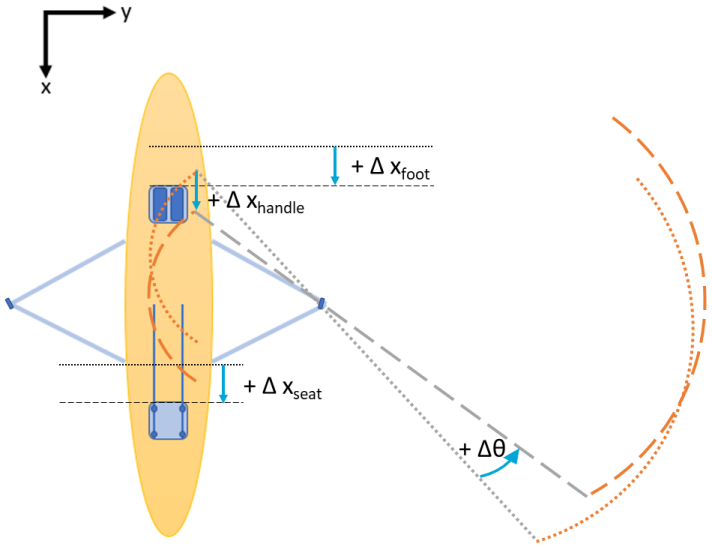

Figure 5.2: A simplified sketch of the effect of changing position of the footstretcher in the model. Δx_{foot} is the change in footstretcher position, Δx_{seat} is the change in the seat position, Δx_{handle} is the change in the (start) position of the handle. The oar angle is calculated with: $\theta = \arcsin(x_{handle}/l_{inboard})$, and $\Delta\theta = \theta_{new} - \theta_{old}$.

5.2. Effects of the parameters

The theoretical effect of the changing rigging parameters is shown in fig. 5.1 and fig. 5.2. Both parameters change the blade path with respect to the boat. In this section the effects of these changed blade paths and forces on the boat acceleration and velocity are discussed. The modeled boat velocity is calculated as the integral of the boat acceleration, using the "standard" initial velocity of the model (eq. (4.16)).

The calculations done in this section result in an incomplete energy balance, this is not realistic. The calculation are done to see if a trend can be found between the changes of the rigging parameters, the boat performance and possibly a better synchronization between the rowers.

5.2.1. Change inboard length oar

To study the effect of the inboard length changes, the inboard length is increased with 4 cm and decreased with 4 cm. Bigger changes in the inboard length are not used often in rowing. Besides, the handle displacement in x-direction can not be guaranteed anymore by a too short inboard length. In appendix A.9 more extreme changes of the inboard length are shown.

In fig. 5.3 the effect of three different inboard lengths on different boat variables is shown. The "original" inboard length of the oars is 0.88 m. A change of the inboard length of the oar results in a different oar angle as shown in fig. 5.3a. The total covered oar angle is increased for a smaller inboard length.

The handle power is slightly changed for different inboard lengths. The new power curves do not deviate much from the original power applied on the handle. Assumed is that the rower is able to deliver the new power at the handle. The work that the rower delivers per stroke is given in the legend of fig. 5.3b. The work per stroke decreases for a longer inboard length. The moment of the handle ($F_{handle} \cdot l_{inboard}$) increases, but the total angle segment of the stroke and the oar angular velocity of the oar decrease. The fluctuations of the handle power around the peak of the curve and in the finish, are caused by the differentiation that is done to determine the oar angular velocity based on the handle displacement.

As shown in fig. 5.3c and fig. 5.3d, the boat motions are changed due to the different inboard lengths. With a longer inboard length, the boat acceleration is increased in the drive phase and slightly decreased around the finish and the beginning of the recovery. The fluctuations of the curve are caused by differentiation of the oar angle. The boat velocity is increased with a longer inboard length of the oar. How much the average velocity of the stroke is influenced by the changed inboard lengths is presented in section 6.4.

Practically, there is an inboard length for which the rower is not able to reach the movements that

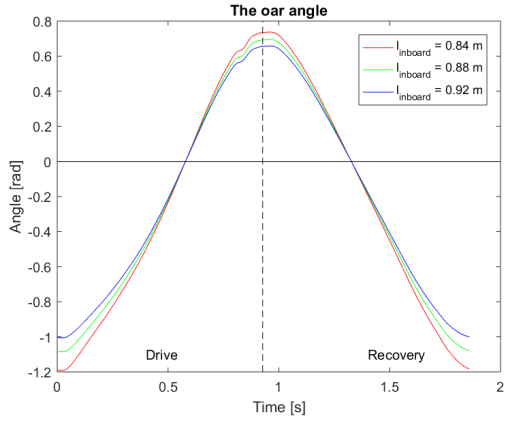

(a) The oar angle for three different $l_{inboard}$.

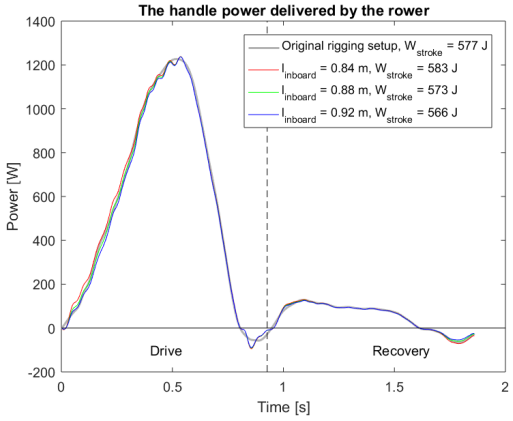

(b) The handle power for three different $l_{inboard}$.

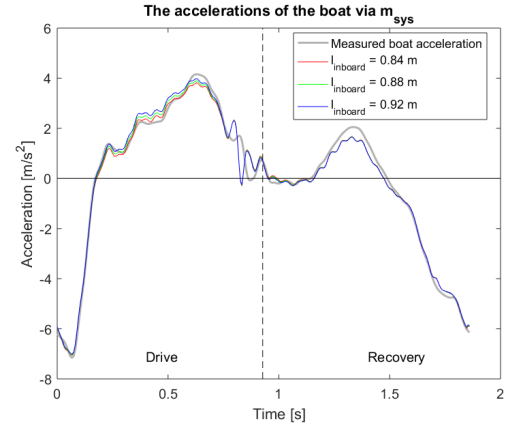

(c) The boat accelerations for three different $l_{inboard}$.

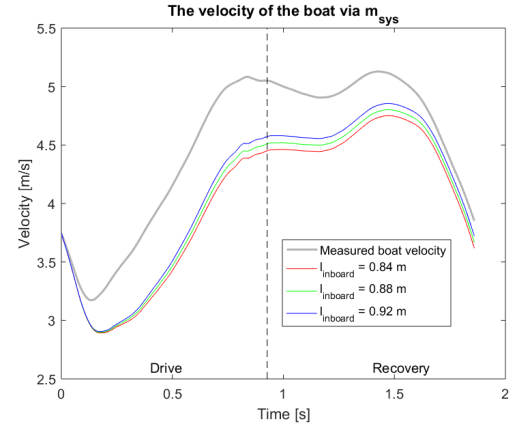

(d) The boat velocity for three different $l_{inboard}$.

Figure 5.3: Four boat variables for three different inboard lengths. The inboard length of rower 1 is changed, while rower 2 uses the original setup. The slight alteration of the boat acceleration just before the finish is probably due to the double derivative of the oar angle needed to calculate F_{blade}.

are imposed by the oar handle. Either the rower has to spread her arms too much for a small inboard length, or the oars have to much overlap for the crossing arms to deal with. These problems can partly be taken care of by changing the span of the boat. This is again limited by practical boundaries.

5.2.2. Change position of the footstretcher

The effect of three different positions of the footstretcher on four different boat variables is shown in fig. 5.4. The absolute original position of the footstretcher is unknown, but as stated in section 5.1, the relative movement of the oar is shifted with the same displacement as the footstretcher. Therefore Δx_{foot} is added to u_{handle} and is introduced into the model.

The chosen values for Δx_{foot} are -5 cm and +5 cm. This means that the footstretcher is moved respectively 5 cm towards the stern and 5 cm towards the bow of the boat. Bigger changes in foot position are practically possible in the boat, but to investigate the influence of the changes in position 5 cm should be enough.

Changing the footstretcher position with 5 cm towards the bow increases the oar angle with 6 °. Placing the footstretcher with 5 cm towards the stern causes a decrease in oar angle of 8 °.

A change of the footstretcher position results in a different oar angle as shown in fig. 5.4a. The total covered oar angle remains the same, but the curve is shifted up or down depending on the direction of the footstretcher position change. The handle power is changed more than for the different inboard lengths, however the deviations from the original applied power on the handle are still not so big that the rower can not deliver the power. The fluctuations due to the derivative of the angular velocity are visible around the peak of the curve and finish.

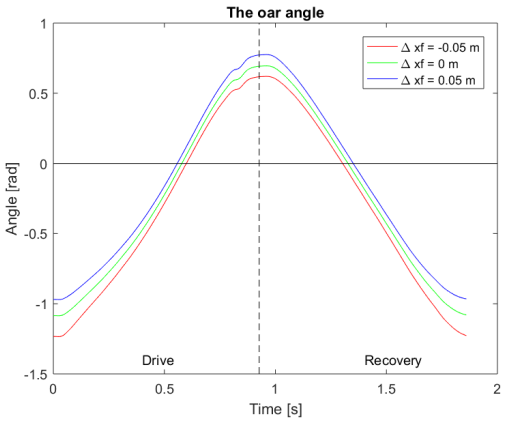

(a) The oar angle for three different Δx_{foot}.

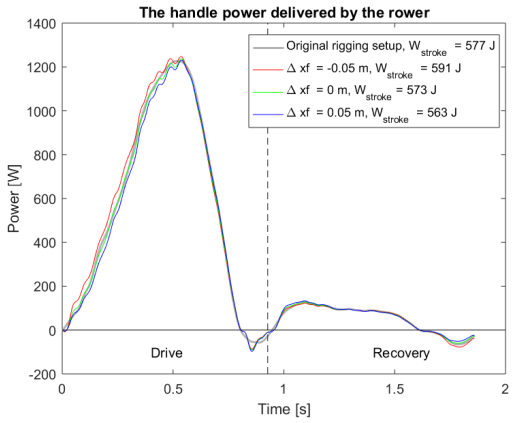

(b) The handle power for three different Δx_{foot}.

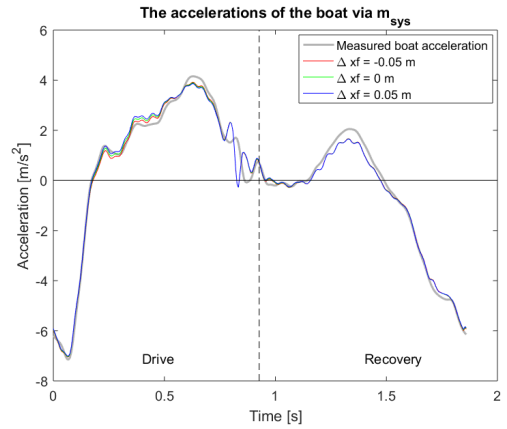

(c) The boat acceleration for three Δx_{foot}.

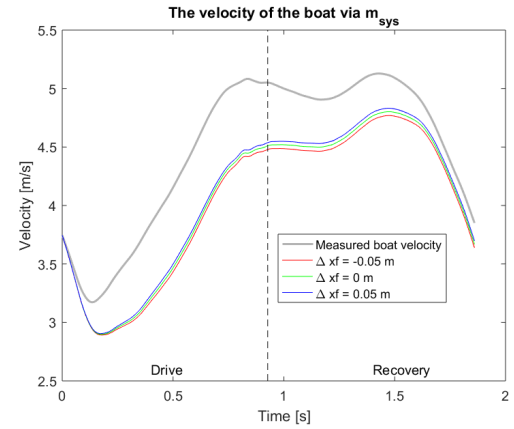

(d) The boat velocity for three different Δx_{foot}.

Figure 5.4: Four boat variables for three different footstretcher positions. The footstretcher position of rower 1 is changed, while rower 2 uses the original setup. The slight alteration of the boat acceleration just before the finish is probably due to the double derivative of the oar angle needed to calculate F_{blade}.

The boat motions are changed for different footstretcher positions. The boat acceleration is increased in the drive phase for a footstretcher position moved in direction of the bow. This leads to an increased boat velocity. How much the average velocity of the stroke is influenced by the changed foot stretcher position is presented in section 6.4.

There is an optimum in the oar movement around the gate. When the oar is positioned perpendicular to the boat, the blade force moment is the largest and the propulsive force on the boat the biggest. When the footstretcher is moved to far towards the bow, the stroke can not be finished, because the oar crashes into the boat. The blade forces for an oar parallel to the boat are not propulsive anymore. In this case the boat acceleration can not be calculated with the model. In appendix A.9 more extreme position changes of the footstretcher are proposed, where the point of improvement of the boat velocity due to the shifted footstretcher position is exceeded.

The boat velocity is increased for a longer inboard length of the oar and a footstretcher position further towards the bow of the boat. The blade forces in these cases are bigger. This is due to the changed blade path, smaller lever ratio and the application of the peak force at a more favorable angle.

An optimization of the two parameters for rower 1 and 2 will not result in surprising new conclusions. Since within the currently used range, the average boat velocity is only increased for a bigger $l_{inboard}$ and Δx_{foot}. An optimization will be limited by the boundaries composed on each parameter.

Summary Chapter 5

The rigging parameters in the model are changed with the assumption that the rower is a force constrained system. The rower's forces and motions in x-direction are assumed to remain constant, as well as the drag force. There are no restrictions on the movements of the handle. The changes in boat motions are caused mainly by changes of the blade forces for a different rigging setup.

Changing the lever ratio of the oar, by increasing the inboard length, leads to a bigger total covered oar angle (in one stroke) and a higher boat velocity. Moving the footstretcher towards the bow of the boat shifts the oar angle and leads to a higher boat velocity as well.

The handle power applied by the rower is decreased when the boat velocity is increased. This indicates a deviation in the energy balance of the system.

6 Results

This chapter presents the results that are obtained by the model; the obtained fits for the boat acceleration and the predicted relative motions of the rowers. Also the found relations between the different variables of the system and the rigging parameters are presented.

The model results are based on different assumptions that are discussed all through the report, therefore in section 6.1, a list of the most important assumptions is given. The found results and predictions are presented in section 6.2, 6.3 and 6.4. In the discussion the effect of the assumptions on the results is discussed and put in the right perspective.

In appendix B the results of other doubles are shown. The data from these doubles is received in a late stage of the project, which is why the results are not further incorporated in this thesis.

6.1. Assumptions

For the boat the following assumptions are made:

- Only the movements of the boat in x-direction are included in the model. This means that the pitch, yaw, roll, heave and sway motions of the boat are neglected.
- The losses due to internal work (bearing friction, etc.) are neglected.
- The drag forces on the boat are assumed to be all viscous and proportional to the square of boat velocity.

For the oar most assumptions are discussed in section 3.3.2, the short list is:

- Distances s and r are zero, causing the CoM of the oar to be at the same point as the pin and the oar rotates around its CoM.
- There is assumed to be no oar flexibility, meaning that the oar will not be able to hold deformation energy and the same axial system is valid for the whole oar.
- The resultant oar blade force is perpendicular to the blade.
- The axial forces at the oar blade are neglected, because they can not be measured.
- The air resistance on the oar is negligible.
- The oars move in symmetry through the boat and the water.

The rower is modeled with the most assumptions and no physiological modeling is done. However, because the data used as input in the model is measured from real rowers, there is certainty that a rower is able to apply the forces on the handle and footstretcher.

- The rower is modeled as a point mass. This means that motions (of the masses) of the different body segments are not taken into account separately.

- The rower's CoM is assumed to only move in x-direction. In reality a rower also has degrees of freedom in y- and z-direction.
- It is assumed that the handle force in x-direction is the only force that acts on the rower in the handle.
- The rower does not gain or return potential energy due to the slight ramp in the slides.
- The rower is not subjected to air drag.
- The rower is assumed to row at a constant speed and pace over the analyzed part of the practice race.
- The rower is assumed to be a force constraint system. This means that she can deliver the same force over the handle displacement despite changes in the rigging setup.
- The handle displacement is linear dependent on displacement of the CoM of the rower and scales linear with a shift in the footstretcher position (with respect to the gate).

With these assumptions the boat and rower motions are modeled. The results will be discussed in the next sections.

6.2. Modeling the boat acceleration

To calculate the boat acceleration, two major methods are developed; the m_{sys} and F_{foots} method. In order to improve the results of these methods, four model parameters are optimized, a virtual resistance force is introduced on the rower and the gain and offset of the foot force are optimized. In fig. 6.1, the boat accelerations calculated via every approach are shown. The qualitative comparison of the curves is done using this graph. Some curves are overlapping slightly, for clarity in appendix A.7 the results are shown separately for the m_{sys} and F_{foots} method.

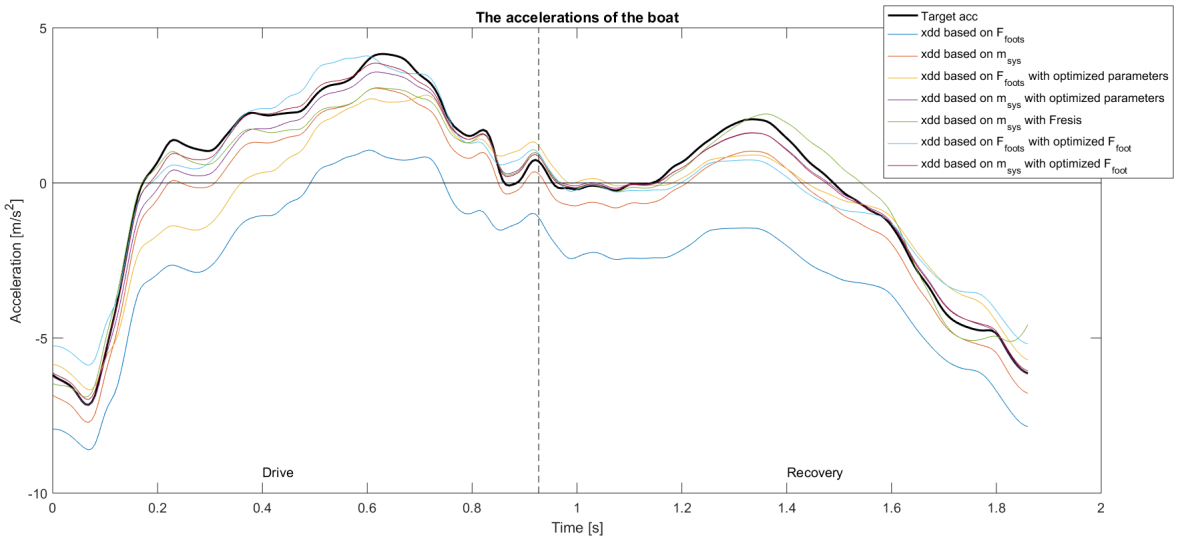

Figure 6.1: The results for $\ddot{x}_b$ via all different methods used in chapter 4.

A qualitative comparison of the modeled acceleration curves is done based on the shape of the curve and the height of the curve with respect to the measured boat acceleration curve.

To quantify the results and compare them, the root mean square error (RMSE) of the difference between the modeled and measured accelerations is calculated. The root mean square errors of the seven different methods that are used to model the boat acceleration are presented in table 6.1, where k are the samples in the vector and N is the total amount of samples in the stroke.

$$\text{RMSE(method)} = \sqrt{\frac{\sum_{k=1}^{N} \left(\ddot{x}_{b,measured}(k) - \ddot{x}_{b,modeled}(k)\right)^2}{N}} \tag{6.1}$$

Method	Shape	Height	RMSE
Based on F_{foots}	+	- -	2.7012 m/s^2
Based on F_{foots} with optimized parameters	+	-	1.1349 m/s^2
Based on F_{foots} with optimized F_{foot}	-	+	0.6805 m/s^2
Based on m_{sys}	++	0	0.8058 m/s^2
Based on m_{sys} with optimized parameters	++	+	0.3775 m/s^2
Based on m_{sys} with F_{resis}	-	++	0.4844 m/s^2
Based on m_{sys} with optimized F_{foot}	++	++	0.2152 m/s^2

Table 6.1: A qualitative and quantitative comparison of the methods used to model the boat acceleration. Where ++ means good, + is reasonable, 0 is neutral, - is bad and - - is very bad. The quantitative measure is the root mean square error (RMSE) of the results of all the methods used to model the boat acceleration.

The best obtained qualitative and quantitative fit for the boat acceleration is found with the m_{sys} method with optimized gain and offset on F_{foot}.

6.3. Predictions of the relative movement of the rower

In section 4.2.2 three methods to approach the relative movement of the rowers are proposed: based on the handle displacement, the forces on the rower (the *Forces* method) and the seat displacement. The *System* method is introduced in section 4.4.1. In order to improve the results of these methods a virtual resistance force on the rower is introduced and the gain and offset of F_{foot} are optimized. In fig. 6.2, the relative rower displacement calculated with every method is shown. The qualitative comparison of the curves is done using this graph. In fig. A.16, the same results are shown, but zoomed into the expected movement range, such that the difference between the methods are better visible.

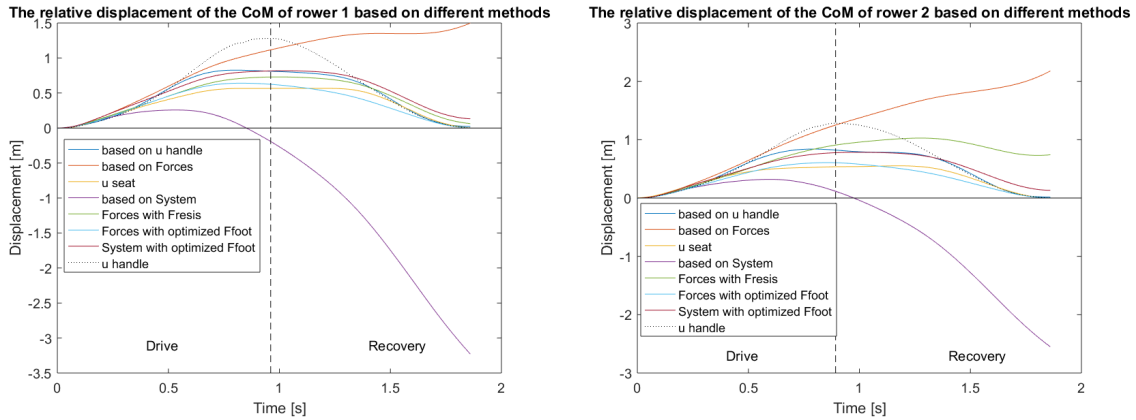

Figure 6.2: The resulting u_r for both rowers via all different approaches. In appendix A.8, the results are shown, zoomed in to the range of the expected rower motions. Such that the differences between the approaches are better visible.

The best result for the relative movement of the rower on both the qualitative and quantitative scale is obtained by the *Forces* method with the optimized gain and offset for F_{foot}. This is also found with data from other doubles in appendix B.

With the best result of the relative rower displacement, the segment of the rower based on her relative displacement is derived. With this segment a force-u_{CoM} curve is drawn (fig. 6.3). The force distribution of the rower over the relative displacement is assumed to be constant, for different rowing paces and rigging setups. The force-u_{CoM} curve can be used as a fingerprint curve for every rower.

In fig. 6.3 is found that the relative movement of rower 1 is over a longer segment than of rower 2. This is probably a rower with longer legs, but the longer stroke can also be the result of a different rowing technique. The calculation of the relative displacement of the rower is highly sensitive to small changes in the foot force. The relative motion of the rower is not absolutely correct for the different paces, a small difference of around 10 cm in the relative displacement is found at a different pace. Therefore in further results only the data of rowing pace 32 str/min will be considered.

Method	Drive	Finish	Recovery	Compare r1&r2	Error r1	Error r2
Based on u_{handle}	+	+	+	0	0.0226 m	0.0151 m
$Forces$ **	-	-	- -	+	1.4997 m	2.1787 m
u_{seat}	+	-	+	++	0 m	0 m
$System$ **	- -	- -	- -	+	-3.2290 m	-2.5500 m
$Forces$ with F_{resis} **	++	++	0	- -	0.0631 m	0.7415 m
$Forces$ with optimized F_{foot}	++	++	+	+	0.00052882 m	0.0010 m
$System$ with optimized F_{foot}	++	+	0	+	0.1317 m	0.1322 m

Table 6.2: A qualitative and quantitative comparison of the methods used to model the relative movement of the rowers. The quantitative measure (error) is the deviation of the rower movement at the end of the stroke from the starting position. r1 is rower 1 and r2 rower 2, ++ means good, + is reasonable, 0 is neutral, - is bad and - - is very bad. ** means that the method used the measured boat acceleration ($\ddot{x}_b$) to predict the relative rower movement.

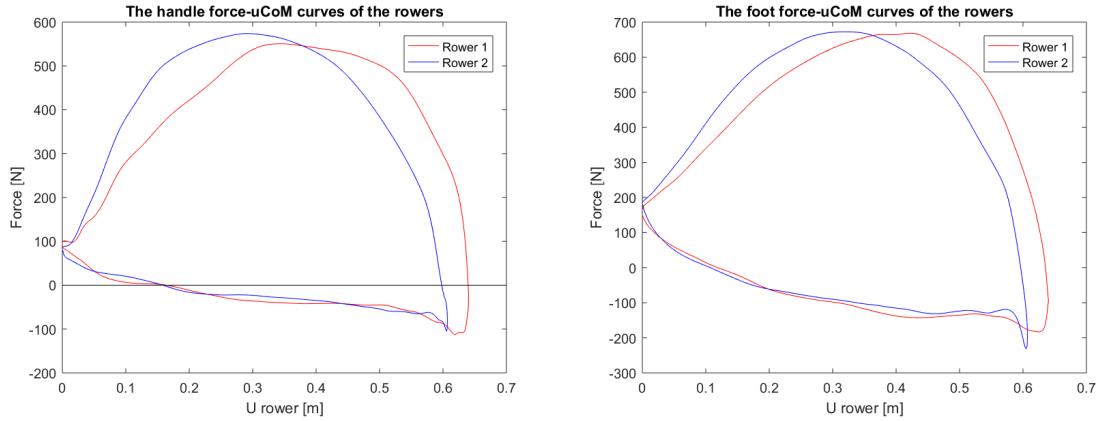

Figure 6.3: The averaged handle force-u_{CoM} curve (right) and averaged foot force-u_{CoM} curve (left) of both rowers. The force distribution of the rower over her own displacement is assumed to be constant, for different rowing paces and rigging setups.

6.4. Effects of the rigging parameters

The different rigging parameters that are changed in the model are introduced in chapter 5 as are the qualitative effects of the changes of these parameters. In this section the quantitative results of the different situations in rigging setup are presented, by taking the average velocity over the stroke.

$$\dot{x}_{stroke,avg} = \dot{x}_{boat,avg} = \frac{\sum_{k=1}^{N} \dot{x}_{boat}(k)}{N} \tag{6.2}$$

6.4.1. Average stroke velocity for changes of the lever ratio

When the inboard length of the oar is changed, the oar angle is changed as well. The blade forces are influenced by the oar angle and the lever ratio of the oar. In table 6.3, the average velocities of one stroke modeled with different inboard lengths for rower 1 and 2 are given.

Table 6.3: The average stroke velocity in nine different combinations of the inboard length of rower 1 and 2.

$\Delta l_{inboard}$		Rower 1		
		- 4 cm	0 cm	4 cm
Rower 2	-4 cm	3.9761 m/s	4.0189 m/s	4.0641 m/s
	0 cm	4.0208 m/s	4.0636 m/s	4.1088m/s
	4 cm	4.0681 m/s	4.1109 m/s	4.1561 m/s

The average velocity of the boat increases for increasing inboard lengths. For a longer inboard length the covered oar angle in the stroke decreases and the handle moment applied by the rower increases. The resulting power applied by the rower on the handle is decreased for a longer inboard length, as is the work done in one stroke.

No big differences between the two rowers are found for changing the inboard length of the oar. Rower 2 applies a bit more force to the handle than rower 1, probably this causes the small differences that are found in the table (compare 4.1109 m/s with 4.1088 m/s).

6.4.2. Average stroke velocity for changes of the footstretcher position

The position of the footstretcher is changed with respect to the boat and thereby with respect to the gate. This means that the rower has to move the handle over a different angle segment, but the total covered angle in a stroke stays the same. A positive displacement of the footstretcher leads to an angle segment that is shifted in positive direction and the other way around.

Table 6.4: The average stroke velocity in nine different combinations of the footstretcher position of rower 1 and 2.

Δx_{foot}		Rower 1		
		- 5 cm	0 cm	5 cm
Rower 2	-5 cm	4.0052 m/s	4.0329 m/s	4.0580 m/s
	0 cm	4.0359 m/s	4.0636 m/s	4.0886 m/s
	5 cm	4.0639 m/s	4.0916 m/s	4.1167 m/s

The average velocity of the boat increases when moving the footstretchers towards the bow. Within the range of the parameters currently studied, every centimeter that the footstretcher is moved towards the bow leads to a profit in boat velocity between 0.005 m/s and 0.006 m/s.

No big differences are found between the two rowers. This is remarkable, because in the original drive an oar angle difference between the two rowers is registered of approximately 0.07 rad (4°), as is shown in fig. 6.4.

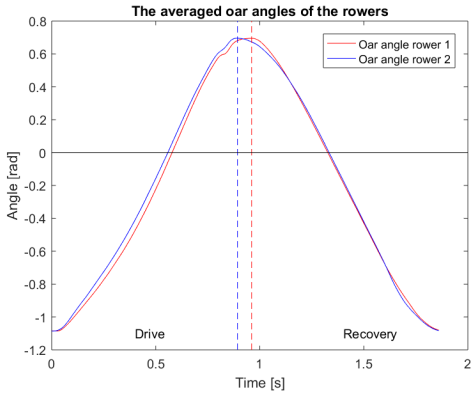

Figure 6.4: The averaged oar angles of rower 1 and 2.

6.4.3. Average stroke velocity for changes in both lever ratio and footstretcher position per rower

It is also possible to change both rigging parameters for the rower at the same time. By changing the inboard length and the footstretcher position at the same time, the path of the blade with respect to the boat is changed both in length and in angle.

The parameters are changed for respectively rower 1 and 2 in table 6.5 and 6.6. The resulting average velocity of the stroke is calculated for nine different rowing setups for every rower. The responses of rower 1 and 2 to the changes in rigging setup result in the same changes in boat velocity. The small differences between the average velocities are probably caused by the fact that rower 2 applies more force on the handle than rower 1.

An optimization of the parameters for rower 1 and 2 will not result in surprising new conclusions. If the rigging parameters are optimized within the currently studied range, the prescribed boundaries will be found as an optimum. Within the currently studied range, the average boat velocity is only increased for a bigger $l_{inboard}$ and Δx_{foot}.

Table 6.5: Average stroke velocity in nine different combinations of inboard length and footstretcher position of rower 1.

Rower 1		$\Delta l_{inboard}$ - 4 cm	0 cm	4 cm
Δx_{foot}	-5 cm	3.9990 m/s	4.0359 m/s	4.0799 m/s
	0 cm	4.0208 m/s	4.0636 m/s	4.1088 m/s
	5 cm	4.0447 m/s	4.0886 m/s	4.1343 m/s

Table 6.6: Average stroke velocity in nine different combinations of inboard length and footstretcher position of rower 2.

Rower 2		$\Delta l_{inboard}$ - 4 cm	0 cm	4 cm
Δx_{foot}	-5 cm	3.9944 m/s	4.0329 m/s	4.0789 m/s
	0 cm	4.0189 m/s	4.0636 m/s	4.1109 m/s
	5 cm	4.0457 m/s	4.0916 m/s	4.1393 m/s

Table 6.7: The work per stroke at the handle for rower 1 in nine different combinations of inboard length and footstretcher position. The work per stroke applied by rower 1 in the original rigging setup is 577 J.

Rower 1		$\Delta l_{inboard}$ - 4 cm	0 cm	4 cm
Δx_{foot}	-5 cm	608 J	591 J	579 J
	0 cm	583 J	573 J	566 J
	5 cm	570 J	563 J	557 J

Table 6.8: The work per stroke at the handle for rower 2 in nine different combinations of inboard length and footstretcher position. The work per stroke applied by rower 2 in the original rigging setup is 561 J.

Rower 2		$\Delta l_{inboard}$ - 4 cm	0 cm	4 cm
Δx_{foot}	-5 cm	596 J	576 J	563 J
	0 cm	567 J	556 J	548 J
	5 cm	551 J	543 J	537 J

The work per stroke delivered by the rower on the handle for different rigging setups is presented in table 6.7 and 6.8. A relation is found between an increase in the inboard length and a decrease in the delivered work for both rowers. This is not in line with the increase in average boat velocity found in table 6.5 and 6.6. The energy balance in the system is not preserved and the obtained results are not completely realistic, due to several assumptions. The results should be interpreted as a sensitivity analysis of the modeled boat performance on changes in the rigging setup.

Summary Chapter 6

Various methods are used to predict the boat acceleration. After comparison with the measured boat acceleration, the best obtained qualitative and quantitative (RMSE = 0.2152 m/s^2) fit for the boat acceleration is found with the m_{sys} method with optimized gain and offset for the foot forces. For predicting the relative motions of the rower also various methods are used. The motions of the rower should be modeled with an individualized approach. The best result for the relative movement of the rower on both the qualitative and quantitative scale is the *Forces* method with the optimized gain and offset for the foot force.

Changing individual rigging parameters did not result in big differences between the rowers. Changing the lever ratio of the oar, by increasing the inboard length leads to a bigger total covered oar angle and a higher boat velocity. Moving the footstretcher towards the bow of the boat shifts the oar angle and leads to a higher boat velocity as well.

The energy balance of the system is not preserved due to several assumptions. The found results of the modeled boat performance on changes in the rigging setup, should be interpreted as a sensitivity analysis and not a realistic prediction.

Discussion

In this chapter, several factors that might influence the results found in chapter 6 are discussed. Also other factors that might improve the results are proposed. The assumptions done in building the model are shown in section 6.1, the effects of some of these assumptions on the results is discussed.

Repeatability

Single dataset One of the possible shortcomings of this research could be the fact that the model is tested build and tested with one dataset. However, only one dataset was available during this study which included measurements of the foot forces. This means that the results and the fit of the model are dependent on the protocol and calibration of this one dataset. The equations are still valid and the results (after fitting the parameters) seem to agree with the measured and expected data.

In appendix B three more datasets have been run through the model. The results of both the boat acceleration and the relative displacement of the rower are approached quite well after compensation of the foot force. This shows that the model is not too dependent on the one dataset. However, there is too little data to gain statistical power from these results. Every dataset needs a different compensation of the foot forces to obtain good results for the relative motions of the rower. These compensations differ per dataset, which makes the results more difficult to compare.

Irregularities within the dataset The relative displacements of the rowers changes between the different rowing paces in the dataset. The movement is either slightly too short or too long. The average difference of the rowers' movement is 15 cm to short at a pace of 28 str/min. This difference is probably the result of too much compensation of the foot force, although the optimized offset of the foot force differs only 5N from the dataset of 32 str/min. Maybe a part of the compensation of the foot force is also based on the noise in the signal.

Measurements of the foot force At one point in the research, the differences between the results of the boat acceleration calculated by the F_{foot} and m_{sys} method drew the suspicion that the measurements at the footstretcher are not coherent with the gate measurements. The negative (pulling) forces of the footstretcher are smaller than expected. Changing the foot force with a slight change in offset and gain created the best results. It is possible that the footstretcher sensor is wrongly calibrated which is compensated for after the optimization. For example the angle of the footstretcher is not correctly taken into account in the sensor settings. However as can be seen in appendix B, in other measurements the foot force had to be compensated as well. So the right calibration will not solve all problems regarding the foot force measurements.

There is also the possibility that some form of backlash occurs in the shoes attached to the footstretcher. Between pushing against the footstretcher in the drive and moving forward (pulling) in the recovery, there is a moment in time that the rower "floats" in her shoes. This depends on how tight the shoes are strapped.

It is difficult to determine what part of the error is caused by the quality of the measurements and what part is due to faults or simplifications in the model.

Optimization of the foot force In the current model the optimization of the gain and offset is done with an error function based on the boat acceleration and the error of the relative displacement of both rowers at the end of the stroke. A choice could be made to keep the boat acceleration out of this function and to only make sure that the rowers return to their initial position. In that case the fit for the boat acceleration slightly decreases and the fit for the relative displacement of the rower increases (even further). With this optimization function the model would be less dependent on the measured data.

The results for the relative displacement of the rower after optimizing the gain and offset at one rowing pace are not consistent at other paces. The difference in the position of the rower at the end of the stroke is highly influenced by small changes in the foot force. The optimal offset for the rowing paces differs with about 5 N. Further research has to be done to find a gain and offset that are constant for all rowing paces of a crew and are not optimized on one specific dataset.

Rower behavior

Constant rower technique The individual biomechanical fingerprint of the rower (the signature force-u_{CoM} curve) is assumed constant for each rower. The biomechanical fingerprint of the rower is not easily changed, but it is unknown how receptive each rower is to changes in her surroundings and how far these changes will influence her technique. In other words, the flexibility of the rower's biomechanical fingerprint is unknown. This also holds for the part of the race over which the fingerprint is constructed, the currently modeled fingerprints could be influenced by adaptation to other rowers, the rigging setup or technical advise from the coach.

To overcome these uncertainties, the measuring and modeling of the rowers' behavior has to be done regularly. This can also be used to observe whether the rowers made progress, or are still doing the same thing and whether the rigging is still suitable for the situation.

The rower as a force constraint system The rower is modeled as a force constraint model when changing the rigging setup. This is done to be able to model the optimal rigging setup for a rower. Adding a power constraint to the model could make it more accurate for rowing at race intensity.

The physiological power of each rower is limited over a certain amount of time (in this case the race duration). Coaches and rowers try to find a rigging setup with which rowers supply a established amount of power, however this is not the same for each rower. The race pace of the crew is fixed, rowers can not deviate from each other in that aspect. Therefore individual rigging per rower can help them achieve their individually established amount of power. By Hill [24] and Monod and Scherrer [36] methods to establish the average power for an athlete over a race time are designed.

The model in this thesis uses a fixed signature force-u_{CoM} curve for every rower. From this curve and the original rigging the applied handle power and work per stroke are calculated. A next step could be to use individually established power per rower as an objective to scale the lever ratio of the rower. With every rower applying her established power, other rigging parameters such as the position of the footstretcher can be used to optimize the synchronization of the crew.

Model simplifications

Rower modeled as a point mass By modeling the rower as a point mass, the movements of the different body segments with respect to each other are neglected and so are also the energy losses that occur here. The rower might be able to generate more power than she delivers on the handle and footstretcher. As long as the rower moves with the same movement pattern these losses are equal for every stroke and nothing changes for the output on the handle or footstretcher. When the rower has learned to move more efficiently or gain extra strength over time due to muscle training, this would result in a different output on the handle and footstretcher and a new model of the movement of the rowers' CoM must be compiled. Therefore regular measurements of all forces and the oar angles are needed.

No restrictions in the oar movement Currently, when changing the rigging parameters, no restrictions are placed on the movements of the handle through the boat and the blade along the boat. However there is a point that the rower is not able to hold both handles anymore, either because her arms overlap to much in the middle of the drive phase, or the handles are to far apart in the catch or the finish. In these cases the rower will not be able to provide the same force on the handles as is assumed. These individual limits, have to be added to the model, in order to create valid outputs outside of a limited range of the original rigging setup.

Boat drag is proportional to square boat velocity All drag forces on the system are considered as viscous drag, with a constant drag coefficient. In reality, the drag coefficient is not constant. It

consists of a hydrodynamic part and an aerodynamic part, both of which are subjected to changes in flow. For example by a gust of wind and the frontal surface. The frontal surface is changing by the movement of the rower.

The currently used drag coefficient C_1 is derived from a study done in 1967 on a racing eight. The derivation is done based on the geometric similarity between all rowing boats. However, the eight used in the drag test probably consists of a heavy men's sweep crew with a coxwain. The generalization of the weight of the rowers (wetted area), skin friction of the boat (wood vs composite) and shape of the hull for the measured eight and the modeled double, is a big simplification.

The boat velocity in the model is not the same as the measured boat velocity. The modeled boat velocity is dependent on the chosen average velocity and the drag force, but the drag force is dependent on the boat velocity. If the boat velocity is increased due to changes in the rigging setup, the drag force should increase and the boat velocity is decreased again. This leads to a chicken-and-egg problem that could be optimized for, but the gain in realism of the model is expected to be small. To overcome this problem, the drag force in the model is based on the measured boat velocity and stays constant for all different rigging setups.

Oar dynamics The blade force is assumed to be always perpendicular to the oar, the component of the blade force parallel to the oar is neglected because it can not be measured. Hofmijster et al. [27] calculated that the estimated power loss at the blade is 18% when the parallel blade force is incorporated. This is a systematic error that is generally excepted.

The blade force in the model is assumed to apply in the center of the blade. But in reality, the location of the application point of the blade force on the blade changes during the stroke (from outwards to inwards). The application point of the blade force has a big result on the blade losses. In the future it is recommended to determine the application point of the blade force through the stroke before modeling the blade.

The oar in the model is assumed to be rigid, this is in reality not completely true. The oar is subject to some deformation, this deformation has an effect of the position of the blade in the water. Next to the position of the blade there is also a fraction of the mechanical energy of the rower stored in the oar in the beginning of the stroke and given back around the finish. To measure the bending of the oar, a force transducer must be applied on the oar shaft next to the oar angle measurements in the gate. Combined this data can show the amount of bending of the oar.

When the rigging is changed, the path of the blade is changed. With the assumptions of the oar blade dynamics in mind, the blade path is more difficult to predict. The effects of the oar deformation, parallel blade force and application point of the blade force change with different rigging setup. It is not possible to say how much the blade forces are influenced. This might explain the curious fact that currently the boat velocity is increased when the work per stroke delivered at the handle is decreased. This is a disruption of the energy balance of the system.

Interpretation of results

Blade path efficiency against synchrony The average boat velocity is increased for a longer inboard length or positive change in footstretcher position. The higher boat velocity could be due to the better blade efficiency, or due to a more optimal synchrony between the rowers. Since the results between changing the rigging of rower 1 and 2 do not differ much, probably the first is true.

The increased boat velocity is not realistic due to the disrupted energy balance. The improvement of the boat velocity due to better synchronisation is currently not registered. This could be because the effect of the synchrony is smaller than the blade efficiency. When the blade forces are modeled more realistically some effect of synchronization might become visible.

Found optimal fits The found optimum values for the boat and rower motions are very similar to the measured and expected values. However there is a large range of parameters that were estimated and probably the reality of their values is not optimal. The sensitivity of the model is not truly investigated. Small errors in the measurements, model or error function used in the optimization may cause deviations in the rowers' motions and boat performance (as seen with small deviations of the foot force). The results after the optimization of the foot forces might not be as detailed as is currently predicted, even if the modeled boat acceleration fits the measured boat acceleration quite well.

Conclusion

A model is constructed based on equations of motions that are derived from free body diagrams. The model is driven with measurements done in the boat. Throughout the model many assumptions have been done, mainly to reduce the complexity of the model.

The individual rower behavior The individual rower behavior can be described by the force that the rower delivers over a constant segment. This segment can be based on the oar angle or the relative movement of the rower. The relative movement of the rower is better equipped to deal with changes in the rigging parameters. The displacement of the handle and seat are used to estimate the relative movement of the rower, but these methods use a generalization on the movement pattern of the rowers.

The measured forces in the boat are used to predict the relative motions of the rower based of the forces on the rower and the boat acceleration (the *Forces* method) or based on the system acceleration together with other rower's motions and the boat acceleration (the *System* method). The best result is found for the *Forces* method when a correction is done on the measured data of the foot force.

Modeling boat motions The boat motions can be modeled by using the forces acting directly on the boat (the F_{foots} method), or by using the system accelerations and the relative accelerations of the rowers (the m_{sys} method). The best obtained qualitative and quantitative fit for the boat acceleration is found with the m_{sys} method with optimized gain and offset for the foot force.

Changing the rigging parameters In the model a rower is assumed who is constraint in force production and has no restrictions in arm movements. Using these assumptions and the m_{sys} method to model the boat acceleration, the blade forces have a leading role in the changes of the boat motions after changing the rigging parameters. However the blade forces might be modeled oversimplified.

Keeping the simplifications in the model in mind some effects of changing the rigging parameters are found. Changing the lever ratio of the oar, by increasing the inboard length leads to a smaller covered oar angle and a higher boat velocity, but a smaller work per stroke delivered at the handle. Moving the footstretcher towards the bow of the boat shifts the oar angle and leads to a higher boat velocity and smaller handle work per stroke as well.

The boat velocity responded similar to changes for the rigging parameters for both rowers. For the two rowers presented here, there are no indications that the boat performance is increased due to better synchronization between the rowers. When the blade forces are more realistically modeled and the energy balance of the system remains valid, there might occur some improvements due to better synchronization.

Can rowing performance be improved by changing the rigging? In this model, the boat performance can be increased by changing the rigging setup of the boat, however there are no indications that this is the result of a better synchrony between the rowers. The increase in boat performance for a longer inboard length or displacement of the footstretcher towards the bow of the boat is caused by the increased in the blade forces. While the work per stroke at the handle is decreased for these rigging setup changes. When the blade forces are modeled in a more realistic way and the energy balance of the system remains valid, maybe there can be found a relation between the boat performance and the synchronization between the rowers.

Recommendations

In future research several things can be changed or added in the model and method to study specific motions (of a part) of the system. In this chapter some recommendations are done in how to improve the reliability of the model and how to validate the results.

Improve reliability model

Construct model based on more data The stroke data that goes in the model is currently averaged from one segment of rowing. The amount of strokes over which are averaged, determines the power of the current average strokes. Therefore data from more strokes would lead to better averages and the outliers (bad strokes as well as a bad part of a stroke) have less influence on quality of the averaged stroke. It could also be interesting to combine different datasets from the same rower in different circumstances. Integrating these datasets would lead to a better insights on for example the flexibility of the technique of the rower. In general, the value generated from integrating different datasets is bigger than looking at the results of the datasets separately.

Calibrate or improve the footstretcher sensor The measurements done with the footstretcher sensor are under discussion. To improve the reliability of the measurements and the modeled boat and rower motions, it is recommended to spend extra energy in studying the accuracy and calibration of the foot force sensor. If the accuracy of the forces that is needed to model the rower motion with good precision is not reached, another measurement system such as OARinspired [38] could be considered, or the load cells in the footstretcher could be replaced.

Smart compensation for F_{foot} At the moment a constant gain and offset to compensate the foot force is applied over the whole stroke. However the effect of the disruptions in the foot force is bigger at the beginning of the stroke than in the end of the stroke, due to the double integration. A smart compensation for F_{foot} could also be used, with a descending correction factor over the stroke. This way a larger compensation is imposed on errors in the beginning of the stroke and smaller compensation on errors in the end of the stroke.

Study flexibility of rower The rower is able to adapt slightly to internal and external feedback. How responsive a rower is to the feedback differs per athlete. More research should to be done to investigate how constant the force-angle or force-u_{CoM} curves are. And how much of the curve is influenced by a specific type of feedback. This way the flexibility of the rower is quantified and more specific improvements on the rigging or feedback in the model can be done per rower. For example a flexible rower may not need much rigging adjustments, because she can adapt to the other rowers herself. While an inflexible rower may benefit more from an individualized rigging setup.

Power constraint per rower Every athlete is able to generate a certain power over a time period, in this case the race duration. Methods to establish the average power for an athlete over time are designed by Hill [24] and Monod and Scherrer [36].

The rigging setup that agrees with this established power is different for each rower. There are certain variables that should be fixed within the crew. The race pace is the same for every rower and each rower is able to generate a specific force over her relative displacement (force-u_{CoM} curve). The lever ratio of the rigging setup can be used to secure the individually established power of each rower. The other rigging parameters can be used to tune the synchronization between the rowers.

More dimensional model Modeling the boat and rower motions in one dimension (and the oar in two dimensions) simplifies a lot of factors that contribute to the propulsion of the boat. If a two-

dimensional model is created (in x- and y-direction) the motions of the rower and boat in this plane can be considered and more limitations regarding the oar movements can be done.

Multiple stroke model The current model is a stroke based model. If there is enough data to average over it might be interesting to model different strokes in a race, for example a start stroke, ”normal” race stroke and a final sprint stroke. Using these different rowing strokes a whole rowing race can be modeled.

Also, in different phases of a race, the stroke length, stroke pace and power is altered considerably. While the biggest part of the race is rowed in a ”normal” race stroke, the differences at the finish between crews are more than once the result of a good start or final sprint. Taking the strokes in these segments of a race also in consideration when optimizing the rigging setup might bring up surprising results.

Drag tests of the rowing boats The currently used drag coefficient C_1 is derived from a study done in 1967 on a racing eight. The derivation is done based on the geometric similarity between all rowing boats. However, in the eight used in the drag test probably a heavy men’s sweep crew with a coxwain is used. The generalization of the weight of the rowers (wetted area), skin friction of the boat (wood vs composite) and shape of the hull, is a big simplification.

In order to have a more suitable drag coefficient for the model, it is recommended that more drag tests are done with the modern rowing boats, with constant speed and speed fluctuations. To find the combined drag force coefficient (C_1), this is preferably done with different crews on board (with different weights and sizes). Without a crew on board the drag coefficient of the hull $C_{drag,boat}$ is derived, but the air drag on the system can not be incorporated in this factor.

Include oar deformation When modeling the extreme cases of the rigging setup, oar deformation and blade forces are becoming more important for the results of the model. Oar deformation can be measured when strain gauges are applied on the oar shaft [5, 52, 57] and these measurements are combined with the measurements at the gate.

Validate results

More measurements with footstretcher sensor Nowadays not a lot of rowing practices are done with a boat that is fully equipped with sensors. Often only the gate sensors are used, while this data only presents a part of the puzzle. In order to accurately model the rowing system, it is crucial that athletes and coaches understand that more data is needed, also of the footstretcher sensor. In order to optimize one crew, it is recommended that this crew rows with the measurement system for a longer period of time. That way technical errors such as ”bum-shoving”, checking the slides and slip losses at the finish can be identified per rower and progress can be registered.

Experiment with rigging setup The results currently obtained by changing the rigging setup can be validated with an experiment. The experiment would be roughly the following: First row under ”normal” circumstances, while measuring the boat acceleration and speed, to create a baseline. Then changing the rigging setup of one (or both) rowers and rowing at the same pace. The resulting boat speed and acceleration can be compared to the results obtained by the model. Also the handle and foot force-u_{CoM} curves of the rowers can be compared to the curves obtained by the model. This procedure should be done several times with different rigging setups.

Compare relative rower motions with other measurement methods There are other ways to determine the movement of the center of mass of the rower. This model is based on the forces measured in the boat, but there could also be looked solely at the kinematics of a rower. With the estimate that the center of mass of the rower lies in the gut, a video analysis could tell something about the movement of the rower with respect to the boat and the global environment.

A magneto inertial suit can be used to measure the kinetics of different body segments of the rowers [33]. With an estimate of the mass of each body segment the motions of the combined CoM of the rower can be calculated.

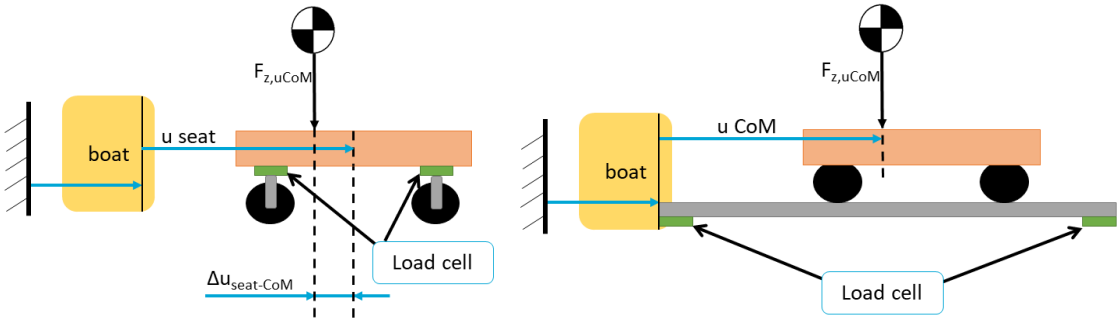

Figure 6.5: Other ways to measure the position of the center of mass

A new idea is to equip the slides or seats with load cells to calculate the position of the center of mass of the rower. With the ratio between the two load cells in the axle of the seat, the relative displacement of the CoM with respect to the seat ($\Delta u_{seat-CoM}$) can be estimated. The same principle can be used for load cells that are mounted under the ends of the slides. Installing slides into the boat with load cells at the ends, is probably more robust than equipping the seat with load cells, due to the wires attaching the load cells to the sensor network.

Bibliography

[1] Alexander, F. (1925). The theory of rowing. *In Proceedings of the University of Durham Philosophical Society*.

[2] Andrews, B., Mandeville, S., Hase, K., E. Halliday, S., and Zavatsky, A. (2002). Biomechanical study of fes rowing and inclined bench sliding systems using simulation models.

[3] Atkinson, W. C. (2001). Modeling the dynamics of rowing. *unpublished*. http://www.atkinsopht.com/row/rowabstr.htm Accessed 26-08-2017.

[4] Barré, S. and Kobus, J.-M. (2010). Comparison between common models of forces on oar blades and forces measured by towing tank tests. *Proceedings of The Institution of Mechanical Engineers, Part P: Journal of Sports Engineering and Technology*, 224:37–50. DOI: 10.1243/17543371JSET43.

[5] Baudouin, A. and Hawkins, D. (2004). Investigation of biomechanical factors affecting rowing performance. *Journal of Biomechanics*, 37(7):969–976. DOI:10.1016/j.jbiomech.2003.11.011.

[6] Blocken, B., Defraeye, T., Koninckx, E., Carmeliet, J., and Hespel, P. (2013). Surprises in cycling aerodynamics. *Europhysics News*, 44:20–23. DOI: 10.1051/epn/2013102.

[7] Brearley, M. N., de Mestre, N. J., and Watson, D. R. (1998). Modelling the rowing stroke in racing shells. *The Mathematical Gazette*, 82(495):389–404. DOI: 10.2307/3619885.

[8] Cabrera, D., Ruina, A., and Kleshnev, V. (2006). A simple 1+ dimensional model of rowing mimics observed forces and motions. *Human Movement Science*, 25(2):192–220. DOI:10.1016/j.humov.2005.11.002.

[9] Caplan, N. and Gardner, T. (2007a). A fluid dynamic investigation of the big blade and macon oar blade designs in rowing propulsion. *Journal of Sports Sciences*, 25(6):643–50. DOI: 10.1080/02640410600809985.

[10] Caplan, N. and Gardner, T. (2007b). Modeling the influence of crew movement on boat velocity fluctuations during the rowing stroke. *International Journal of Sports Science and Engineering*, 01(03):165–176.

[11] Coker, J. (2010). *Using boat instrumentation system to measure and improve elite on-water sculling performance*. Phd thesis, School of sport and recreation, Auckland University of Technology.

[12] Concept2 (2017a). Choosing your oar components. http://www.concept2.com/oars/oar-components Accessed 25-11-2017.

[13] Concept2 (2017b). Indoor rowers. http://www.concept2.nl/nl/indoor-rowers Accessed 20-06-2017.

[14] Consiglieri, L. and Pires, E. (2009). An analytical model for the ergometer rowing: inverse multibody dynamics analysis. *Computer Methods in Biomechanics and Biomedical Engineering*, 12(4):469–479. DOI: 10.1080/10255840802687400.

[15] Cuijpers, L. S., Passos, P. J. M., Murgia, A., Hoogerheide, A., Lemmink, K. A. P. M., and de Poel, H. J. (2016). Rocking the boat: does perfect rowing crew synchronization reduce detrimental boat movements? *Scandinavian Journal of Medicine & Science in Sports*. DOI:10.1111/sms.12800.

[16] Debraux, P., Grappe, F., Manolova, A. V., and Bertucci, W. (2011). Aerodynamic drag in cycling: methods of assessment. *Sports Biomechanics*, 3:197–218. DOI: 10.1080/14763141.2011.592209.

[17] Dudhia, A. (2008). The physics of ergometers. http://eodg.atm.ox.ac.uk/user/dudhia/rowing/physics/ergometer.html Accessed 05-09-2017.

[18] Empacher (2017). Welcome to empacher. http://www.empacher.de/en/ Accessed 20-12-2017.

[19] Formaggia, L., Miglio, E., Mola, A., and Montano, A. (2009). A model for the dynamics of rowing boats. *International Journal For Numerical Methods in Fluids*, 1(61):119–143. DOI: 10.1002/fld.1940.

[20] Formaggia, L., Mola, A., Parolini, N., and Pischiutta, M. (2010). A three-dimensional model for the dynamics and hydrodynamics of rowing boats. *Proceedings of The Institution of Mechanical Engineers, Part P: Journal of Sports Engineering and Technology*, 224:51–61. DOI: 10.1243/17543371JSET46.

[21] Gianchandani, M. (2010). Fisa rowing boat rigging survey. https://www.rowperfect.co.uk/fisa-rigging-survey/ Accessed 15-05-2017.

[22] Gravenhorst, F., Muaremi, A., Draper, C., Galloway, M., and Tröster, G. (2015). Identifying unique biomechanical fingerprints for rowers and correlations with boat speed - a datadriven approach for rowing performance analysis. *International Journal of Computer Science in Sport*, 14:4–33.

[23] Greene, A. J., Sinclair, P. J., Dickson, M. H., Colloud, F., and Smith, R. M. (2013). The effect of ergometer design on rowing stroke mechanics. *Scandinavian Journal of Medicine & Science in Sports*, 23(4):468–477. DOI:10.1111/j.1600-0838.2011.01404.

[24] Hill, A. V. (1925). The physiological basis of athletic records. *The Lancet*, pages 481–486.

[25] Hill, D. W., Alain, C., and Kennedy, M. D. (2003). Modeling the relationship between velocity and time to fatigue in rowing. *Medicine and Science in Sports and Exercise*, 35(12):2098–2105. DOI:10.1249/01.MSS.0000099111.78949.0.

[26] Hill, H. (2002). Dynamics of coordination within elite rowing crews: evidence from force pattern analysis. *Journal of Sports Sciences*, 20(2):111–117. DOI:10.1080/026404102317200819.

[27] Hofmijster, M. J., de Koning, J. J., and van Soest, A. J. (2010). Estimation of the energy loss at the blades in rowing: Common assumptions revisited. *Journal of Sport Sciences*, 28(10):1093–1102. DOI:10.1080/02640414.2010.495994.

[28] Hofmijster, M. J., van Soest, A. J., and de Koning, J. J. (2008). Rowing skill affects power loss on a modified rowing ergometer. *Medicine & Science in Sports & Exercise*, 40:1101–1110. DOI:10.1249/MSS.0b013e3181668671.

[29] In Motion Software & Sports Technology (2016). The rowing in motion system. https://www.rowinginmotion.com/ Accessed 02-06-2017.

[30] Ishiko, T. (1971). *Biomechanics of Rowing in Biomechanics II*.

[31] Kleshnev, V. (2011). *Biomechanics of Rowing In: Nolte V, editor. Rowing faster.* Human Kinetics, 2 edition.

[32] Lazauskas, L. (1997). A performance prediction model for rowing races. *Technical report, University of Adelaide, Australia*.

[33] Lintmeijer, L., Hofmijster, M., Beek, P., Fischedick, G. S., Zijlstra, P., and Soest, A. (2016). Rowers' on-water power output is commonly underestimated. *21st annual ECSS Congress Vienna/Austria, July 6-9 2016*.

[34] Manuel, M. (2014). mattymanuel's blog: Gps (global positioning system) in sport.

[35] McMahon, T. A. (1971). Rowing: A similarity analysis. *Science*, (173):349–351. DOI: 10.1126/science.173.3994.349.

[36] Monod, H. and Scherrer, J. (1965). The work capacity of a synergic muscular group. *Ergonomics*, pages 329–338. DOI: 10.1080/00140136508930810.

[37] Nevill, A. M., Allen, S. V., and Ingham, S. A. (2011). Modelling the determinants of 2000 m rowing ergometer performance: a proportional, curvilinear allometric approach. *Scandinavian Journal of Medicine & Science in Sports*, 21:73–78. DOI:10.1111/j.1600-0838.2009.01025.x.

[38] OARinspired (2017). Technology. http://www.oarinspired.com/technology-2/ Accessed 07-06-2017.

[39] Ottenhoff, E. (2003). Modelling the rowing stroke. Master thesis, University of Groningen.

[40] O'Brien, C. (2011). *Effortless rowing. In: Nolte V, editor. Rowing faster.* Human Kinetics, 2 edition.

[41] Peach-Innovations (2014). Powerline rowing instrumentation and telemetry: The ultimate analysis tool for coaches and athletes. http://www.peachinnovations.com/ Accessed 22-06-2017.

[42] Pelz, P. F. and Vergé, A. (2014). Validated biomechanical model for efficiency and speed of rowing. *Journal of Biomechanics*, 47(13):3415–3422. DOI:10.1016/j.jbiomech.2014.06.037.

[43] Peterman, J. E., Lim, A. C., Ignatz, R. I., Edwards, A. G., and Byrnes, W. C. (2015). Field-measured drag area is a key correlate of level cycling time trial performance. *PeerJ*. DOI:10.7717/peerj.1144.

[44] Pettersson, R., Nordmark, A., and Eriksson, A. (2014). Simulation of rowing in an optimization context. *Multibody System Dynamics*, 32(3):337–356. DOI:10.1007/s11044-013-9384-5.

[45] Pope, D. L. (1973). On the dynamics of men and boats and oars. *Mechanics and Sport. ASME*, pages 113–130. DOI: 10.1243/17543371JSET38.

[46] Richardson, M., Marsh, K., and Schmidt, R. (2005). Effects of visual and verbal interaction on unintentional interpersonal coordination. *Journal of Experimental Psychology: Human Perception and Performance*, 31(1):62–79. DOI: 10.1037/0096-1523.31.1.62.

[47] Ritchie, A. C. (2008). Dynamic modeling of ergometer and on-water rowing. *Sports Technology*, 1(2-3):110–116. DOI: 10.1002/jst.15.

[48] Rongere, F., Khalil, W., and Kobus, J.-M. (2011). Dynamic modeling and simulation of rowing with a robotics formalism. *16th International Conference on Methods & Models in Automation & Robotics*. DOI: 10.1109/MMAR.2011.6031355.

[49] Roosendaal, S. (2010). A model of rowing. https://sanderroosendaal.wordpress.com/.

[50] Schwanitz, P. (1991). Applying biomechanics to improve rowing performance. *FISA Coach*, 2(3):1–7.

[51] Serveto, S., Barré, S., Kobus, J.-M., and Mariot, J.-P. (2009). A three-dimensional model of the boat–oars–rower system using adams and lifemod commercial software. *Proceedings of the Institution of Mechanical Engineers, Part P: Journal of Sports Engineering and Technology*, 224(1):75–88. DOI:10.1243/17543371JSET42.

[52] smartOar (2017). Oars. http://www.smartoar.com/oars/ Accessed 08-06-2017.

[53] Soper, C. and Hume, P. A. (2004). Towards an ideal rowing technique for performance: The contributions from biomechanics. *Sports Medicine*, 34(12):825–848. DOI:10.2165/00007256-200434120-00003.

[54] unkown (2011). *Werktuigbouw.nl Formuleboekje*. mikrocentrum. ISBN/EAN:978-90-810406-2-4.

[55] van Holst, M. (2017). Theory and model. *unpublished*. http://home.hccnet.nl/m.holst/RoeiWeb.html Accessed 29-08-2017.

[56] Voordouw, J. (2018). Overview of measurement systems and models that can be used for optimization in rowing. Literature research.

[57] Webasport (2014). Our product line. http://www.weba-sport.com/en/ Accessed 06-06-2017.

[58] Wellicome, J. (1967). *Report on resistance experiments carried out on three racing shells. Technical report*. NPL Ship T. M.

[59] White, F. M. (2011). *Fluid Mechanics*. McGraw-Hill. ISBN 978-007-1131121-2.

[60] Wing, A. and Woodburn, C. (1995). The coordination and consistency of rowers in a racing eight. *Journal of Sport Sciences*, 13:187–197. DOI: 10.1080/02640419508732227.

A

Additional data & results

A.1. Boat motion sensors

The original sensors of the PowerLine system that can measure the boat motions are impeller with an IMU. The IMU measures the linear acceleration in three axis and yaw, pitch and roll angles. For the measurements to be accurate, the IMU should be placed horizontally on a flat surface. It must line up with the longitudinal axis of the boat. The impeller should attached to the bottom of the hull, where it measures the speed of the water along the boat.

Another way to measure the boat motions is to install a high frequency GPS device, such as a MiniMax S4. This device is used by the measurements of the M4x. Unfortunately, in the dataset obtained from the measurements on the LW2x no boat velocity sensor is used.

(a) The IMU (top) and the impeller (bottom) of the PowerLine system [41]. The IMU is to be placed horizontally on a flat surface on the hull. The impeller is attached to the bottom of the hull.

(b) The MiniMax S4 is a sensor that combines GPS with accelero-, gyro- and magnetometer data. It is used to measure the motions of the rowing boat with a frequency of 100 Hz [34]. The device is attached to the inside of the hull and used during the M4X race.

Figure A.1: The boat motion sensors; the IMU, the impeller and MiniMax S4.

A.2. Raw data measured by the sensors on the boat.

The sensor in the boat each supply data that is logged at a frequency of 50 Hz. In this section the raw data (only converted to SI-units) of the IMU, footstretcher and seat position sensor are shown.

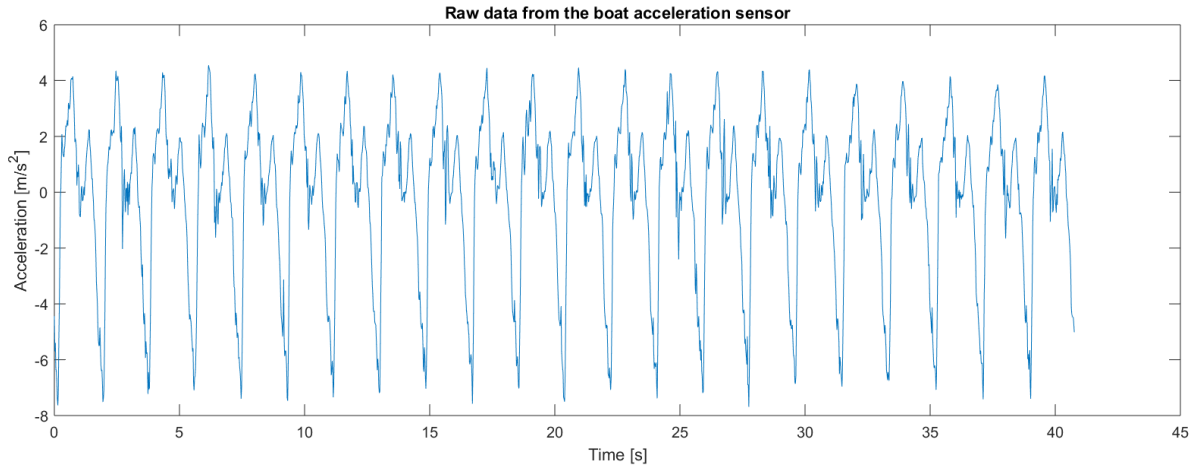

Figure A.2: Raw data of the boat acceleration sensor (IMU) from the PowerLine system from the LW2x at pace 32 str/min, for a period of ±40 seconds.

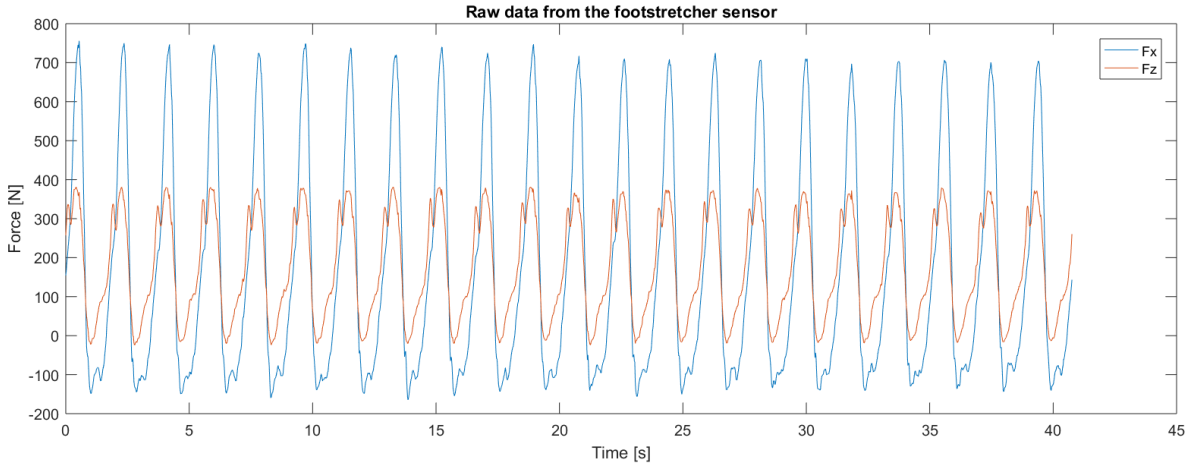

Figure A.3: Raw data obtained with the PowerLine footstretcher from a LW2x at pace 32 str/min, for a period of ±40 seconds.

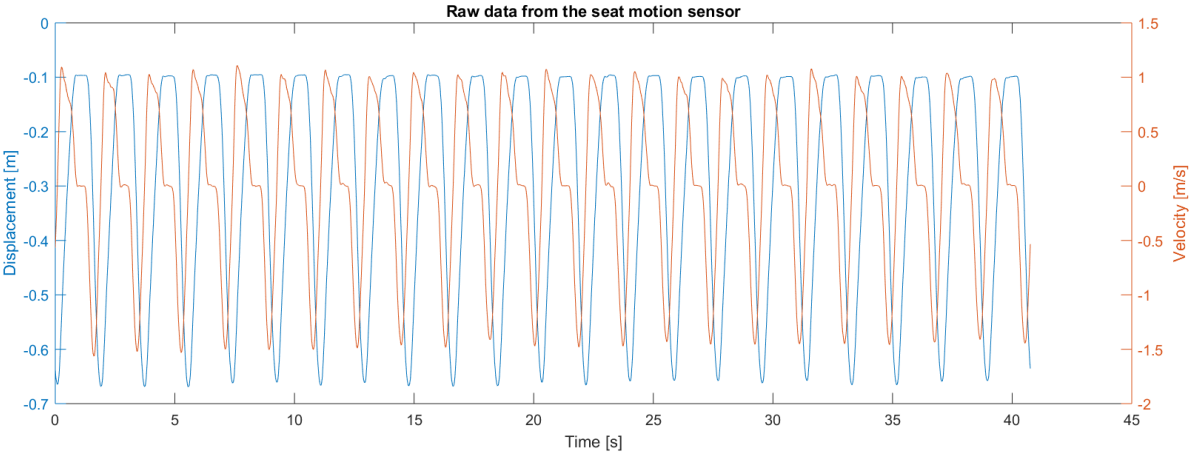

Figure A.4: Raw data of the seat motions from the PowerLine seat position sensor from the LW2x at pace 32 str/min, for a period of ±40 seconds.

A.3. Normalized gate force-angle curves for a M4x

The thesis started with the analysis of the rowers and boat of a M4x. The dataset of the M4x is not suitable to model the rowers motions with, however rower specific force-angle curves could be created. In fig. A.5, the average normalized force-angle curves of the four rowers of the quad are shown. Clear differences in force pattern over the angle are found between the rowers.

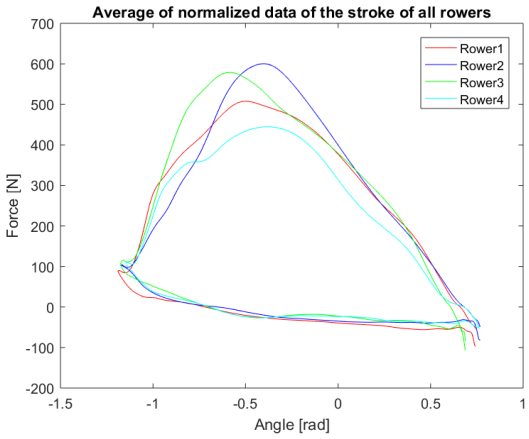

Figure A.5: The normalized averaged gate force-angle curves for all rowers in a M4x.

A.4. Effects of s, $\ddot{v}_{oar}$, I_{gate} and the oar deformation on the oar forces.

The equations to calculate the handle forces are presented in section 3.3.2, but for convenience they are repeated below.

$$F_{handle,v} = \frac{F_{pin} \cdot {l_{outboard}}^{*} + I_{gate} \cdot \ddot{\theta} + m_{oar} \cdot \ddot{v}_{oar}(s - {l_{outboard}}^{*}) + m_{oar} \cdot \ddot{w}_{oar} \cdot r}{{l_{outboard}}^{*} + {l_{inboard}}^{*}} \tag{3.9}$$

$$F_{handle,w} = F_{gate,w} + m_{oar} \cdot \ddot{w}_{oar} \tag{3.10}$$

$$F_{handle,x} = F_{handle,v} \cdot \cos(\theta) + F_{handle,w} \cdot \sin(\theta) \tag{3.12}$$

In fig. A.6, $F_{handle,X}$ is shown for different distances s. s is changed from 0 to 0.6 m in steps of 0.1 m, that way the effect of changing distance s is visualized. In the overall graph of $F_{handle,X}$ there is barely an effect visible of a changed s. If there is zoomed in in the start of the stroke (here the effect should be the largest), there are found some differences for a different s. However the absolute difference between a s of 0 and 0.6 m is only 2 N. The accuracy of the gate force sensor is only 2 % (2 % of the max force is approximately 10 N) of which is bigger than the difference in force caused by the changes in s. Therefore the effect of s on the handle forces is neglected and for simplicity reasons, s is assumed zero.

The effect of the $\ddot{v}_{oar}$ on the handle force is shown in fig. A.7. In eq. (3.9) is shown where $\ddot{v}_{oar}$ is introduced in the equation of $F_{handle,v}$. The effect is visible in the overall graph of $F_{handle,X}$, but for more details a zoomed version is presented as well. The differences in $F_{handle,X}$ are the biggest halfway the drive, because that is where $\ddot{v}_{oar}$ is the largest. The maximum difference cause by $\ddot{v}_{oar}$ is approximately 5 N, which is negligible, but since this assumption does not lead to a more simplified model, there is no harm in keeping the component in the handle force calculations.

The effect of the oar inertia around the gate (I_{gate}) on $F_{handle,X}$ is shown in fig. A.8. This is done with three values for I_{gate}, so that a trend is shown. In eq. (3.9) is shown where I_{gate} is introduced in the equation of $F_{handle,v}$. The effect is visible in the overall graph of $F_{handle,X}$, but for more details a zoomed version is presented as well. The differences in $F_{handle,X}$ are the biggest around in the finish. The maximum difference between an I_{gate} of 0.5 and 2 kgm^2 is approximately 14 N, this is a definite difference, so the I_{gate} must be taken into account. However a difference of the oar inertia between 1.1 or 1.2 does not lead to a big difference in the handle force.

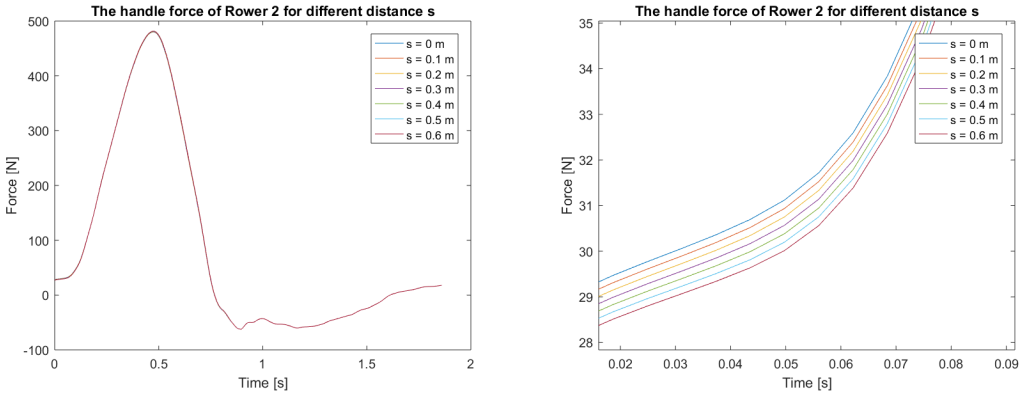

Figure A.6: The effect of the distance s on handle force $F_{handle,X}$. In the overall graph of $F_{handle,X}$ (left) there is barely an effect visible of a changed s. If there is zoomed in (right) in the start of the stroke (here the effect should be the largest), there are found some differences for a different s. However the absolute difference between a s of 0 and 0.6 m is only 2 N which is smaller than the accuracy of the gate force sensor.

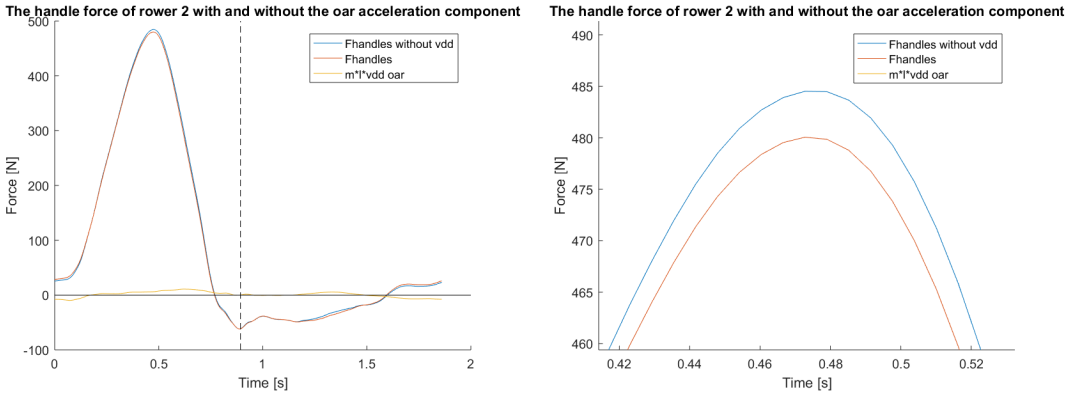

Figure A.7: The effect of the component of the oar acceleration on handle force $F_{handle,X}$. In the overall graph of $F_{handle,X}$ (left) there an effect visible of the introduction of $\ddot{v}_{oar}$. If there is zoomed in (right) to forces in the the middle of the drive phase, there is found that the maximum effect of $\ddot{v}_{oar}$ is approximately 5 N.

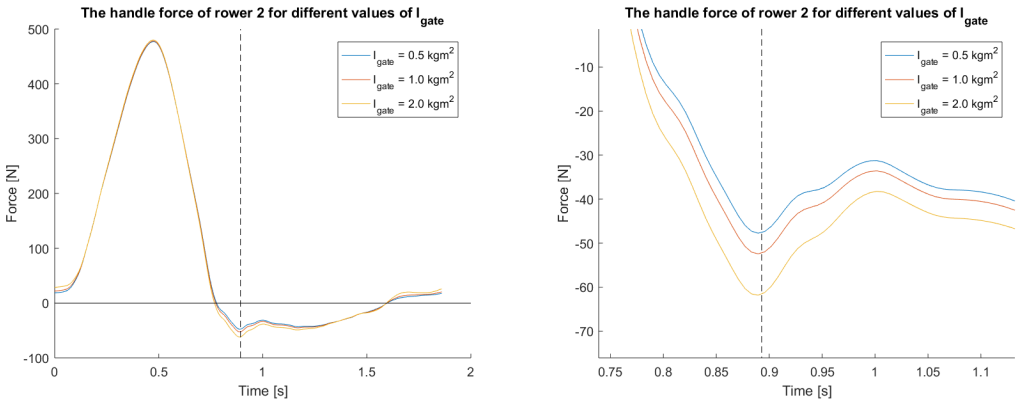

Figure A.8: The effect of three different values for I_{gate} on handle force $F_{handle,X}$. In the overall graph of $F_{handle,X}$ (left) there an effect visible of between the three values. If there is zoomed in to forces around the finish (right), the maximum difference between the three values is shown, this is a difference of approximately 14 N between the I_{gate} of 0.5 and 2 kgm^2.

In fig. A.9 the theoretical effect of the oar deformation on the blade forces is shown in a schematic representation. During the drive phase the path of the blade through the water is different if oar deformation is introduced. The forces on the blade with oar deformation can not be placed in the same axial system as the boat or the oar without deformation (v,w in fig. 3.6). The oar deformation can not

be measured or calculated based on the currently used data, therefore it is neglected.

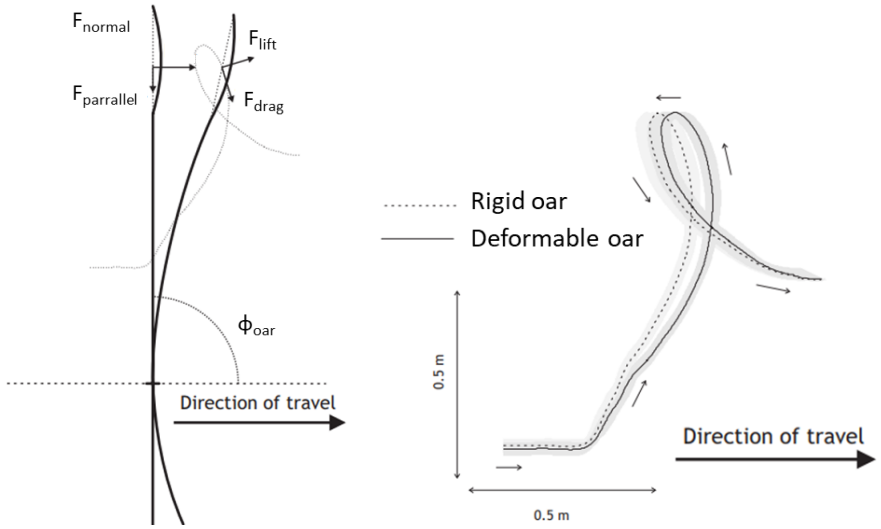

Figure A.9: A schematic representation of the effects of the oar deformation on the blade forces and path, during the drive phase. The rigid and the oar under deformation are both shown (left). $F_{parallel}$ and F_{normal} are oriented in the boat axial frame. F_{lift} and F_{drag} are oriented along the an axial frame, aligned with the movement direction of the center of the blade. Due to the oar deformation, this axial system is not the same as the oar axial system v,w in fig. 3.6. In the right graph the effects of the oar deformation on the path of the center of the blade is shown. Figures adjusted from Hofmijster et al. [27].

A.5. Effects of separate parameters on the F_{foots} method

In fig. 4.13 the effect of the different model parameters on the boat acceleration calculated via the m_{sys} method is already shown. In fig. A.10, the effect of the same parameter variation on the boat acceleration calculated via the F_{foots} method is shown. The effect of the parameter changes on the shape of the acceleration curve is quite similar for both methods.

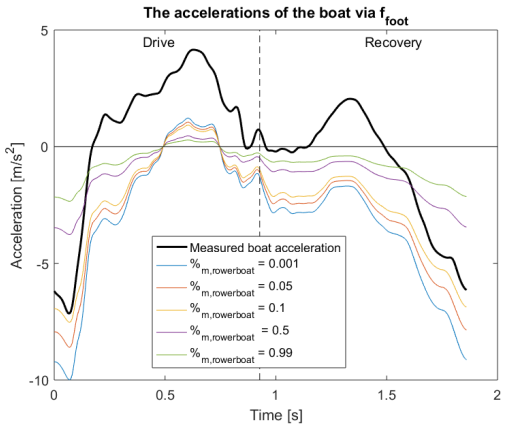

(a) The effect of the percentage of the rowers mass attached to the boat ($\%_{m,rowerboat}$).

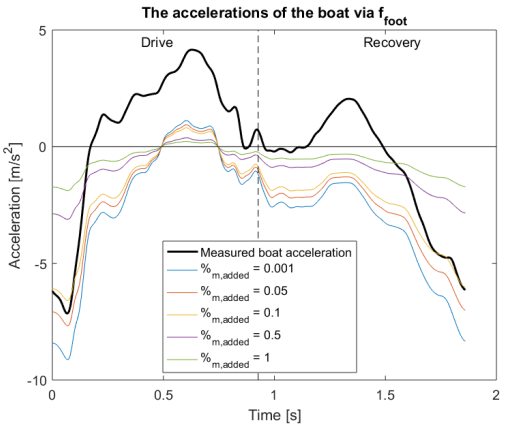

(b) The effect of the percentage of the system mass used as added mass on the boat ($\%_{m,added}$).

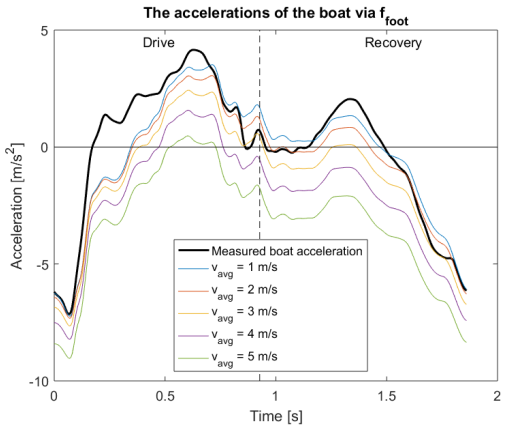

(c) The effect of the average velocity at the beginning of the stroke (v_{avg}).

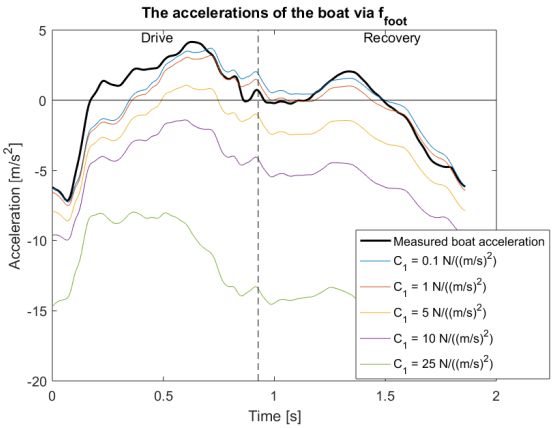

(d) The effect of the drag coefficient of the hull drag (C_{drag}).

Figure A.10: The effects of different parameters on the modeled boat acceleration calculated via the F_{foots} method (eq. (3.1))

A.6. Relative movements rower

Function $\Delta u_{handle-CoM}$

In section 4.2 the relative displacement of the rower is calculated based on the handle displacement in x-direction (u_{handle}). This method generalizes the relative distance between the handle and the CoM of the rower ($\Delta u_{handle-CoM}$). The function of $\Delta u_{handle-CoM}$ is equal to the length of the arms during the leg drive a cosine with the amplitude of half of the arms length in the back-arms swing.

$$\Delta u_{handle-CoM}(i) = \begin{cases} l_{arms} & \text{for the legdrive} \\ \frac{l_{arms}}{2}\cos(2\pi \cdot f^*_{back-arms}(i)) + \frac{l_{arms}}{2} & \text{for back-arms swing} \end{cases}$$

The period of the back-arms swing ($T_{back-arms}$), is defined as the period in which the oar angle is bigger zero, plus a custom amount of time (0.3 sec) to make the curve a bit smoother. $f^*_{back-arms}$ is $\frac{1}{T_{back-arms}}$.

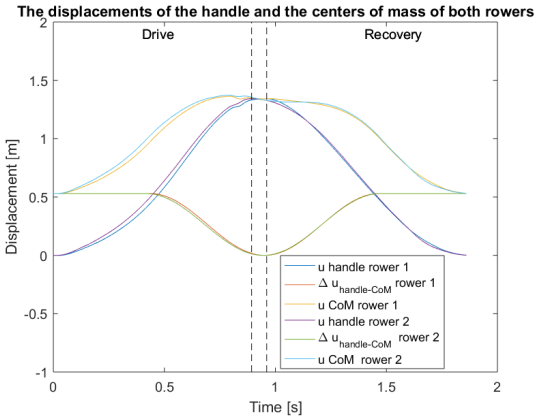

(a) The displacement of the handle (u_{handle}), the function for the relative movement of the handle and the CoM ($\Delta u_{handle-com}$) and the displacement of the CoM (u_{CoM}) for both rowers.

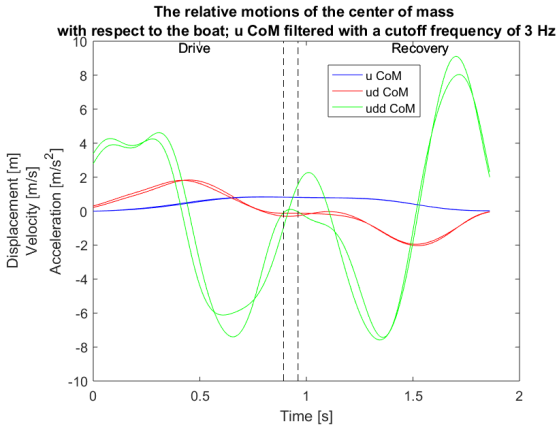

(b) The relative motions of the center of masses of the rowers, after u_{CoM} is filtered with a cutoff frequency of 3 Hz.

Figure A.11: The motions of the center of mass of both rowers, derived from the handle displacement (u_{handle}).

In fig. A.11a the displacement of the handle, the relative movement of the handle and the CoM of the rower and the displacement of the CoM of the rower are shown for both rowers. Fig. A.11b shows the acceleration, velocity and displacement of both CoM's. Clear differences are found in the motions of the CoM's of the rowers in a crew. Small changes in the displacement of the CoM result in big changes in the accelerations of the center of mass and will thereby cause a change in the net forces that the rowers apply on the boat.

Improving $\ddot{u}_r$

To study the influence of rower 2 on the relative motion of rower 1, several inquiries are done. In fig. A.12, the relative acceleration of rower 2 is based on the measured seat acceleration. The relative acceleration of rower 1 has bigger peaks in the drive phase. The relative displacement of rower 1 almost returns to the catch position at the end of the stroke. However, the CoM of the rower is bigger than the handle displacement, which is unexpected. Using the seat acceleration to predict the motions of rower 2 is not really using a self-containing model and is not in line with the goal to create a more precise estimate of the relative motions of the rowers.

When the relative acceleration of rower 2 is completely neglected, the relative displacement of rower 1 is still returning to the catch position, however much bigger than the handle displacement (fig. A.13).

These tests of the model are not very realistic and will therefore not be included in further modeling of the rower's motions.

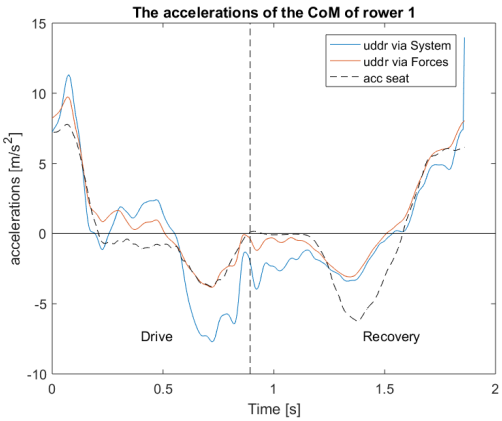

(a) The relative acceleration of rower 1, with the seat acceleration of rower 2 used as her relative acceleration in the *System* method.

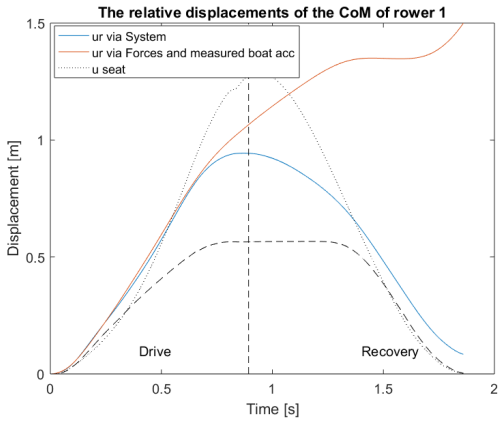

(b) The relative displacement of rower 1, with the seat acceleration of rower 2 used as her relative acceleration in the *System* method.

Figure A.12: The relative acceleration and displacement of rower 1, with the seat acceleration of rower 2 used as her relative acceleration, calculated via the *System* method.

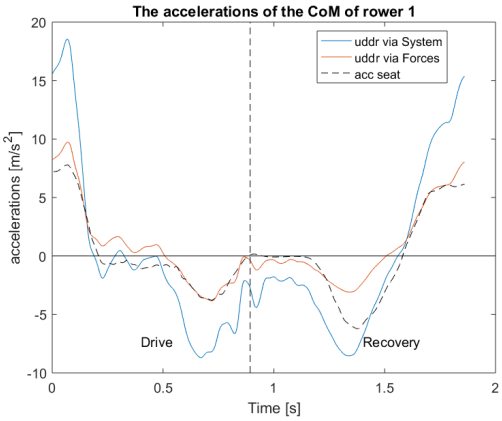

(a) The relative acceleration of rower 1, when the relative acceleration of rower 2 is neglected in the *System* method.

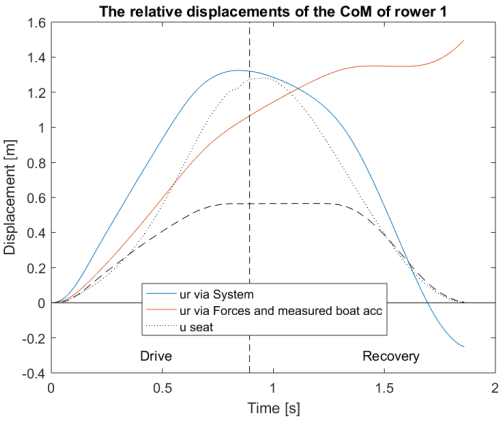

(b) The relative displacement of rower 1, when the relative acceleration of rower 2 is neglected in the *System* method.

Figure A.13: The relative acceleration and displacement of rower 1, calculated via the *System* method when the relative acceleration of rower 2 is neglected.

Function F_{resis}

The function of the virtual resistance force is build up from different combinations of the absolute rower displacement and velocity and boat displacement and velocity.

$$states_r(t) = \begin{bmatrix} 1 \\ xdr(t) \\ xdr(t)^2 \end{bmatrix} * \begin{bmatrix} 1 \\ xr(t) \\ xr(t)^2 \end{bmatrix}$$

$$states_b(t) = \begin{bmatrix} 1 \\ xdb(t) \\ xdb(t)^2 \end{bmatrix} * \begin{bmatrix} 1 \\ xb(t) \\ xb(t)^2 \end{bmatrix}$$

$$Fresis(t) = \begin{bmatrix} xpar_r \\ xpar_b \end{bmatrix} * \begin{bmatrix} states_r(t) \\ states_b(t) \end{bmatrix}$$

$xpar_r$ is a vector of 9 parameters each multiplied with a state of the rower and $xpar_b$ is a vector of 9 parameters each multiplied with a state of the boat. For each parameter the lower boundary is set to 0.0001 lower boundary and the upper boundary to 100.

The found optimum for $xpar_r$ and $xpar_b$ are:

$$xpar_{r,opt} = [0.0015 \quad 0.0002 \quad 0.0001 \quad 0.0003 \quad 0.0001 \quad 0.0001 \quad 0.0001 \quad 0.0001 \quad 0.0001]$$
$$xpar_{b,opt} = [0.0015 \quad 0.0003 \quad 0.0001 \quad 0.0009 \quad 0.0005 \quad 0.3547 \quad 49.9519 \quad 0.0049 \quad 5.6040]$$

From this optimal parameters can be concluded that the seventh and ninth state of $states_b$ are dominant in the resistance force. These states are $xdb(t) * xb(t)^2$ and $xdb(t)^2 * xb(t)^2$, this means that the boat velocity and displacement are leading for the resistance force.

A.7. Results for the boat acceleration per method

The results of modeled boat accelerations are shown in fig. 6.1 for the the seven different approaches together. To be able to judge the quality of the results, figures with the results per method are presented in this section.

Three approaches are based on the F_{foots} method: the original, with optimized parameters and with an optimized offset and gain for F_{foot}. The results are shown in fig. A.14. The original approach has the worst fit with the measured boat acceleration, although the shape of the curve is neat. The optimized parameters did improve quite well, but the height of the curve is still to low. The F_{foots} method with optimized offset and gain for F_{foot} has the best fit in this figure, although the shape of the curve does not match the measured boat acceleration at every point in the stroke.

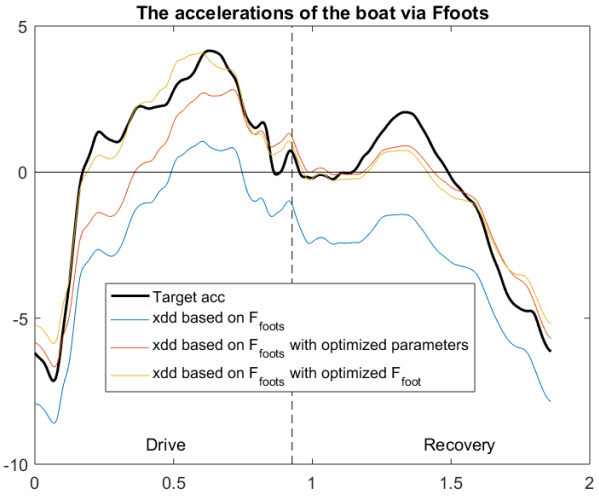

Figure A.14: The modeled boat accelerations based three different approaches based on the F_{foots} method.

Four approaches use the m_{sys} method: the original, with optimized parameters, a virtual resistance force and with an optimized offset and gain for F_{foot}. The results are shown in fig. A.15. The original approach has the worst fit with the measured boat acceleration. The optimized parameters did improve quite well, but the height of the curve is a bit lower then the measured boat acceleration curve. Adding a virtual resistance force on the rower results in a curve that has a better height, but worse shape. The m_{sys} method with optimized offset and gain for F_{foot} the best fit found in this figure, the shape of the curve remains good and the height is better than for the original or optimized parameters.

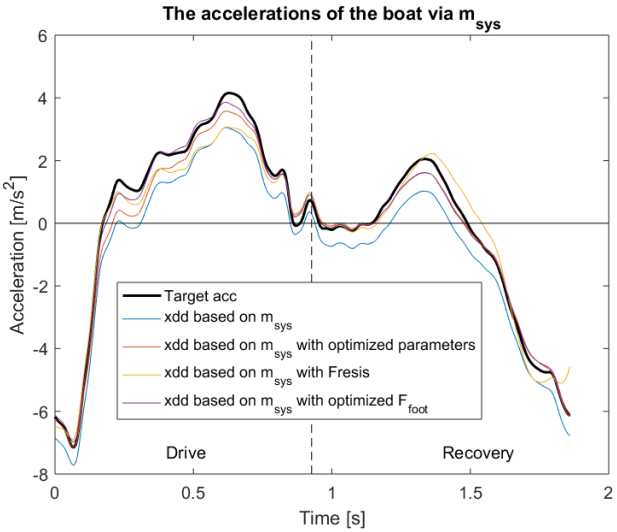

Figure A.15: The modeled boat accelerations based four different approaches based on m_{sys}.

A.8. Results for the relative displacement of the rowers

In fig. A.16 the relative motions of rower 1 and 2 are shown, zoomed in to the range of the expected rower motions. In these graphs, the differences between the methods that have a result that lies within this range are better visible.

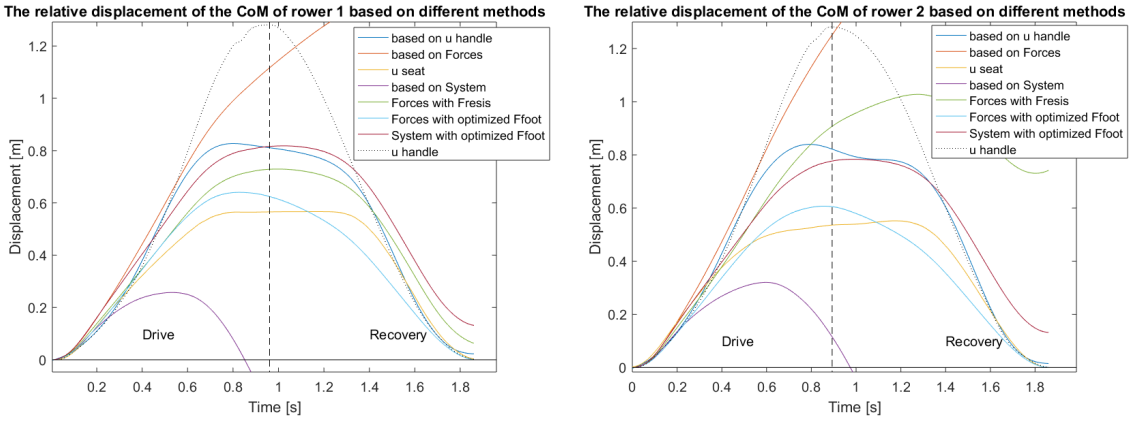

Figure A.16: The resulting u_r for both rowers via the different approaches. Zoomed in to the range of the expected rower motions, so that the differences between the approaches are better visible.

A.9. More extreme rigging setup changes

In chapter 5 rigging parameter changes have been studied that are within a reasonable range for the rower. However in the model, more extreme cases of changes in the rigging setup can be tried. In this section, two extreme cases of an inboard length of the oar and three extreme cases of the footstretcher position are presented.

Extreme changes in the inboard length of the oar are tricky, because from some point the rower is not able to follow the handle movement anymore. In fig. A.17, two extreme versions of a change in the inboard length are shown; a $\Delta l_{inboard}$ of -10 cm and +10 cm. For a decrease of the inboard length of 10 cm, the total covered oar angle is grown so much, that the oar can not reach the furthest point in the catch. This leads to a constant angle in the first part of the drive phase. This leads to a jump in the handle power curve of the rower, due to a sudden change of the oar angular velocity.

The overlap of the oars for a inboard length of 98 cm is not punished by the model. However practically this would be very uncomfortable for the rower, because the arms should be far crossed in front of the body, while in the mean time providing the same force on the handles.

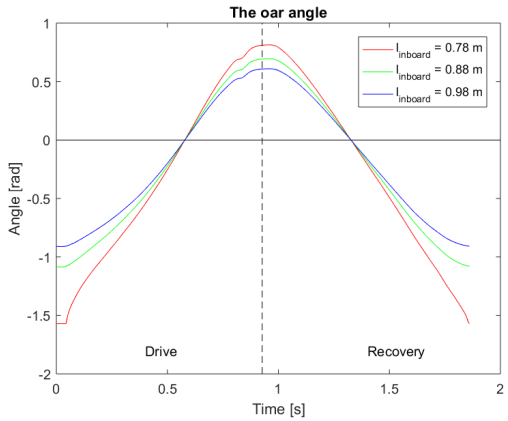

(a) The oar angle for three different $l_{inboard}$.

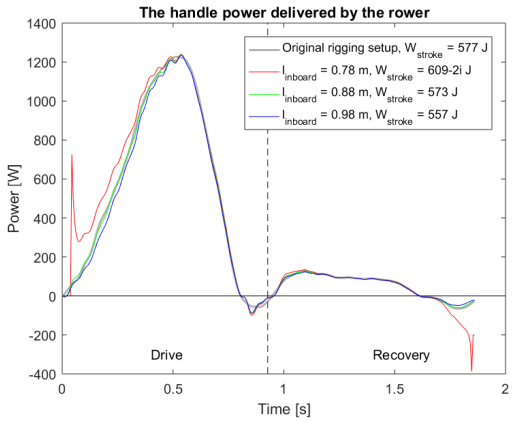

(b) The handle power for three different $l_{inboard}$.

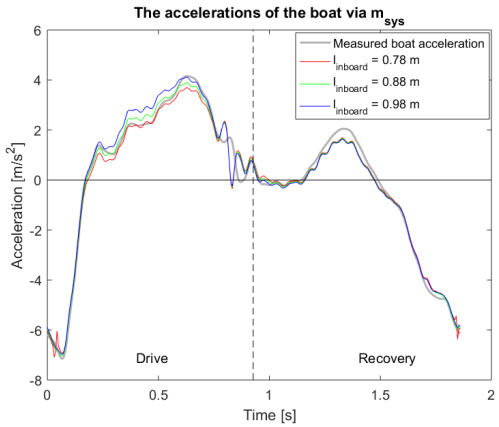

(c) The boat acceleration for three $l_{inboard}$.

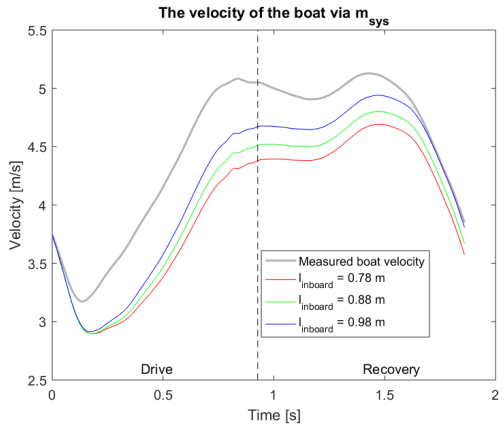

(d) The boat velocity for three different $l_{inboard}$.

Figure A.17: Four boat variables for three more extreme inboard lengths of the oar. The inboard length of rower 1 is changed, while rower 2 uses the original setup.

In fig. A.18 more excessive changes are applied to the position of the footstretcher, there is found that the footstretcher can not be moved towards the bow of the boat ongoing. A shift of 20 cm still has a positive effect on the boat velocity, but for a shift of 30 cm, the boat velocity decreases.

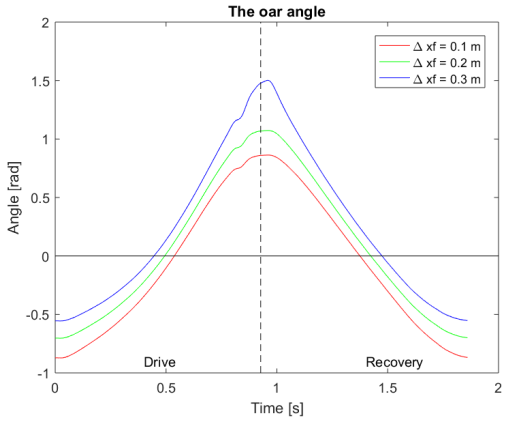

(a) The oar angle for three different Δx_{foot}.

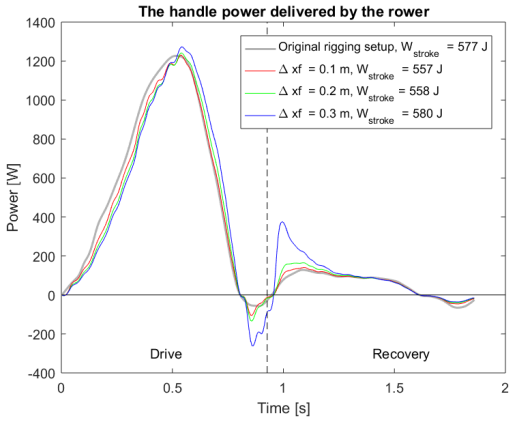

(b) The handle power for three different Δx_{foot}.

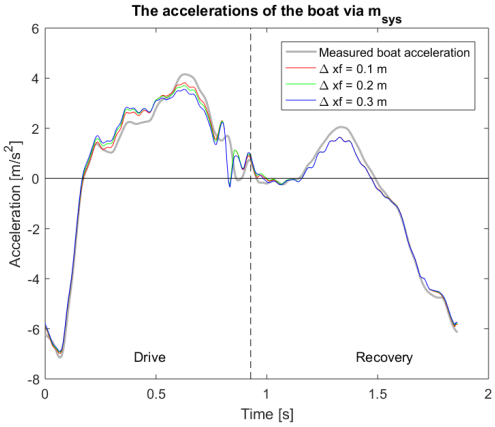

(c) The boat acceleration for three Δx_{foot}.

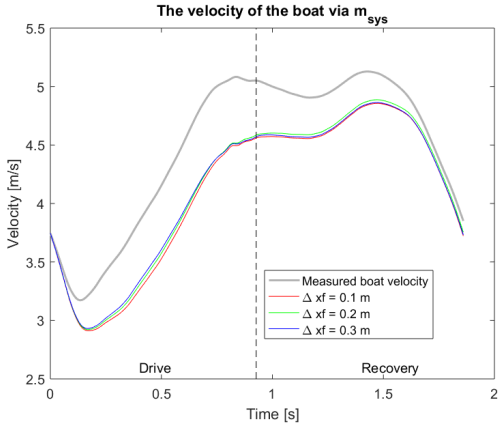

(d) The boat velocity for three different Δx_{foot}.

Figure A.18: Four boat variables for three more extreme footstretcher positions. The footstretcher position of rower 1 is changed, while rower 2 uses the original setup.

B

Results of an Australian dataset

One week before the hand-in date of the thesis, more data is received from different women's doubles from Australia.

The obtained results are approximately the same as the results for the Dutch LW2x. The best prediction of the boat acceleration is done with the m_{sys} method, and after a small correction of the foot force gain and offset, the results did improve.

The other methods to calculate the relative displacement of the rower and the boat accelerations are not applied in this case. The extra datasets are all over a period of approximately 30 second, and included data obtained from the footstretcher sensor. The stroke rate is between 30 and 33 str/min.

A second LW2x

This dataset is measured in a lightweight women's double, competing at the World Championships under 23. The level of rowing is thus quite comparable to the Dutch LW2x that is used in the thesis.

Parameters	Value
Span	1.58 m
$l_{inboard}$	0.865 m
l_{oar}	2.86 m

(a) Rigging parameters of the LW2x.

Rower	Weight
Bow (1)	57.5 kg
Stroke (2)	58.1 kg

(b) Rower masses of the LW2x.

Table B.1: The settings of the LW2x from Australia.

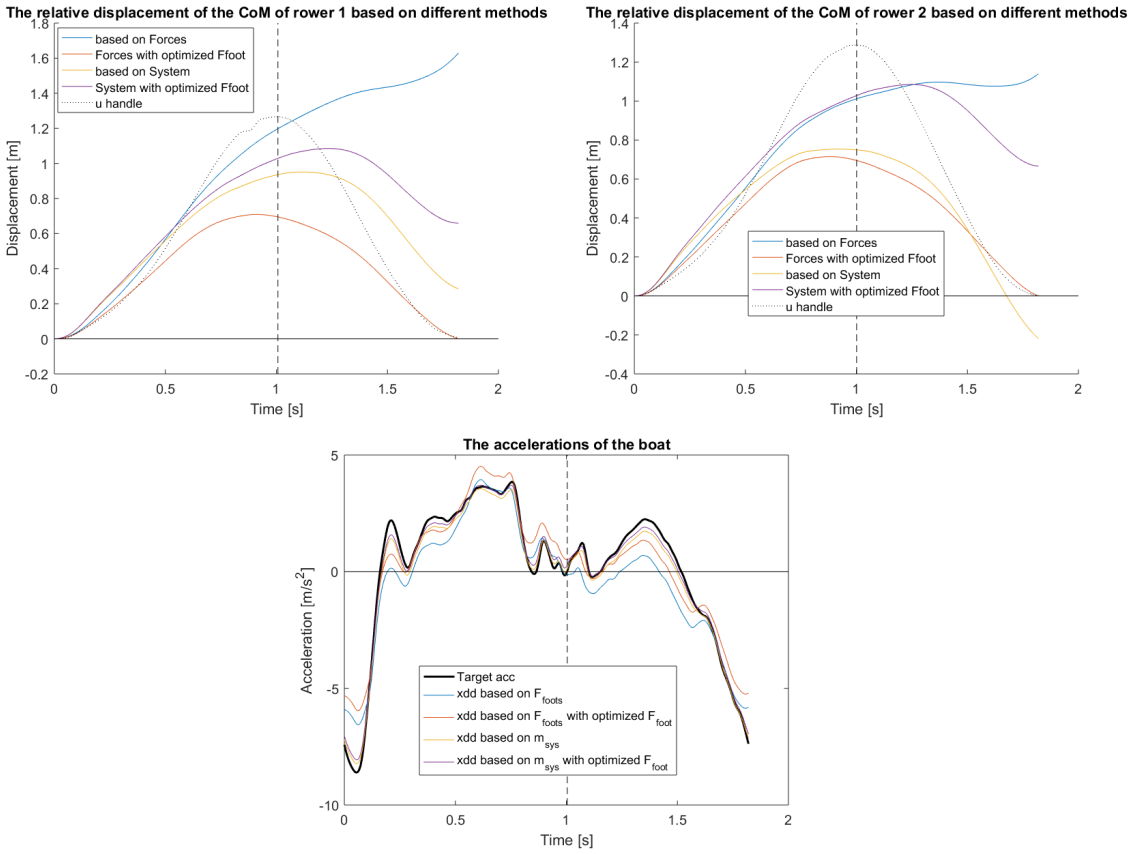

Figure B.1: The results of $\ddot{x}_b$ for a LW2x, original and with optimized gain and offset for F_{foot}. The optimized offset and gain are respectively -17.9753 N and 0.9894 (3.9% change in total) for rower 1 and -8.6492 N and 1.0150 (0.3% change in total) for rower 2.

Method	Shape	Height	RMSE
Based on F_{foots}	-	-	1.0569 m/s^2
Based on F_{foots} with optimized F_{foot}	-	+	0.9294 m/s^2
Based on m_{sys}	++	+	0.3284 m/s^2
Based on m_{sys} with optimized F_{foot}	++	++	0.2565 m/s^2

Table B.2: A qualitative and quantitative comparison of the methods used to model the boat acceleration of the Australian LW2x. Where ++ means good, + is reasonable, 0 is neutral, - is bad and - - is very bad. The quantitative measure is the root mean square error (RMSE) of the results of all the methods used to model the boat acceleration.

Method	Drive	Finish	Recovery	Compare r1&r2	Error r1	Error r2
$Forces$	-	-	- -	+	1.6291 m	1.1399 m
$Forces$, optimized F_{foot}	++	++	+	+	-2.0592 e-07 m	4.2377e-10 m
$System$	-	+	-	0	0.2848 m	-0.2184 m
$System$, optimized F_{foot}	-	-	- -	+	0.6595 m	0.6664 m

Table B.3: A qualitative and quantitative comparison of the methods used to model the relative movement of the rowers of the Australian LW2x. The quantitative measure (error) is the deviation of the rower movement at the end of the stroke from the starting position. r1 is rower 1 and r2 rower 2, ++ means good, + is reasonable, 0 is neutral, - is bad and - - is very bad. ** means that the method used the measured boat acceleration ($\ddot{x}_b$) to predict the relative rower movement.

Two different W2x

The rigging set up of both the W2x is slightly different from the rigging setup of the lightweight rowers in the LW2x. The crew of first W2x consisted of the rowers and settings in table B.4.

Parameters	Value
Span	1.58 m
$l_{inboard}$	0.865 m
l_{oar}	2.87 m

(a) Rigging parameters of the W2x.

Rower	Weight
Bow (1)	76.4 kg
Stroke (2)	85.2 kg

(b) Rower masses of the first Australian W2x.

Table B.4: The settings of the first W2x from Australia.

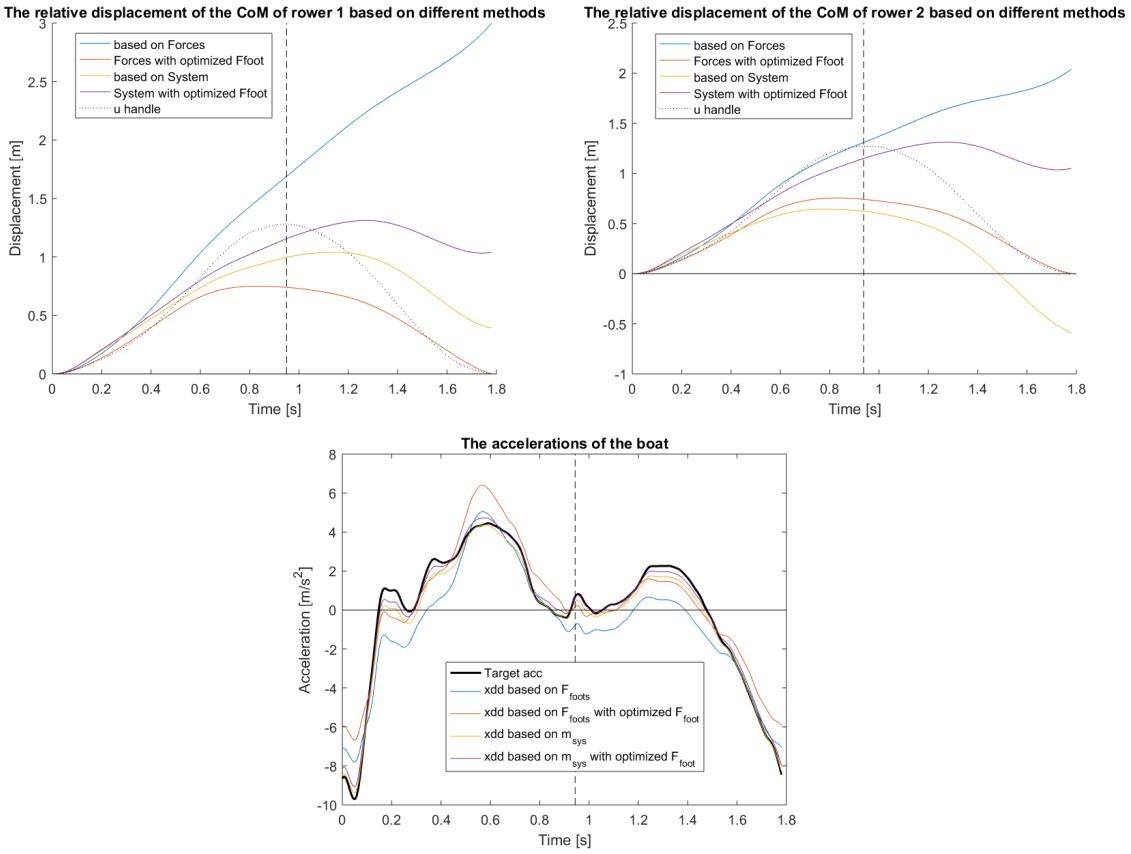

Figure B.2: The results of $\ddot{x}_b$ for the first Australian W2x, original and with optimized gain and offset for F_{foot}. The optimized offset and gain of F_{foot} are respectively -26.2631 N and 0.9572 (7.4% change in total) for rower 1 and -14.4635 N and 1.0233 (0.6% change in total) for rower 2.

Method	Shape	Height	RMSE
Based on F_{foots}	-	-	1.2891 m/s^2
Based on F_{foots}, optimized F_{foot}	-	0	1.0759 m/s^2
Based on m_{sys}	+	+	0.4073 m/s^2
Based on m_{sys}, optimized F_{foot}	+	++	0.2755 m/s^2

Table B.5: A qualitative and quantitative comparison of the methods used to model the boat acceleration of the first Australian W2x. Where ++ means good, + is reasonable, 0 is neutral, - is bad and - - is very bad. The quantitative measure is the root mean square error (RMSE) of the results of all the methods used to model the boat acceleration.

Method	Drive	Finish	Recovery	Compare r1&r2	Error r1	Error r2
$Forces$	- -	- -	- -	+	2.9982 m	2.0401 m
$Forces$, optimized F_{foot}	++	++	+	+	8.9192e-08 m	-1.2020e-08 m
$System$	+	+	-	-	0.3921 m	-0.5932 m
$System$, optimized F_{foot}	0	+	- -	+	1.0401 m	1.0510 m

Table B.6: A qualitative and quantitative comparison of the methods used to model the relative movement of the rowers of the first Australian W2x. The quantitative measure (error) is the deviation of the rower movement at the end of the stroke from the starting position. r1 is rower 1 and r2 rower 2, ++ means good, + is reasonable, 0 is neutral, - is bad and - - is very bad. ** means that the method used the measured boat acceleration ($\ddot{x}_b$) to predict the relative rower movement.

The second W2x had the same rigging setup as the first, but the stroke rower is changed (see table B.7). The boat acceleration pattern is also quite different from the first W2x, but the model is able to predict both boat accelerations with an RMSE error of around 0.3 m/s^2. The relative movement of the bow rower (1) is shown for both races together in fig. B.4. There is found that the movements of the bow rower are quite consistent with different rowing partners. So the rower does not change her movements to much to adapt to the boat average. This supports the assumption that u

Parameters	Value
Span	1.58 m
$l_{inboard}$	0.865 m
l_{oar}	2.87 m

(a) Rigging parameters of the W2x.

Rower	Weight
Bow (1)	76.4 kg
Stroke (2)	77.5 kg

(b) Rower masses of the second Australian W2x.

Table B.7: The settings of the second W2x from Australia.

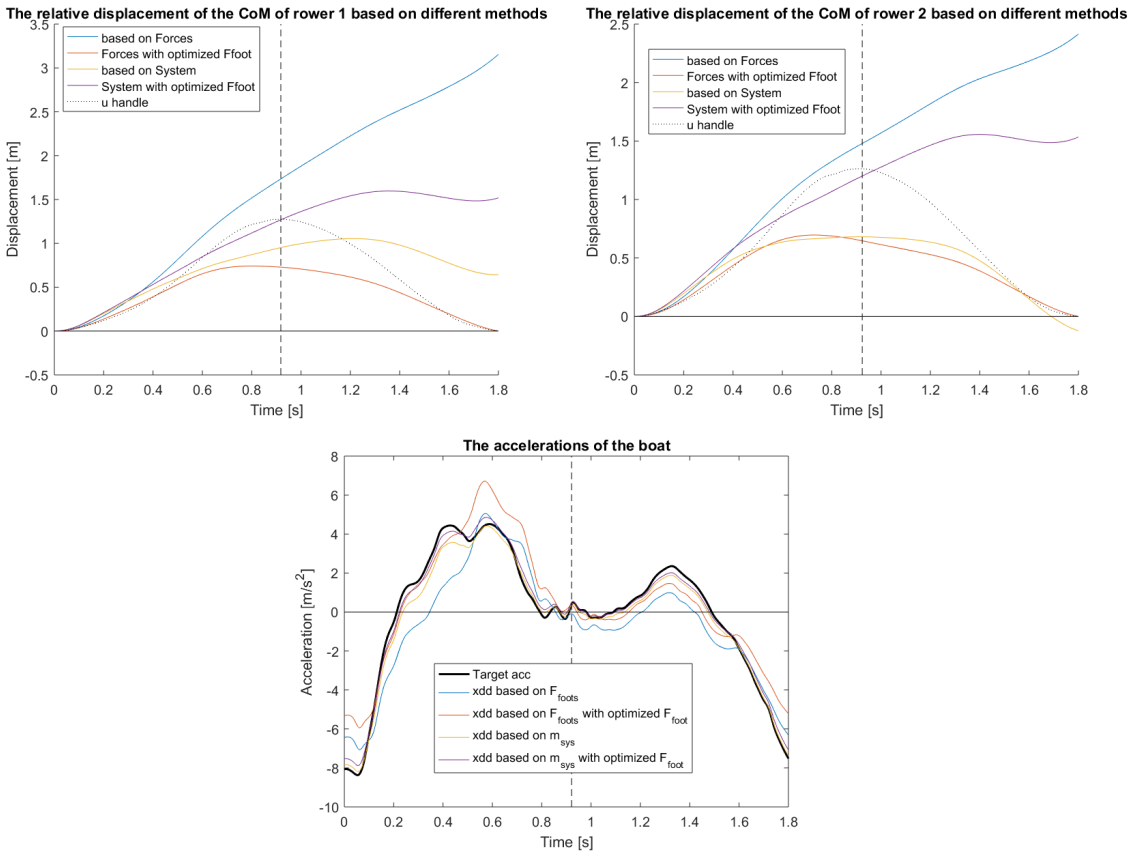

Figure B.3: The results of $\ddot{x}_b$ for the second Australian W2x, original and with optimized gain and offset for F_{foot}. The optimized offset and gain of F_{foot} are respectively -27.7257 N and 0.9662 (6.5% change in total) for rower 1 and -0.2435 N and 0.9610 (3.9% change in total) for rower 2.

Method	Shape	Height	RMSE
Based on F_{foots}	-	-	1.3800 m/s^2
Based on F_{foots} with optimized F_{foot}	-	0	1.2057 m/s^2
Based on m_{sys}	+	+	0.4432 m/s^2
Based on m_{sys} with optimized F_{foot}	++	++	0.2946 m/s^2

Table B.8: A qualitative and quantitative comparison of the methods used to model the boat acceleration of the second Australian W2x. Where ++ means good, + is reasonable, 0 is neutral, - is bad and - - is very bad. The quantitative measure is the root mean square error (RMSE) of the results of all the methods used to model the boat acceleration.

Method	Drive	Finish	Recovery	Compare r1&r2	Error r1	Error r2
$Forces$	- -	- -	- -	+	3.1547 m	2.4147 m
$System$	-	+	-	0	0.6436 m	-0.1225 m
$Forces$, optimized F_{foot}	++	++	+	+	-4.4536e-08 m	1.7875e-08 m
$System$, optimized F_{foot}	-	-	- -	+	1.5184 m	1.5342 m

Table B.9: A qualitative and quantitative comparison of the methods used to model the relative movement of the rowers of the second Australian W2x. The quantitative measure (error) is the deviation of the rower movement at the end of the stroke from the starting position. r1 is rower 1 and r2 rower 2, ++ means good, + is reasonable, 0 is neutral, - is bad and - - is very bad. ** means that the method used the measured boat acceleration ($\ddot{x}_b$) to predict the relative rower movement.

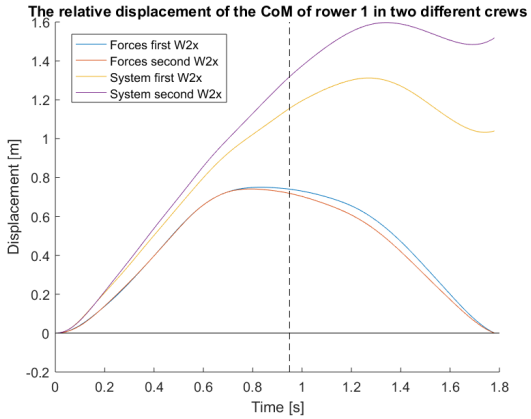

Figure B.4: The relative displacement of rower 1 in two different crews calculated with two different methods.

C

Graphical User Interface with the rigging parameters

To gain more insight in the result of changing a rigging parameter on other rigging parameters and the oar movements, a graphical interface is build (shown in fig. C.1). In this interface various rigging parameters can be changed (more than in chapter 5). The tool is currently used as an interface to visualize the parameters of the rigging setup of the boat. The changes in boat velocity are not processed, due to the many assumptions that have to be made, before this can be properly done.

The ”Show” button presents the user with a schematic boat figure that visualizes the currently selected rigging setup and the modeled handle and blade movements. The slide bars ”Drive” and ”Recovery” allow to the user go gradually through different points of the drive and recover in the force-angle and boat speed curves. The oar movements are also shown during the drive in the schematic boat figure. The recovery is not yet implemented in the oar movements. The ”Save” button allows the user to save the modeled rigging setup in the workspace and use it for other applications.

The assumptions between the relative movement of the rower and the displacement of the oar is the most difficult to model. The handle displacement in x-direction is assumed to stay constant and the covered oar angles change for different rigging setups. The relative movement of the rower is based on the position of the footstretcher. The handle and CoM movements of the rower are not coupled to each other.

Restrictions

The parameters in the GUI have a big range in which they can vary. Basically the parameters are whatever the user uses as input. However, some combinations of parameters can not be modeled, the combinations are physically impossible implement such as:

- All inputs must be numeric values.
- The length of the oar l_{oar} can not be smaller then l_{in}, otherwise the oar can not be put through the gate.
- The span of the boat can not be smaller then the boat width or l_{in}.
- Rower segments can not overlap; a warning is given that the rowers collide (fig. C.2a). (in reality, could be a little).
- The footstretcher of one rowing spot can not be placed behind the gate of the same spot (fig. C.2b).
- The blades can not collide with the hull, therefore, they may not go closer towards the hull then the y-coordinates of the gates (span/2). This is a restriction on l_{in}.

If a restriction is crossed, the graphical interface is programmed such that it gives a warning To the user, in fig. C.2 two examples of these warnings are given.

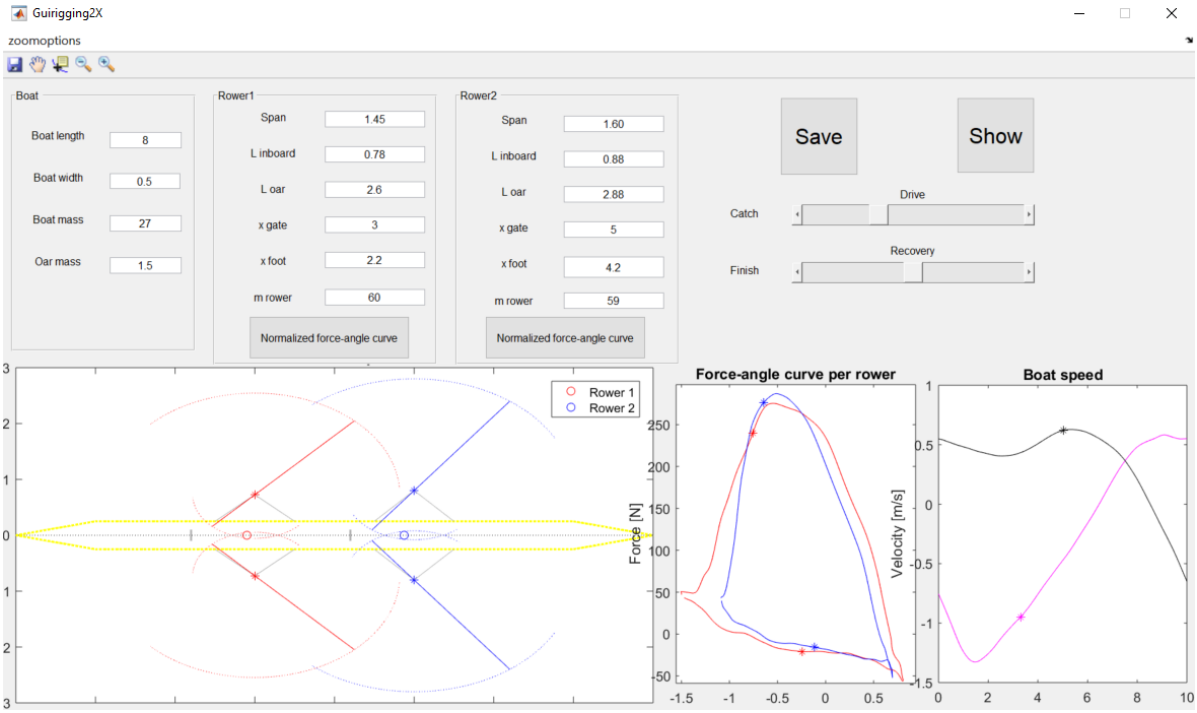

Figure C.1: GUI of rigging parameters

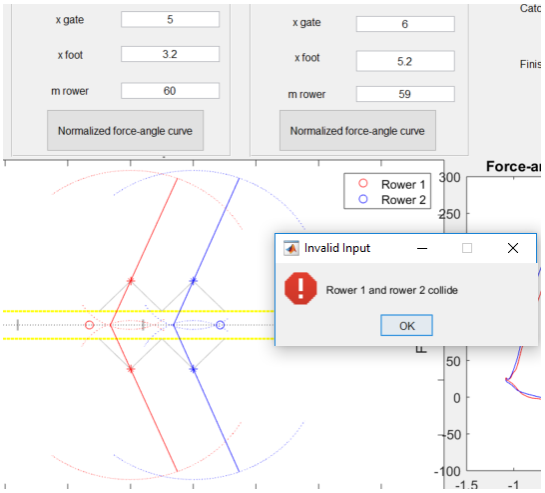

(a) The warning given when x_{gate} of rower 1 is to close too x_{gate} of rower 2 and their stroke segments overlap.

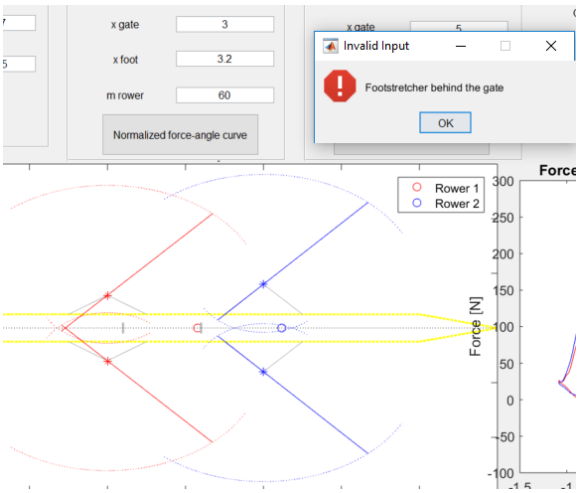

(b) The warning given when the footstretcher of rower 1 is placed behind the gate of rower 1. $x_{foot} > x_{gate}$

Figure C.2: Warnings given by the GUI, when the restrictions of the parameters are not met.

Figures

Schematic boat figure When the show button is pushed, the figure on the left shows the setup in a schematic boat. Also the blade and handle path are shown. This graph will provide insight for a coach, what would happen to the oar movements when certain parameters are changed. The ”Drive”-slide bar does approximately the same thing, only it can also move the oar through the stroke, depending on how far the slide bar is progressed (the beginning is the catch and the end the finish).

In fig. C.1 the graphical interface is shown with a changed setup of rower 1 with respect the original setup, that is still used by rower 2. The span of rower 1 is smaller, as well as the inboard length and the oar length. The effect on the blade path and handle movement is shown in the schematic boat figure. The oar movements that are studied by moving the ”Drive” slide bar are different as well.

Force-angle curves The middle figure shows the force-angle curves for the two rowers. When the rigging parameters are changed, the shape of the force-angle curve can change as well. For the new rigging setup of rower 1 the shape of the force-angle curve is changed. The force-angle curve of rower 1 is broadened with respect to the original rigging setup (compare with fig. 2.12b). The total angle covered by the handles and blades of rower 1 is increased.

Speed calculations The most right figure shows the boat speed. In the current version of the interface, the boat speed is a graph of the measured boat speed. It does not change with new rigging parameters. The two lines show the speed development through the drive and recover separately. In time this graph is supposed to show the calculated boat speed, based on the model and the changed parameters of the boat setup. In that case the user can see whether the new rigging setup has improved the boat speed.